





On the validity of the spectroscopic age indicators [Y/Mg], [Y/Al], [Y/Si], [Y/Ca], and [Y/Ti] for giant stars

Orlando J. Katime Santrich^{1,2}★ , Leandro Kerber¹ , Yuri Abuchaim² ,
and Geraldo Gonçalves² 

¹Universidade Estadual de Santa Cruz, UESC, Rodovia Jorge Amado km 16, Ilhéus, 45662000, Bahia, Brazil.

²Universidade de São Paulo, Instituto de Astronomia, Geofísica e Ciências Atmosféricas, Departamento de Astronomia, Rua do Matão 1226, 05508-090 São Paulo/SP, Brazil.

Accepted in MNRAS 2022

ABSTRACT

The abundance ratios [Y/Mg], [Y/Al], [Y/Si], [Y/Ca], and [Y/Ti] have been suggested as chemical clocks for solar-metallicity dwarf stars in the field as well as for giant stars in open clusters. To verify this last hypothesis, we derived these abundances ratios of 50 giant stars belonging to seven open clusters. To calculate the abundances, we analyzed FEROS spectra assuming the LTE-hypothesis. We confirmed that [Y/Mg], [Y/Al], [Y/Si], [Y/Ca], and [Y/Ti] work as chemical clocks for field dwarf stars at the local region ($d < 1$ kpc) whereas for the field giants the [Y/Mg], [Y/Al] and [Y/Si] also present trends with the ages but high scattering. [Y/Ca] and [Y/Ti] do not present any correlation with age in the field giants. In Our open clusters, the behaviour is similar, [Y/Mg], [Y/Al] and [Y/Si] present evident trends, whereas [Y/Ca] vs ages is a flat and [Y/Ti] vs ages is less steep. We also confirmed that the chemical clocks have high scatter at the early ages. The chemical clocks for the cluster giants of compiled samples, are similar to our results in some cases whereas in other situations there are differences but always keeping the general trend. Several relations between abundance ratios and ages may be obtained when dwarfs and giants are analyzed, confirming the non-universality of the spectroscopic age indicators.

Key words: stars: abundances - stars: fundamental parameters - stars: late-type - Galaxy: evolution - open clusters and associations

1 INTRODUCTION

The spectroscopic ratios [Y/Mg]¹, and [Y/Al]² have been important in last years owing to possibility to obtain reliable ages for the stars. This fact is striking because stellar ages are hard to derive and have always been a topic of discussion in Astrophysics. These spectroscopic clocks have been studied in field dwarf stars, while in giants the results are limited for some open clusters.

The ratio [Y/Mg] has been the most studied spectroscopic indicator in literature mainly for field dwarf stars, being proposed as a promising age indicators for solar twin stars by Nissen (2015) and Tucci Maia et al. (2016). Afterwards, Feltzing et al. (2017) used a sample of 714 dwarf stars in the solar neighbourhood (Bensby et al. 2014) to conclude that [Y/Mg] vs Age relation is unique to solar analogues. Delgado Mena et al. (2019), using more than 1000 FG K

field dwarfs, confirmed the negative correlation between [Y/Mg] and the ages (Nissen 2015). More recently, Titarenko et al. (2019) used 342 turn-off stars in the solar neighborhood and also found the same negative tendency but they did not see dependency on the metallicity. Skúladóttir et al. (2019) studied [Y/Mg] in the dwarf galaxy Sculptor obtaining the same negative inclination with the ages, although their [Y/Mg] ratios have presented lower values relative to the Galactic objects. This result was the first to report such clock in other galaxies.

Despite the validation of the ratio [Y/Mg] as a chemical clock for field dwarf stars, the use of this (or any other) spectroscopic age indicator to study the chemical evolution of our Galaxy is limited by the faintness of such stars. The natural solution to probe the distant regions in the Galactic disk are the giant stars, whose luminosity can reach several magnitudes brighter. Although the correlation between abundance ratios and age for giant stars can be verified using those in the Galactic field, it is evident that open clusters are the ideal laboratories for such studies since the stars have similar initial chemical composition and age. In particular, the ages can be

★ E-mail: ojksantrich@uesc.br and ojkatime@gmail.com (KTS)

¹ It was obtained from [Y/Fe] and [Mg/Fe], in turn derived from abundance definition $[A/B] = \log(A/B)_\star - \log(A/B)_\odot$.

² from [Y/Fe] and [Al/Fe].

very well determined in open clusters by means of isochrone fitting techniques, reaching uncertainties in $\log(\text{age})$ of ~ 0.01 if $[\text{Fe}/\text{H}]$ are known with an accuracy of ~ 0.06 dex (Bossini et al. 2019), which, translate in linear age, corresponds to just 2%.

The first work dedicated to study the $[\text{Y}/\text{Mg}]$ vs Age in giants was Slumstrup et al. (2017) who analyzed five red clump stars in four open clusters (NGC 6811, NGC 6819, M 67, and NCG 188) ranging ages from ~ 1 Gyr to 6 Gyr. They claimed an evident negative tendency between $[\text{Y}/\text{Mg}]$ and their ages, in excellent agreement with the one presented by Nissen (2016) for solar twins. On the other hand, Peña Suárez et al. (2018) also investigated $[\text{Y}/\text{Mg}]$ vs Age in giant stars in three open clusters younger than ~ 2 Gyr (NGC 3680, NGC 2360, and NCG 5822), concluding that there is no evidence favouring the negative trend.

The relation $[\text{Y}/\text{Al}]$ vs Age was studied in first studied by Nissen (2016) who analyzed 21 solar twin stars, Spina et al. (2018) increased the sample analyzing 79 solar twins. The two works concluded that the ratio $[\text{Y}/\text{Al}]$ is an excellent candidate to be spectroscopic age indicator because of the low scattering shown. Later, Delgado Mena et al. (2019) also confirmed this ratio as age indicator in field dwarf stars.

Casali et al. (2020) studied the ratios $[\text{Y}/\text{Mg}]$, $[\text{Y}/\text{Al}]$, $[\text{Y}/\text{Si}]$, $[\text{Y}/\text{Ca}]$, $[\text{Y}/\text{Ti}]$ and $[\text{Y}/\text{TiII}]$ in open cluster giants and solar-like stars. These abundance ratios presented a clear scattering for giant stars with ages < 2.0 Gyr. The authors concluded that this result was due to the variation of the star formation histories at different Galactocentric distances, and to the role of metallicity in the efficiency of the neutron-capture element production.

More recently, Casamiquela et al. (2021) studied these abundance ratios and the ages for open clusters in the inner and outer disks. They concluded that the tendencies exist but with differences in the two galactic disks.

This paper is organized as follow. In Section 2, we present the data employed in this study. In section 3 we describe spectroscopic techniques needed to calculate the abundance ratios. In Section 4, we present and discuss the spectroscopic clocks. Finally, Section 5 shows our conclusions.

2 DATA

We have applied a detailed spectroscopic analysis for 50 giant stars in the open clusters NGC 5316, NGC 6633, IC 4756, NGC 5822, NGC 6940, IC 4651 and NGC 2682 (M 67) (Table 1). These clusters have solar-like metallicities and ages ranging from 150 Myr to 3.6 Gyr.

In order to calculate the chemical abundances and age indicators, we used high-resolution spectra obtained with the Fiberfed Extended Range Optical Spectrograph (FEROS, Kaufer et al. 1999). Its spectral resolving power is $R = 48000$, corresponding to 2.2 pixels of 15μ , and the wavelength coverage is $[3800, 9200]\text{\AA}$. FEROS is installed in the MPI 2.2 mts telescope in La Silla/Chile. We have taken the reduced spectra from phase III form in the ESO/archive³. The nominal S/N ratio was evaluated by measuring the *rms* flux fluctuation in selected continuum windows, and the typical values were $S/N = [120, 180]$. The Juno solar spectrum used in the analysis has a $S/N = 800$. Therefore, the spectra have good quality to carry out the spectroscopic analysis and to obtain reliable results. This

fact is shown in Figure 1 where Y II and Sr I absorption lines are identified in two stars of the clusters IC 4651 and NGC 2682.

Figure 2 presents the Hertzsprung-Russell (HR) diagram of the seven clusters in our sample as well as the position of the 50 giant stars with FEROS spectra. This HR diagram was built using the Gaia DR2 photometry (Gaia Collaboration, et al. 2018a) and Cantat-Gaudin et al. (2018b) catalogs, which include cluster membership determination. The isochrone fits obtained by Gaia Collaboration, et al. (2018b) and Bossini et al. (2019) were used to convert the observational magnitudes to the absolute ones. Table 1 shows the physical parameters of our cluster sample and the number of stars analyzed in each cluster. We directly used these cluster ages to develop the analysis presented in this work. We adopted conservative age uncertainties of 20% since the estimates from Bossini et al. (2019) are only the formal ones, which are clearly underestimated in the most cases. Furthermore, it seems that only such level of age uncertainty can explain the differences with the results found by Cantat-Gaudin et al. (2020) analysing the same Gaia DR2 data. These last authors do not provide individual uncertainties but informed that the $\log(\text{age})$ uncertainty ranges from 0.15 to 0.25 for young clusters and from 0.1 to 0.2 for old clusters, which are in agreement with our conservative assumption. Table A1 shows the 50 cluster giants analyzed in this work.

3 SPECTROSCOPIC ANALYSIS

We applied the Local Thermodynamical Equilibrium (LTE) approximation to derive the abundance ratios in the cluster sample. The Stellar Atmospheric Parameters (SAP), effective temperature (T_{eff}), surface gravity ($\log g$), microturbulence velocity (ξ) and metallicity $[\text{Fe}/\text{H}]$ are prerequisite to find the chemical abundances. Specifically, T_{eff} were obtained from excitation equilibrium, $\log g$ from ionization equilibrium between Fe I and Fe II lines, ξ from zero slope between Fe I abundances and reduced equivalent width and $[\text{Fe}/\text{H}]$ were established from the final value fixed by the ionization equilibrium. To avoid the dependency on the $\log gf$ -values we have employed the line-by-line (lbl) method relative to the Juno solar spectrum.

All abundances were obtained via Equivalent Width (EWs) measurements, with the exception of Ba and Eu that were computed via spectral synthesis technique. To measure the EQW we used the Gaussian fit of splot/IRAF⁴, and to obtain the stellar parameters and chemical abundances we employed the python-code qoyllur-quipu⁵. This code uses the Kurucz atmospheric grids⁶ and spectral code MOOG⁷. The list of the Fe-lines were taken from Lambert et al. (1996) & Castro et al. (1997) and for the other elements from several sources such as it is shown in the Appendix (Tables A2, A3, A4, A5, A6 and A7).

We have computed $[\text{Mg}/\text{Fe}]$, $[\text{Al}/\text{Fe}]$, $[\text{Sr}/\text{Fe}]$, $[\text{Y}/\text{Fe}]$, $[\text{Zr}/\text{Fe}]$, $[\text{Ba}/\text{Fe}]$, $[\text{La}/\text{Fe}]$, $[\text{Ce}/\text{Fe}]$, $[\text{Nd}/\text{Fe}]$, $[\text{Eu}/\text{Fe}]$, $[\text{hs}/\text{ls}]$ ⁸,

⁴ IRAF is developed by NOAO and available on <http://iraf.noao.edu/>

⁵ this code was developed by (Ramírez et al. 2014) and it is available on <https://github.com/astroChasqui/q2>

⁶ These grids are available on <http://kurucz.harvard.edu/>

⁷ MOOG is available in its last version on <https://www.as.utexas.edu/~chris/moog.html>

⁸ Obtained from $[\text{hs}/\text{Fe}] - [\text{ls}/\text{Fe}]$; where $[\text{hs}/\text{Fe}]$ is the mean value for the second-peak Ba, La, Ce, and Nd whereas $[\text{ls}/\text{Fe}]$ is for the first-peak Sr, Y, and Zr

³ <http://archive.eso.org/cms.html>

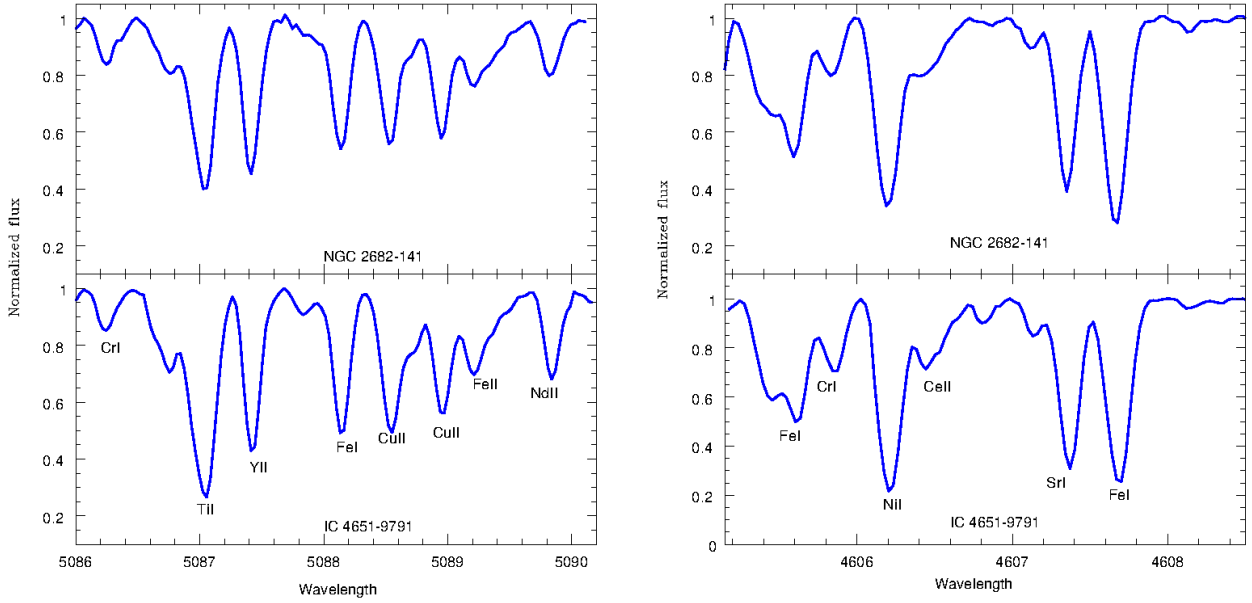


Figure 1. Spectral regions around Y II and Sr I absorption lines in the stars IC 4651–9791 and NGC 2682–141. Some lines of other elements are also identified.

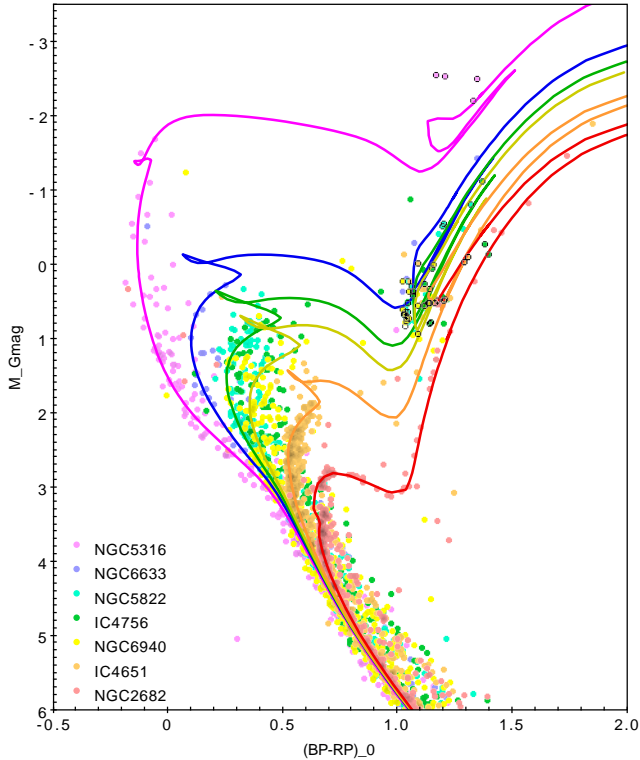


Figure 2. Gaia DR2 Hertzsprung-Russell diagram for all open clusters analyzed in this work. Giant stars with FEROS spectra are marked by black circles. PARSEC isochrones (Marigo, et al. 2017) with the parameters presented in Table 1 are overplotted. The original Gaia DR2 data come from Cantat-Gaudin et al. (2018b). Only stars with membership probability ≥ 0.50 are presented.

[Ba/Eu], [Y/Mg], [Y/Al] and [s/Fe]⁹ abundance ratios. This process was made for six open clusters of our sample.

For IC 4651, we have taken SAP, [Y/Fe], [Zr/Fe], [La/Fe], [Ce/Fe], and [Nd/Fe] from [Katime Santrich and Rossi \(2017\)](#) to derive the other abundance ratios and chemical clocks. These authors used FEROS spectra and the same methodology employed by us.

For our entire sample, the abundance ratios of Mg, Al, Sr, and Zr were obtained from the neutral state whereas for the elements Y, Ba, La, Ce, Nd, and Eu the ratios were derived from their first-ionization state.

We have compared our results with those from the works of [Luck \(2015, 2018\)](#) in which the author has developed an homogeneous analysis of high-resolution spectra corresponding to giant and dwarf stars with ages until 8 Gyr and 12 Gyr, respectively. An important detail is that this author did not derive the spectroscopic age indicators, therefore we have used his results to derived [Y/Mg], [Y/Al], [Y/Si], [Y/Ca], and [Y/Ti], as well as [s/Fe], [hs/lr], and [Ba/Eu] abundance ratios. The giant sample of [Luck \(2015\)](#) will be also useful because offer a opportunity to compare the giant stars within two scenarios, the field and open clusters. The inclusion of the field dwarfs studied by the same author will allow to test if the spectroscopic clocks also work in dwarfs such as it was reported by other authors, if work, this would indicate that the spectroscopic analysis carry out by [Luck \(2015, 2018\)](#) is consistent. From these papers, we have directly taken the stellar ages whereas for carry out our analysis, the cluster non-members were used as well as the stars within the metallicity interval of $[-0.30, 0.30]$ dex. It is also import to add that we have selected only the field stars whose chemical abundances of YII, MgI, AlI, SiI, CaII, TiI, SrI, BaII and EuII were calculated from more than two absorption lines (with the exception

⁹ This ratio represents the mean value of the heavy-element abundances. In this work, it was derived from abundance ratios [x/Fe] of Sr, Y, Ba, La, Zr, Ce, and Nd.

of SrI and EuII). As well as we have also taken the field stars with ages derived from at least two isochrones.

For comparison, we have used the open cluster samples of literature whose ages and abundances were obtained in homogeneous form. We have used the open clusters also studied by Luck (2015): Me 25, NGC 2287, NGC 2632, IC 2391, NGC 3532, Me 111, NGC 6475 and NGC 6705. As well as the samples of Reddy et al. (2012, 2013, 2015); Reddy & Lambert (2019) and the work of Blanco-Cuaresma et al. (2015) who studied dwarf and giant stars within several open clusters.

3.1 Solar abundances

Our solar atmospheric parameters (5777 ± 24 K; 4.45 ± 0.05 dex; 7.48 ± 0.02 dex; 0.94 ± 0.09 km s⁻¹) were used to find the abundances of the chemical species studied in this work. In general terms, the solar chemical abundances of Juno spectrum are similar to the reported in literature (Table 2). However, some Juno abundances present differences >0.10 dex, specially in relation to Asplund et al. (2009) and the giant stars in the open cluster M67 studied in Gaia-ESO iDR5.

For example, although the our determinations of AlI are similar to Sun iDR5 and Grevesse et al. (2007), when it is compared to Asplund et al. (2009) we see that there is a difference of $+0.12$ dex. In the same way, the abundance of SiI has $+0.12$ dex in relation to the Giants of M67 iDR5 and the CaI presents a difference of $+0.17$ dex in relation to M67 iDR5. Other elements with important differences are the ZrI which presents -0.12 dex and -0.11 dex between iDR5 (Sun and M67) and Juno respectively. Finally, chemical abundances of LaII and EuII have a difference of -0.17 dex when they are compared to M67 iDR5.

These differences can affect in direct way the comparisons between our values and literature. More detailed comparisons, star by star in relation to open clusters and field stars of literature will be made in section 4.4. The implications of these differences in our analyses of the spectroscopic clocks will be discussed in section 4.

3.2 Stellar parameters and abundances

The SAP obtained in this work are in the intervals: $T_{eff} = [4347, 5335]$ K; $\log g = [1.36, 3.38]$ dex; $\xi = [1.45, 2.82]$ km s⁻¹; and $[Fe/H] = [-0.15, 0.17]$ dex. Therefore the obtained SAP, shown in Table 3, indicate that our sample correspond to cool RGB stars with solar metallicity. The abundances of the chemical species derived here are shown in Table 4.

The absorption line 4607 Å, whose profile is well-defined in our spectra (Figure 1), was used to obtain the Sr abundances. To measure the Ba abundances, we used the absorption lines 5853 Å, 6141 Å and 6497 Å and taken into account the hyperfine structure (HFS) corrections of McWilliam and Lambert (1988). In the case of Eu, the abundance calculations were more complicated because the line 6645 Å always presented a blending with CrI and SiI. Following the process explained in Bensby et al. (2005), these absorption lines and the CN bands were included in the line list around 6645 Å and therefore reliable Eu abundances were obtained in our sample. Figure 3 shows the spectral synthesis of EuII in the stars NGC 2682-141 and IC 4651-9791. For the first time, we provide chemical abundance determinations of Sr, Ba, and Eu for some stars in IC 4651, NGC 5822, and NGC 2682. The EuII line 4129 Å never presented a well-defined profile and therefore abundances from this

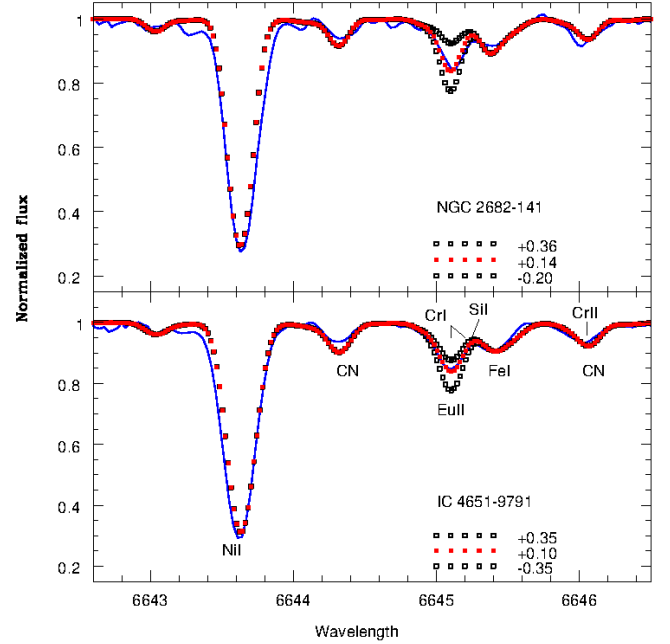


Figure 3. Spectral synthesis to the Eu II line at $\lambda 6645$ Å. Black dotted lines are the synthetic spectra whereas red dotted lines represent the final solutions. Other absorption lines are identified.

line were not obtained. The HFS corrections of Mucciarelli et al. (2008) were used to derive the Eu abundances.

Figure 4 shows the chemical abundances of Sr, Ba and Eu obtained in this work. We compared our abundances with the field giants and also with Gaia and Hi-Res open clusters. As it can be observed, there is similarity between field and open cluster giants. Therefore our abundances of Sr, Ba and Eu are consistent to the previously found in the Galactic disk.

3.3 Abundance uncertainties

In order to evaluate the effect of the stellar atmospheric parameters in the final chemical abundances, we have obtained the propagation of the uncertainty in all calculated abundances. Furthermore, we also included the line to line abundance scatter as another error source. The total error of the abundances were obtained from the quadratic sum of the previously variables mentioned. In Table 6 are shown these errors for the star IC 4756-38. This star has errors similar to the other stars studied here.

4 SPECTROSCOPIC AGE INDICATORS

It is known from the stellar evolution theory that ISM pollution from low-mass AGB stars increases the abundances of Y and Ba with time (Travaglio et al. 2004; Fishlock et al. 2017). Otherwise, considering that Mg and Al elements are mainly produced by core-collapse SNe, the final stage of high-mass stars ($>8M_{\odot}$), and that the ISM chemical enrichment occurs in short time-scales, it is reasonable to assume that $[Mg/Fe]$ and $[Al/Fe]$ decrease with time (Matteucci et al. 2014). Consequently, we can deduce that younger stars have higher $[Y/Mg]$ and $[Y/Al]$ ratios than older stars.

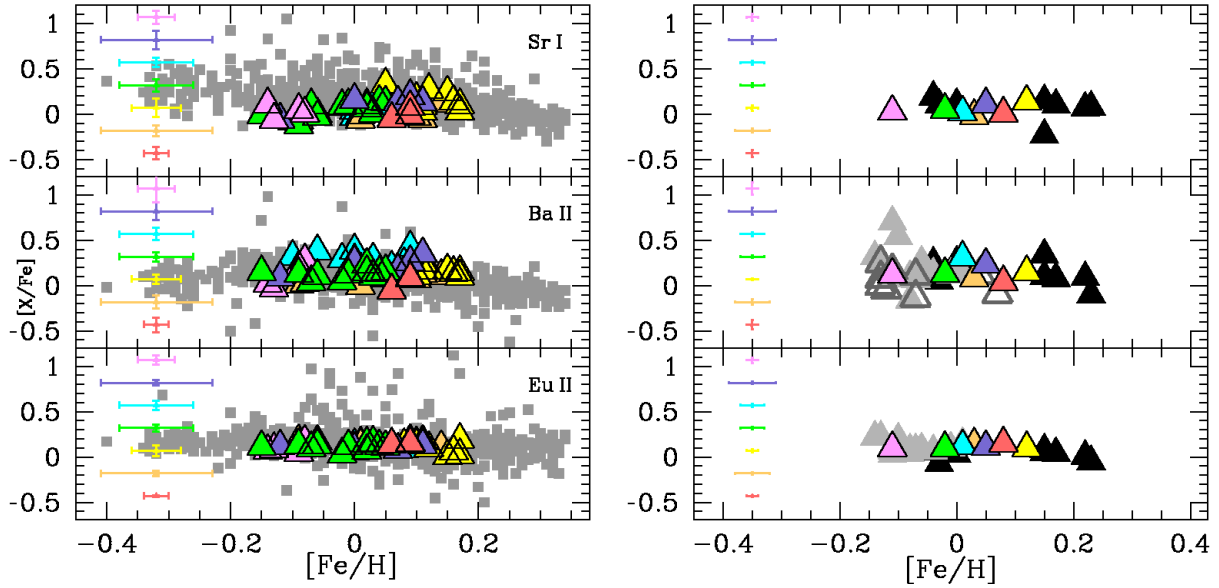


Figure 4. Left: Chemical abundances of Sr, Ba & Eu star by star in IC 4756 (green triangles), IC 4651 (light orange triangles), NGC 5316 (magenta clear triangles), NGC 6633 (blue triangles), NGC 6940 (yellow triangles), NGC 5822 (cyan triangles) and NGC 2682 (light red triangles) compared with field giants of Luck (2015) (gray squares). Error bars represent the standard deviation. Right: comparisons with open cluster samples studied from giant stars: Luck (2015) (black triangles); Reddy et al. (2012, 2013, 2015); Reddy & Lambert (2019) (grey triangles) and Blanco-Cuaresma et al. (2015) (open triangles). Error bars represent the standard deviation of the mean.

This behavior is found when solar twins are analyzed from high-resolution spectroscopy (Nissen 2015; Tucci Maia et al. 2016; Spina et al. 2016, 2018). According to Feltzing et al. (2017), the $[Y/Mg]$ –age relation only works for solar analogue stars because it depends on the $[Fe/H]$. This same behaviour was also reported by Delgado Mena et al. (2019) using FGK field dwarf stars. In fact, they have found that the linear functions to calculate the ages, using spectroscopic clocks, are limited by metallicity. These last results do not match those found by Titarenko et al. (2019) who, considering solar neighbourhood turn-off stars, have concluded that $[Y/Mg]$ negative trend with stellar ages is independent of the metallicity.

Slumstrup et al. (2017) analyzed five stars in the clusters NGC 6811, NGC 6819, M 67, and NGC 188, with $[Fe/H]$ close to the solar metallicity. This paper concluded that the $[Y/Mg]$ clock also works for giant stars in the helium-core-burning phase (i.e., Red Clump stars). More recently, Peña Suárez et al. (2018) analyzed giant stars in the open clusters NGC 2360, NGC 3680, and NGC 5822 (which is in common with the present work). They concluded that $[Y/Mg]$ seems to be promising as age indicator but they also pointed out the necessity to have clusters with a wider age range and more studied stars per cluster.

The first work reporting a non-universality of the spectroscopic clocks was Casali et al. (2020), attributing this fact to differences in Galactocentric distances or star formation histories. However, in their fig. 7, these authors found that the abundances ratios $[Y/Mg]$, $[Y/Al]$, $[Y/Ti]$, $[Y/Ca]$, and $[Y/Si]$, for a sample of 19 open clusters from the Gaia-ESO survey present a high scattering in the age range < 2.0 Gyr. Surprisingly these authors did not examine the possibility that the origin of an apparent non-universality of the spectroscopic clocks could reside on the use of giant stars despite dwarf stars.

4.1 Giants and dwarfs in the local region

Figure 5 shows the relations $[Y/Mg]$, $[Y/Al]$, $[Y/Si]$, $[Y/Ca]$, $[Y/Ti]$ vs. age for the giant and dwarf stars of Luck (2015, 2018), our open clusters and also the clusters analyzed by Luck (2015). Further, we present the result for linear least squares regressions for the field stars. The slope (S) and y-axis intercept (y) parameters, as well as the Pearson correlation coefficients (r), are presented in Table 8. The uncertainties in these parameters, which correspond to 84% confidence intervals, were calculated using the bootstrapping technique. It also allowed us to estimate the p -values under the null hypothesis that the correlation coefficient is null. We performed linear fits using the whole samples of Luck (2015, 2018).

As can be seen from Table 8, for field giants the $[Y/Mg]$, $[Y/Al]$, and $[Y/Si]$ are weakly anti-correlated with age ($r \lesssim -0.30$), besides we can assume that exist a non-null correlation with more than 99% confidence level since the p -value is lower than 0.01. Possibly the correlations were dilute by the scattering that was caused by the uncertainties in abundance ratios and age, but unfortunately Luck (2015) did not provide this information. From the standard deviation of the abundance ratio values for the age range between 1 and 2 Gyr, we estimated that the typical uncertainties range from ~ 0.10 dex ($[Y/Mg]$ and $[Y/Al]$) to ~ 0.10 dex ($[Y/Si]$). Furthermore, assuming the age uncertainties are the standard deviation of the ages that were obtained by Luck (2015) using different stellar evolutionary models, the typical relative age uncertainties would be ~ 40 – 60% . Concerning $[Y/Ca]$ and $[Y/Ti]$, the almost null S and r values, as well as the high p -values, clearly attest that these parameters do not correlate with age.

The situation for the field dwarfs is different, they present a clear anti-correlation between abundance ratios and stellar ages, with $-0.48 \leq r \leq -0.36$ and p -values $\ll 0.01$. This includes $[Y/Ca]$ and $[Y/Ti]$, whose correlation is null for giant stars from Luck (2015). From comparisons with the Pearson coefficients in the

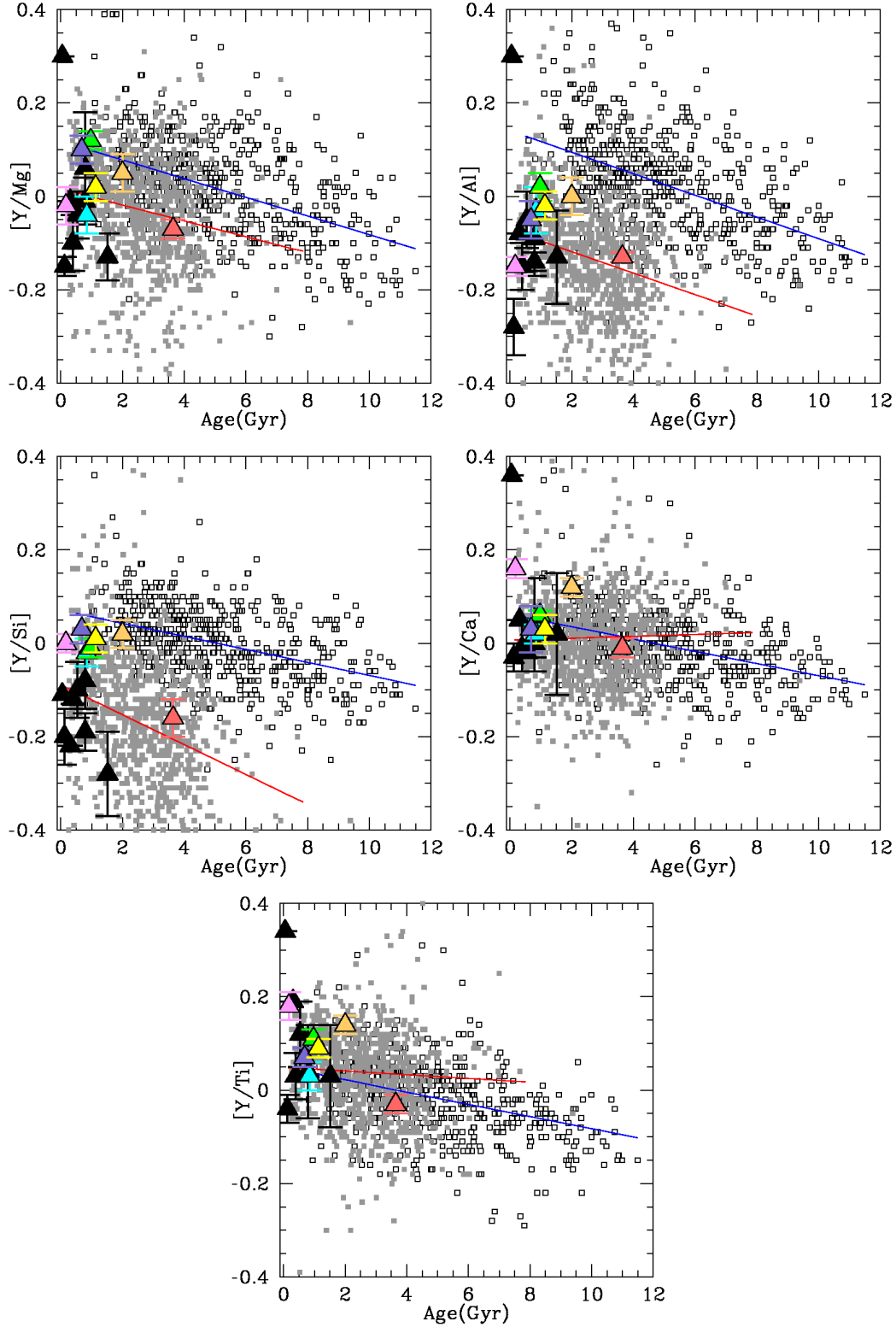


Figure 5. Abundance ratios as function of age for our sample, field giants (grey squares) and open clusters (black triangles) of (Luck 2015) as well as the field dwarfs (open squares) of (Luck 2018). The red and blue lines represent the least squares fitting for the giants and dwarfs respectively. (See Table 8).

dwarf stars of [Casali et al. \(2020\)](#), we could think that the works of [Luck \(2015, 2018\)](#) have no high precision in their abundances and in this form producing the scattering found in the spectroscopic clocks. However, it is necessary consider that the samples of [Luck \(2015, 2018\)](#) were homogeneously studied and therefore their differences in the Pearson coefficients and p -values may be a real fact. In other words, the giant stars could have intrinsically higher scattering than the dwarfs.

4.2 Open cluster giants

Figure 6 shows a comparison between our sample and literature. In the two cases the open clusters are restricted to the local region ($d < 1$ kpc). We have found that our sample falls along a very probable tendency with the ages as it has been previously reported. This fact is specially notable for the clocks $[Y/Mg]$, $[Y/Al]$, $[Y/Si]$ and $[Y/Ti]$ whereas for the ratio $[Y/Ca]$ the slope is less steeper. From our results it also possible to see that our slopes are similar to the obtained slopes for the field stars of [Luck \(2015, 2018\)](#) as it can be observed in Table 8. In spite that we have a small sample, we seen that scatter reported by [Casali et al. \(2020\)](#) and [Casamiquela et al. \(2021\)](#) at the early ages is also present in our clusters.

To verify this early scatter, we have compiled other samples from literature. We found that the works of [Reddy et al. \(2012, 2013, 2015\)](#); [Reddy & Lambert \(2019\)](#) and [Blanco-Cuaresma et al. \(2015\)](#) obtained chemical abundances and ages for several open clusters in homogeneous form. Despite that these authors derived abundances and ages, they did not discuss the spectroscopic clocks. We have used these results and applied the same restriction ($d < 1$ kpc) to these clusters. These derived clocks are directly compared to our results in Figure 6.

From last figure we seen that the scatter seems to exist despite the restriction ($d < 1$ kpc). In these two samples there is also the same problem than in ours, no points between ~ 2.0 Gyr and ~ 4.0 Gyr and also not clusters with ages > 4.0 Gyr. However, the few old clusters are not an exclusive problem of this work, [Casali et al. \(2020\)](#) and [Casamiquela et al. \(2021\)](#) also have few points and it is those older clusters that are defining the anti-correlation with the ages. In our sample we have taken the abundances of NGC 3680 ([Peña Suárez et al. 2018](#)) for calculating the clocks and including them in our sample. This cluster was analyzed using the same line lists and methodology than us and the spectra are also from FEROS. Besides, NGC 3680 has age ~ 2.0 Gyr and distance $\lesssim 1.0$ kpc.

Thus, it is probable that we are observing only a partial behaviour for the open clusters since the field giants shown the existence of clear trends of $[Y/Mg]$, $[Y/Al]$, and $[Y/Si]$ with age. Then the question that arises is whether the scattering found in the giants is due to the method of obtaining abundances and ages which would hamper the tendencies. This last could be discarded because the field dwarfs, investigated with the same methodology, shown a clear trend with less scattering.

4.3 Cluster dwarfs and other samples

The best scenario to study the probable existence of age-abundance relation differences between giants and dwarfs are the open clusters, thus we need to investigate the clusters that were spectroscopically studied from giants and dwarf stars.

On this direction, we have used the table 8 from [Blanco-Cuaresma et al. \(2015\)](#) to derive these relations which shown in Figure 7. we observe that the literature tendencies also seem to exist

in giants and dwarfs but with different slopes. In opposite direction to the field stars, the four chemical clocks in the sample of [Blanco-Cuaresma et al. \(2015\)](#) show that the cluster giant stars have steeper slopes than the dwarfs.

In the specific case of $[Y/Mg]$, our results, [Luck \(2015\)](#), and [Blanco-Cuaresma et al. \(2015\)](#) present similar slopes -0.045 ± 0.023 ; -0.035 ± 0.039 and -0.048 ± 0.012 respectively. Whereas the sample of [Reddy et al. \(2003, 2012, 2013, 2015\)](#); [Reddy & Lambert \(2019\)](#) present a almost flat slope. In the cluster dwarfs, this chemical clock present a flatter slope -0.025 ± 0.009 that is very similar to the field dwarfs.

The case of $[Y/Si]$ is complex, our results and [Blanco-Cuaresma et al. \(2015\)](#) have similar slopes -0.057 ± 0.014 and -0.048 ± 0.018 respectively but the other samples present different behaviours, sample of [Luck \(2015\)](#) has a positive slope 0.015 ± 0.034 whereas Reddy's sample present a flat. The cluster dwarfs present a flatter slope whose agrees with the field dwarfs, ie -0.014 ± 0.009 .

Our $[Y/Ca]$ vs age is flat -0.005 ± 0.019 , similar to the flat of [Reddy et al. \(2003, 2012, 2013, 2015\)](#); [Reddy & Lambert \(2019\)](#) 0.000 ± 0.019 whereas the samples of [Luck \(2015\)](#) and [Blanco-Cuaresma et al. \(2015\)](#) present similar behaviours with slopes -0.030 ± 0.029 and -0.023 ± 0.008 . The cluster dwarfs also present a flat slope in this chemical clock.

Our $[Y/Ti]$ vs age = -0.024 ± 0.019 is similar to the value -0.034 ± 0.007 from the sample of [Blanco-Cuaresma et al. \(2015\)](#) and also similar to -0.043 ± 0.025 from [Luck \(2015\)](#). Whereas Reddy's sample has a flat. This chemical present a flatter slope -0.014 ± 0.009 in the cluster dwarfs.

Only seven open clusters were studied using giants and dwarfs, the number of analyzed stars by cluster is also low. However, [Luck \(2018\)](#) analyzed Melotte 25 using 42 dwarfs and [Blanco-Cuaresma et al. \(2015\)](#) used 28 giants and 14 dwarfs to analyze NGC 2682.

There are some exceptions that are precisely in these two clusters. The chemical clocks $[Y/Si]$ and $[Y/Al]$ in Melotte 25 and $[Y/Si]$ in NGC 2682, these clocks present differences ≥ 0.15 dex between giants and dwarfs. Consequently, to confirm/refuse differences between giants and dwarfs, more open clusters and stars by cluster need to be analyzed.

4.4 Comparisons with literature

We did comparisons between our ratios $[Y/Mg]$, $[Y/Al]$, $[Y/Si]$, $[Y/Ca]$, and $[Y/Ti]$ and other authors that done detailed studies of the same clusters. This means the authors that have the tables, of the analyzed stars, available for star-by-star comparisons. These comparisons are shown in Tables 10, 11 and 12.

Some stars of the clusters IC 4651 and NGC 2682 were also analyzed by [Luck \(2015\)](#), we have done a direct comparison with the six stars in common. As it is shown in Table 11, the differences in relation to our values are very low. This is more evidence when we see the mean of the differences. Those similarities are also observed in Figure 5, which shows that our results fall along the global behaviour of the field giants of [Luck \(2015\)](#).

In Table 10, we see that our results are very similar to the obtained abundances by [Peña Suárez et al. \(2018\)](#) in the cluster NGC 5822, the quantities $\Delta[Y/Mg]$, $\Delta[Y/Al]$, $\Delta[Y/Si]$, $\Delta[Y/Ca]$, and $\Delta[Y/Ti]$ that represent the mean differences of the abundances have values near to zero. Further NGC 5822, these authors also studied NGC 3680 that was added to our results. ([da Silveira et al. 2018](#)) were studied in the same way that in this work, that is to say using the same line lists and FEROS spectra such as in this work.

The case of NGC 6940 is similar to NGC 5822, the mean values

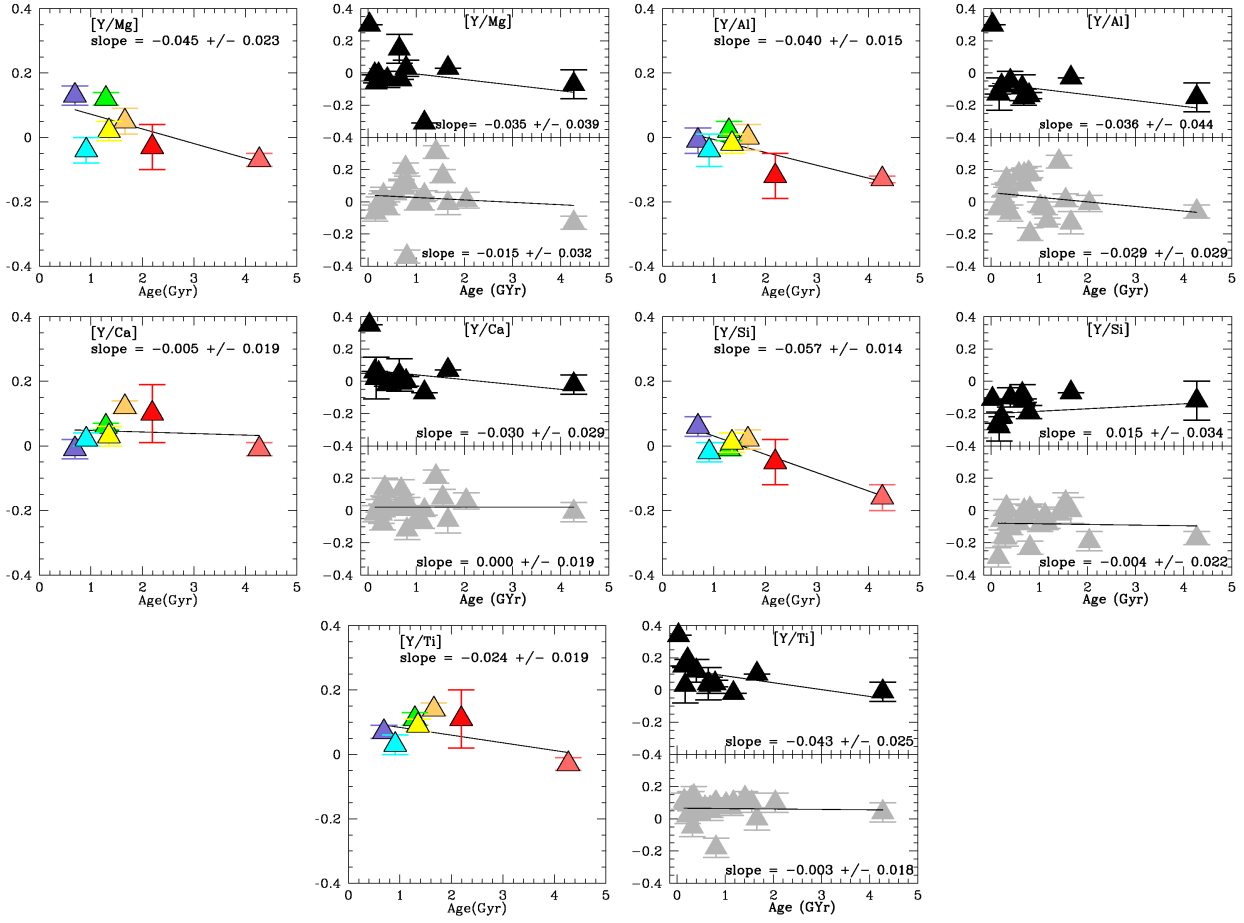


Figure 6. Chemical clocks for our clusters and samples of Luck (2015) and Reddy et al. (2012, 2013, 2015); Reddy & Lambert (2019). All samples have open clusters with $d < 1$ kpc. Grey lines are the least-square fitting for our sample.

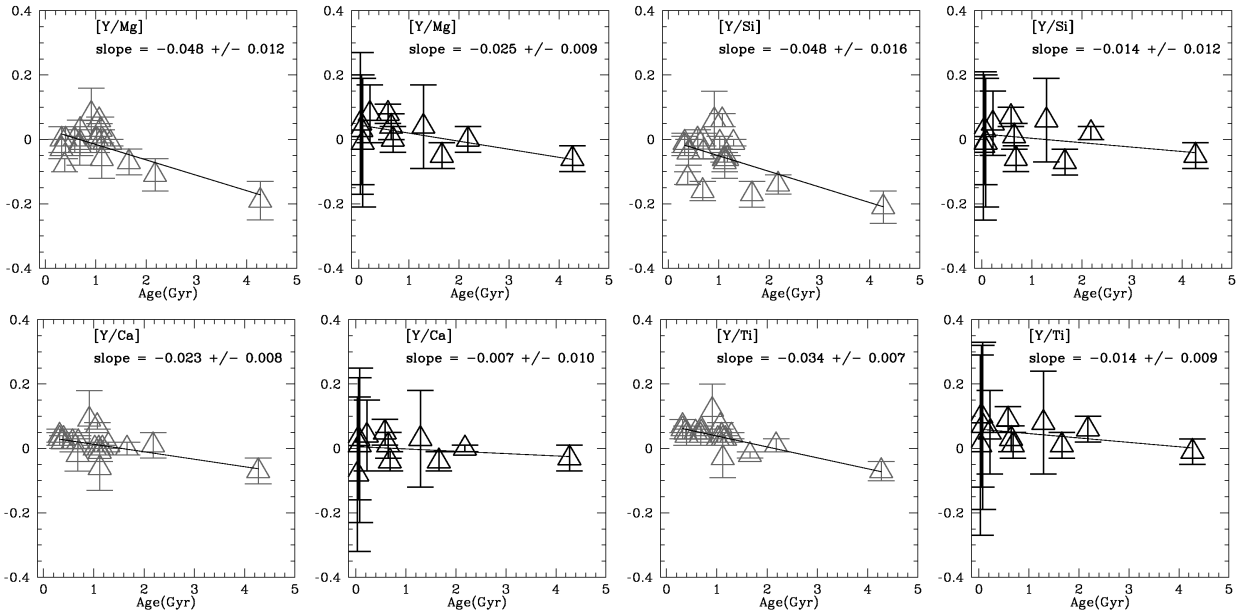


Figure 7. Chemical clocks for giant stars (grey open triangles) and dwarfs (black open triangles) in several open clusters studied by Blanco-Cuadros et al. (2015).

of Bocek Topcu et al. (2016) are similar to the found in this work in spite that they did not use the lbl method nor the line lists used by us. Bocek Topcu et al. (2015) also studied NGC 752 which was normalized to the Juno values.

Also in Table 10 we see that IC 4756 presents notable differences in [Y/Mg] and [Y/Si] obtained by Bagdonas et al. (2018) and this work. These authors reported lower values and they did not apply the lbl method. Their iron line lists are not the same than us, originating discrepancies in the atmospheric parameters that will also produce differences in the abundance determinations. In the specific case of [Y/Mg], these authors only used two absorption lines for obtaining the Mg-abundances in all stars of their sample. In any case, our relations [Y/Mg] & [Y/Al] –age are more near to the literature tendencies than the results of Bagdonas et al. (2018).

Great differences in NGC 5316 appear when our results are compared to Drazdauskas et al. (2016). Our abundance ratios seem to be more congruent in the context of the spectroscopic clocks, the [Y/Mg] and [Y/Si] from these authors are lightly higher to field giants of Luck (2015) such as it is observed in the Figure 5.

Comparisons with Casali et al. (2020) are shown in Table 12, there are non-negligible differences for the clock [Y/Al] in NGC 6633 & NGC 2682 as well as for [Y/Si] in NGC 2682. In the case of NGC 2682, Casali et al. (2020) reported solar values for the chemical clocks whereas our results also shown values near to the solar but excepting the clocks [Y/Al] & [Y/Si] which have presented lower values. A study with more giant stars is necessary to determine if these stars within NGC 2682 also have solar abundance ratios. In literature there are extensive analysis about M67 but in the majority of these works the number of giant stars is low or simply these stars were not included in the analysis. The open cluster M67 was also analyzed by Slumstrup et al. (2017) and Önehag et al. (2014). When comparing with this work and Casali et al. (2020), we can see that our value [Y/Mg] = -0.07 ± 0.02 dex is closer to -0.04 ± 0.05 dex found by Önehag et al. (2014), whereas the results of 0.01 ± 0.03 dex (Slumstrup et al. 2017) and 0.00 ± 0.01 dex (Casali et al. 2020) are very similar. In the case of [Y/Al] in NGC 6633, the interpretation is similar. Our results are within the trend set by the field giants whereas the value reported by Casali et al. (2020) is on the upper limit of the tendency of Luck (2015). Unfortunately, Casali et al. (2020) did not specify the studied giant stars in the two clusters, the identifying of the giants would have facilitated the direct comparison.

5 SUMMARY AND CONCLUSIONS

In this work we have investigated the spectroscopic age indicators [Y/Mg], [Y/Al], [Y/Si], [Y/Ca], and [Y/Ti] in giant stars. For such purpose, we have done a homogeneous spectroscopic analysis of 50 solar-metallicity giant stars of seven open clusters (NGC 5316, NGC 6633, NGC 5822, IC 4756, NGC 6940, IC 4651, and NGC 2682). With the goal to generalize our results, we have compared with other homogeneous samples of literature where giants and dwarfs, in the field and open clusters, were investigated. The main results and conclusions that emerge from this work are:

- From the slopes, correlation coefficients and p -values derived in the field dwarf stars, we confirmed that the aforementioned spectroscopic age indicators work in this type of stars. This fact is in agreement with the reported in literature for dwarf stars in the inner disk.
- For the field giant stars, [Y/Mg]- and [Y/Al]-age relations

present weaker correlations than the ones from dwarf stars, although the slopes are similar. The [Y/Si] vs. age relation shows a correlation coefficient near to the values found in the dwarf stars and a steeper slope. These abundance relations for field giant stars present a remarkable scattering. The ratios [Y/Ca] and [Y/Ti] have flatter slopes and null correlations with age, indicating that they cannot be considered as age indicators for evolved stars of the inner disk.

- Our open clusters and the homogeneous literature samples shown that the scattering reported by Casali et al. (2020) to seem to be real independently of the galactic region ($7 < R_{gc} < 8.5$ kpc and/or $d < 1$ kpc). This behaviour is observed in the results obtained from giant stars as well as from dwarfs.

- Despite that the scattering at the early ages, our open clusters shown that the tendency between abundance ratios and ages very probably exist as it has been reported by other authors. This fact is evident for the spectroscopic clocks [Y/Mg], [Y/Al] and [Y/Si] whose slopes -0.045 ± 0.023 , -0.040 ± 0.015 and -0.057 ± 0.014 , respectively, are close to the literature. Our slope for [Y/Ca] is a flat, it agrees with the field giants and other cluster samples.

- Except for the spectroscopic clock [Y/Ca], our cluster stars present steeper slopes than the field stars. This fact could be due to the high number of field stars studied in Luck (2015, 2018). Our sample is limited, only two open clusters with ages > 2.0 GYrs and none cluster with ages > 4.0 GYr. The clusters NGC 3680 and NGC 2682 are the objects that really are defining the anti-correlation for our spectroscopic clocks. However, this situation is very similar to the found in Casali et al. (2020) and Casamiquela et al. (2021), in these works, two or three clusters are also defining the anti-correlations. These facts reinforce the need to analyze the older open clusters.

- Because of the behaviour found in Melotte 25 and NGC 2682, it is also need to study more giant stars and dwarfs by cluster to confirm/refuse the differences between giants and dwarfs.

- From this work and the literature, we seen that several relations between abundance ratios and ages seem to exist in the Galactic disk when giants and dwarfs are analyzed. This fact point to the probable non-universality of the spectroscopic age indicators.

- The abundance ratios [Sr/Fe], [Ba/Fe], [s/Fe] and [Eu/Fe] derived in our open clusters follow the Galactic disk trend reported in other clusters and field stars of literature.

DATA AVAILABILITY STATEMENT

The authors confirm that the all data supporting the findings of this study are openly available in ESO/archive at <http://archive.eso.org/cms.html> and can be accessed in free way. As well as there are available data within the article and/or its supplementary material.

ACKNOWLEDGEMENTS

The authors would like to acknowledge to CNPq for partial financial support. This study was financed in part by the Coordenação de Aperfeiçoamento de Pessoal de Nível Superior - Brasil (CAPES) - Finance Code 001. Data was obtained from the ESO Science Archive Facility under request numbers 216546 and 230944 and username ojsantrich. This work presents results from the European Space Agency (ESA) space mission *Gaia*. *Gaia* data are being processed by the *Gaia* Data Processing and Analysis

Consortium (DPAC). Funding for the DPAC is provided by national institutions, in particular the institutions participating in the *Gaia* MultiLateral Agreement (MLA). The *Gaia* mission website is <https://www.cosmos.esa.int/gaia>. The *Gaia* archive website is <https://archives.esac.esa.int/gaia>.

REFERENCES

- Barker, Adrian J.; Ogilvie, Gordon I. 2010, MNRAS 404, Issue 4, pp. 1849
- Bagdonas, V.; Drazdauskas, A.; Tautvaišienė, G.; Smiljanic, R. and Chorniy, Y. 2018, A&A 615, 13
- Antipova, L. I., Boyarchuk, A. A., Pakhomov, Yu. V., and Yushkin, M. V. 2005, ARep, 49, 535
- Ansong, J. K.; Sutherland, B. R. 2010, JFM 648, 405
- Asplund, M.; Grevesse, N.; Sauval, A. J.; Scott, P. 2009, ARA&A 47, Issue 1, 481
- Bensby, T.; Feltzing, S.; Lundström, I. and Ilyin, I. 2005, A&A 433, Issue 1, 185
- Bensby, T.; Feltzing, S. and Oey, M. S. 2014, A&A 562, id.A71, 28
- Bertelli Motta, C.; Pasquali, A.; Richer, J.; Michaud, G.; Salaris, M., et al. 2018, MNRAS 478, 425
- Blanco-Cuadras, S.; Soubiran, C.; Heiter, U. et al. 2015, A&A 577, id.A47, 15
- Bossini, D.; Vallenari, A.; Bragaglia, A., et al. 2019, A&A, 623, A108
- Bocek Topcu, G.; Afşar, M. and Sneden, C., 2016, MNRAS 463, 580
- Bocek Topcu, G.; Afşar, M.; Schaeuble, M. and Sneden, C., 2015, MNRAS 446, 3562
- Bonato, C.; Kerber, L. O.; Bica, E.; Santiago, B. X., 2006, A&A 446, 121
- Bobylev, V. V.; Bajkova, A. T. 2021, Astronomy Reports 65, Issue 6, 498
- Busso, M.; Palmerini, S.; Maiorca, E.; Cristallo, S.; Straniero, O.; Abia, C.; Gallino, R.; La Cognata, M. 2010, ApJ 717, Issue 1, L47-L51pp
- Brummell, Nicholas H.; Clune, Thomas L.; Toomre, Juri. 2002, ApJ 570, 825
- Cantat-Gaudin, T.; Jordi, C.; Vallenari, A.; Bragaglia, A.; Balaguer-Núñez, L. et al., 2018, A&A 618, A93
- Cantat-Gaudin T., Anders F., Castro-Ginard A., Jordi C., Romero-Gómez M., Soubiran C., Casamiquela L., et al., 2020, A&A, 640, A1
- Casamiquela, L.; Soubiran, C.; Jofré, P.; Chiappini, C.; Lagarde, N.; Tarricq, Y.; Carrera, R.; Jordi, C.; Balaguer-Núñez, L.; Carbajo-Hijarrubia, J.; Blanco-Cuadras, S. 2021, A&A 652, id.A25, 17 pp
- Casali, G.; Spina, L.; Magrini, L. et al. 2020, accepted in A&A doi:10.1051/0004-6361/202038055
- Charbonnel, C.; Lagarde, N.; Jasiewicz, G.; North, P. L.; Shetrone, M.; Krugler Hollek, J.; Smith, V. V.; Smiljanic, R.; Palacios, A.; Ottoni, G. 2020, A&A 633, id.A34, 15
- Castro, S.; Rich, R. M.; Grenon, M.; Barbuy, B.; McCarthy, J. K. 1997, AJ 114, 376
- Chanamé, Julio; Pinsonneault, Marc; Terndrup, Donald M. 2005, ApJ 631, 540
- Charbonnel, C.; Zahn, J. P. & 476, Issue 3, L29
- Dintrans, Boris; Brandenburg, Axel; Nordlund, Åke; Stein, Robert F. 2003, Ap&SS 284, 237
- da Silva, M. D.; Pereira, C. B.; Drake, N. A. 2018, MNRAS 476, Issue 4, 4907D
- Drazdauskas, Arnas; Tautvaišienė, Gražina; Smiljanic, Rodolfo; Bagdonas, Vilius; Chorniy, Yuriy. 2016, MNRAS 462, 794D
- Denissenkov, Pavel A.; Tout, Christopher A. 2003, MNRAS 340, 722
- Denissenkov, Pavel A.; Pinsonneault, Marc.; MacGregor, Keith B. 2009, ApJ 696, 1823
- Delgado Mena, E.; Moya, A.; Adibekyan, V. et al. 2019, A&A 624, A78
- Dotter, Aaron.; Conroy, Charlie.; Cargile, Phillip.; Asplund, Martin. ApJ 840, Issue 2, id. 99, 9 pp
- Dias, W. S.; Alessi, B. S.; Moitinho, A.; Lépine, J. R. D. 2002, A&A 389, 871
- Edvardsson, B., Andersen, J., Gustafsson, B., et al. 1993, Å, 275, 101
- Feltzing, Sofia; Howes, Louise M.; McMillan, Paul J.; Stenket, Edit., 2017, MNRAS 465, L109
- Fishlock, C. K.; Yong, D.; Karakas, A. I. et al. 2017, MNRAS 466, 4672
- Gaia Collaboration, et al., 2018, A&A 616, A10
- Gaia Collaboration, et al., 2018, A&A 616, A1
- Gaia Collaboration; Magrini, L.; Spina, L.; Randich, S.; Friel, E.; Kor-dopatis, G. et al. 2018, arXiv: 1806.03068
- Gao, Xudong; Lind, Karin; Amarsi, Anish M.; et al. 2018, MNRAS 481, 2666
- Garaud, P.; Kumar, A.; Sridhar, J. 2019, ApJ 879, Issue 1, id. 60, 16pp
- Gossage, S.; Conroy, C.; Dotter, A.; Choi, J.; Rosenfield, P.; Cargile, P.; Dolphin, A., 2018, ApJ 863, 67
- Grevesse, N.; Asplund, M. and Sauval, A. J. 2007, SSRv 130, Issue 1-4, 105
- Gilmore, G.; Randich, S.; Asplund, M.; Binney, J.; Bonifacio, P. et al., 2012, The Messenger, 147, 25
- Holanda, N.; Pereira, C. B.; Drake, N. A. 2019, MNRAS 482, Issue 4, 5275p
- Jacobson, H. R.; Friel, E. D.; Jilková, L.; Magrini, L.; Bragaglia, A. et al., 2016, A&A 591, A37
- Joshi, Y. C.; Dambis, A. K.; Pandey, A. K.; Joshi, S., 2016, A&A 593, A116
- Kaufer, A.; Stahl, O.; Tubbesing, S.; Norregaard, P.; Avila, G.; Francois, P.; Pasquini, L. and Pizzella, A., 1999, The Messenger, 95, 8
- Karakas, A.I.; Lugaro, M. 2016, ApJ 825, 26
- Katime Santrich, Orlando J.; Pereira, C. B.; Drake, N. A., 2013, A&A 554, A2
- Katime Santrich, Orlando J.; Rossi, Silvia., 2017, CaJPH 95, 862
- Kharchenko, N. V.; Piskunov, A. E.; Schilbach, E.; Röser, S.; Scholz, R.-D. 2013, A&A 558, A53
- Korn, A. J.; Grundahl, F.; Richard, O.; Mashonkina, L.; Barklem, P. S.; Collet, R.; Gustafsson, B. and Piskunov, N. 2007, ApJ 671, 402
- Lagarde, N.; Decressin, T.; Charbonnel, C.; Eggenberger, P. Ekström, S.; Palacios, A. 2012, A&A 543, id.A108, 14
- N. Lagarde, N.; Reylé, C.; Robin, A. C.; et al. 2019, A&A 621, A24
- Lambert, D. L.; Heath, J. E.; Lemke, M.; Drake, J. 1996, ApJ 103, 183S
- Luck, R. E., 2015, AJ 150, 88
- Luck, R. E., 2018, AJ 155, 111
- Magrini, L.; Vescovi, D.; Casali, G.; Cristallo, S.; Viscasillas Vázquez, C.; Cescutti, G.; Spina, L.; Van Der Swaelmen, M.; Randich, S. 2021, A&A 646, id.L2, 5
- Maiorca, E.; Randich, S.; Busso, M.; Magrini, L. and Palmerini, S. 2011, ApJ 736, 120
- Masseron, T.; Lagarde, N.; Miglio, A.; Elsworth, Y.; Gilmore, G. 2017, MNRAS 464, 3021
- Matteucci, F.; Romano, D.; Arcones, A.; Korobkin, O.; Rosswog, S. 2014, MNRAS 438, 2177
- McWilliam, Andrew; Lambert, David L. 1988, MNRAS 230, 573
- McWilliam, A., and Rich, M. R. 1994, ApJS, 91, 749
- Mucciarelli, A.; Carretta, E.; Origlia, L. and Ferraro, F. R. 2008, AJ 136, Issue 1, 375
- Nissen, P. E. 2015, A&A 579, 52A
- Nissen, P. E. 2016, A&A 593, A65
- Nollett, K. M.; Busso, M.; Wasserburg, G. J. 2003, ApJ 582, 1036
- Önehag, A.; Gustafsson, B.; Korn, A. 2014, A&A 562, A102, 14pp
- Palacios, A.; Charbonnel, C.; Talon, S.; Siess, L. & 453, 261
- Palmerini, S.; Busso, M.; Maiorca, E.; Guandalini, R.
- Palmerini, S.; La Cognata, M.; Cristallo, S.; Busso, M. 2011, ApJ 729, Issue 1, id. 3, 21pp
- Peña Suárez, V. J.; Sales Silva, J. V.; Katime Santrich, O. J.; Drake, N. A.; Pereira, C. B. 2018, ApJ 854, 184
- Ramírez, I.; Meléndez, J.; Bean, M. et al. 2014, A&A 572, A48
- Ratnasingham, R. P.; Edelman, P. V. F.; Rogers, T. M. 2019, MNRAS 482, Issue 4, p.5500
- Reddy, B. E.; Bakker, E. J., and Hrivnak, B. J. 1999, ApJ 524, 831
- Reddy, B. E., Tomkin, J., Lambert, D. L., and Allende Prieto, C. 2003, MNRAS, 340, 304
- Reddy, A. B. S.; Giridhar, S.; Lambert, D. L. 2012, MNRAS 419, Issue 2, 1350
- Reddy, A. B. S.; Giridhar, S.; Lambert, D. L. 2013, MNRAS 431, Issue 4, 3338

- Reddy, A. B. E.; Giridhar, S.; Lambert, D. L. 2015, MNRAS, 450, Issue 4, 4301
- Reddy, A. B. E. and Lambert, D. L. 2019, MNRAS485, Issue 3, 3623
- Reyniers, M., Van Winckel, H., Gallino, R., and Straniero, O. 2004, A&A, 417, 269
- Rodgers, T. M.; McElwaine, J. N. 2017, ApJ 848, L1, 6pp
- Rogers, T. M.; Lin, D. N. C., McElwaine, J. N. Lau, H. H. B. 2013 ApJ 772, 21
- Skúladóttir, Á.; Hansen, C. J.; Salvadori, S.; Choplin, A. 2019, A&A 631, A171, 13pp
- Slumstrup, D.; Grundahl, F.; Brogaard, K. et al. 2017, A&A 604, L8
- Smith, V. V., Cunha, K., Jorissen, A., and Boffin, H. M. J. 1996, A&A, 315, 179
- Souto, Diogo; Allende Prieto, C.; Cunha, Katia; et al.; 2019, ApJ 874, article id. 97, 28 pp.
- Souto, Diogo; Cunha, Katia; Smith, Verne V. et al.; 2018, ApJ 857, article id. 14, 19pp
- Snedden, C., McWilliam, A., Preston, G. W., et al. 1996, ApJ, 467, 819
- Sweigart, A. V.; Mengel, J. G. 1979, ApJ 229, 624.
- Marigo P., et al., 2017, ApJ, 835, 77
- Randich, S.; Tognelli, E.; Jackson, R.; Jeffries, R. D.; Degl’Innocenti, S., et al. 2018, ApJ, 863, 67
- Spina, Lorenzo; Meléndez, Jorge; Ramírez, Ivan. 2016, A&A 585, 152A
- Spina, Lorenzo; Meléndez, Jorge; Karakas, Amanda I. 2018, MNRAS 474, 2580
- Tautvaišienė, G.; Viscasillas Vázquez, C.; Mikolaitis, Š.; Stonkutė, E.; Minkevičiūtė, R.; Drazdauskas, A.; Bagdonas, V. 2021, A&A 649, id.A126, 20
- Titarenko, A., Recio-Blanco, A., de Laverny, P., Hayden, M.,; Guiglion, G. 2019, A&A 622, A59
- Travaglio, Claudia; Gallino, Roberto; Arnone, Enrico et al. 2004, ApJ 601, 864
- Tucci Maia, M.; Ramírez, I.; Meléndez, J.; Bedell, M.; Bean, J. L.; Asplund, M., 2016, A&A 590, A32
- Van Winckel, H., and Reyniers, M. 2000, A&A, 345, 135
- Wachlin, F. C.; Vauclair, S.; Althaus, L. G. 2014, A&A 570, A58
- Wiese, W. L., Smith, M. W., and Miles, B. M. 1969, NSDRS-NBS, 68

Table 1. Physical parameters of the seven open clusters analyzed in this work. [Fe/H] is the spectroscopic metallicity used for the isochrone fitting in each work, the last column presents the number of giant stars with FEROS spectra.

Cluster	RA (J2000)	Dec (J2000)	Age (Gyr)	[Fe/H]	distance (kpc)	E(B-V)	Reference	N_{spectra}
NGC 2682	132.846	+11.814	$3.64^{+0.02}_{-0.02}$	0.00	0.88	0.04	Bossini et al. (2019)	3
			4.3	0.00*	0.89	0.02	Cantat-Gaudin et al. (2020)	
NGC 5316	208.516	−61.883	$0.153^{+0.002}_{-0.004}$	0.13	1.44	0.25	Bossini et al. (2019)	4
			0.17	0.00*	1.45	0.30	Cantat-Gaudin et al. (2020)	
NGC 5822	226.051	−54.366	$0.891^{+0.000}_{-0.002}$	0.08	0.81	0.11	Bossini et al. (2019)	9
			0.91	0.00*	0.85	0.13	Cantat-Gaudin et al. (2020)	
IC 4651	261.212	−49.917	2.0	0.12	0.95	0.04	Gaia Collaboration, et al. (2018b)	7
			1.7	0.00*	0.98	0.14	Cantat-Gaudin et al. (2020)	
NGC 6633	276.845	+06.615	$0.773^{+0.055}_{-0.011}$	−0.08	0.37	0.15	Bossini et al. (2019)	5
			0.69	0.00*	0.42	0.10	Cantat-Gaudin et al. (2020)	
IC 4756	279.649	+05.435	$0.971^{+0.031}_{-0.011}$	0.00	0.48	0.13	Bossini et al. (2019)	11
			1.3	0.00*	0.51	0.09	Cantat-Gaudin et al. (2020)	
NGC 6940	308.626	+28.278	$1.02^{+0.07}_{-0.07}$	0.15	1.03	0.15	Bossini et al. (2019)	11
			1.3	0.00*	1.10	0.13	Cantat-Gaudin et al. (2020)	

Table 2. Juno abundances compared with Gaia-ESO Sun iDR5, G 2007([Grevesse et al. 2007](#)), A 2009([Asplund et al. 2009](#)) and giants M67 iDR5.

Spec	Juno	Sun iDR5	G 2007	A 2009	M67 iDR5
FeI	7.48±0.06	7.49±0.03	7.50±0.05	7.50±0.04	7.45±0.01
MgI	7.55±0.07	7.51±0.07	7.53±0.09	7.60±0.04	7.51±0.05
AlI	6.33±0.03	6.34±0.04	6.37±0.06	6.45±0.03	6.41±0.04
SiI	7.43±0.07	7.48±0.06	7.51±0.04	7.51±0.03	7.55±0.06
CaI	6.27±0.06	6.31±0.12	6.31±0.04	6.34±0.04	6.44±0.10
TiI	4.92±0.07	4.90±0.08	4.90±0.06	4.95±0.05	4.90±0.09
SrI	2.85	—	2.97±0.07	2.87±0.07	—
YII	2.23±0.05	2.19±0.12	2.21±0.02	2.21±0.05	2.14±0.09
BaII	2.20±0.07	2.17±0.06	2.13±0.05	2.18±0.09	2.07±0.07
ZrI	2.65±0.09	2.53±0.13	2.60±0.02	2.58±0.04	2.54±0.05
LaII	1.17±0.02	—	1.17±0.07	1.10±0.04	1.00±0.12
CeII	1.60±0.06	1.70±0.11	1.58±0.07	1.58±0.04	1.71±0.01
NdII	1.51±0.08	—	1.50±0.06	1.42±0.04	—
EuII	0.59	0.52±0.06	0.51±0.08	0.52±0.04	0.42±0.04

Table 3. Stellar atmospheric parameters calculated in this work. The line numbers of Fe I and Fe II are represented by #1 and #2. Whereas σ and σ_n represent the standard deviation and standard error of the mean, respectively.

Star	$T_{eff} \pm \sigma$ K	$\log g \pm \sigma$ dex	$\xi \pm \sigma$ km s ⁻¹	[Fe/H] $\pm \sigma$ (#1, #2) dex
IC 4756–12	5124±21	2.96±0.09	1.61±0.06	-0.02±0.08 (76, 14)
IC 4756–14	4765±52	2.56±0.12	1.74±0.08	-0.06±0.11 (76, 14)
IC 4756–28	4689±34	2.34±0.15	1.76±0.07	-0.15±0.11 (75, 14)
IC 4756–38	5224±27	3.20±0.08	1.66±0.06	0.02±0.07 (76, 14)
IC 4756–42	5228±29	3.16±0.08	1.61±0.06	0.03±0.08 (76, 14)
IC 4756–44	5177±28	3.17±0.08	1.58±0.07	0.02±0.08 (77, 13)
IC 4756–52	4503±47	2.08±0.11	1.91±0.07	-0.09±0.10 (68, 12)
IC 4756–101	5241±29	3.17±0.08	1.62±0.06	0.05±0.07 (74, 14)
IC 4756–109	5070±29	2.85±0.10	1.75±0.07	-0.01±0.08 (77, 14)
IC 4756–125	5172±20	2.94±0.09	1.80±0.06	-0.07±0.06 (69, 14)
IC 4756–164	5176±39	3.09±0.09	1.74±0.07	0.04±0.09 (77, 14)
Mean $\pm \sigma_n$	5060±67	2.89±0.10	1.68±0.03	-0.01±0.02
NGC 5822–6	5195±27	3.07±0.06	1.55±0.06	0.01±0.06 (64, 13)
NGC 5822–8	5069±18	2.83±0.07	1.60±0.05	-0.02±0.05 (62, 12)
NGC 5822–102	5183±39	3.05±0.09	1.65±0.06	-0.06±0.08 (67, 12)
NGC 5822–224	5202±33	3.07±0.08	1.45±0.07	0.09±0.08 (70, 10)
NGC 5822–240	4605±37	2.18±0.11	1.87±0.06	-0.10±0.08 (57, 11)
NGC 5822–316	5183±25	3.03±0.05	1.67±0.05	0.08±0.06 (75, 11)
NGC 5822–348	5202±23	3.18±0.07	1.57±0.05	0.06±0.06 (74, 13)
NGC 5822–375	4802±41	2.52±0.09	1.79±0.06	0.00±0.08 (70, 13)
NGC 5822–443	4817±50	2.62±0.13	1.82±0.07	0.03±0.09 (68, 9)
Mean $\pm \sigma_n$	4980±84	2.75±0.13	1.66±0.04	0.00±0.02
NGC 6940–28	5156±31	3.09±0.07	1.53±0.06	0.12±0.07 (69, 14)
NGC 6940–30	5034±33	2.85±0.12	1.69±0.08	0.11±0.11 (73, 12)
NGC 6940–67	5118±40	3.05±0.09	1.59±0.07	0.16±0.09 (72, 12)
NGC 6940–87	5091±36	3.04±0.08	1.45±0.06	0.17±0.08 (70, 11)
NGC 6940–101	5137±31	3.24±0.09	1.59±0.07	0.15±0.09 (68, 12)
NGC 6940–105	4874±43	2.66±0.12	1.67±0.07	0.08±0.11 (70, 11)
NGC 6940–108	5335±38	3.38±0.13	1.99±0.10	0.05±0.10 (66, 8)
NGC 6940–132	5070±32	2.99±0.10	1.59±0.07	0.17±0.09 (74, 11)
NGC 6940–138	5086±18	2.95±0.08	1.54±0.05	0.05±0.07 (72, 13)
NGC 6940–139	5136±34	3.04±0.07	1.62±0.06	0.10±0.08 (71, 10)
NGC 6940–152	5049±42	3.02±0.08	1.72±0.06	0.11±0.08 (71, 12)
Mean $\pm \sigma_n$	5099±33	3.03±0.06	1.63±0.04	0.12±0.01
NGC 6633–78	4420±22	1.78±0.09	2.01±0.05	-0.12±0.05 (44, 10)
NGC 6633–100	5080±20	2.75±0.07	1.62±0.04	0.07±0.05 (60, 13)
NGC 6633–106	5172±20	2.96±0.09	1.52±0.07	0.11±0.08 (63, 12)
NGC 6633–119	5241±31	3.14±0.08	1.63±0.07	0.00±0.07 (64, 14)
NGC 6633–126	5232±34	3.11±0.08	1.56±0.07	0.09±0.08 (64, 13)
Mean $\pm \sigma_n$	5029±155	2.75±0.25	1.67±0.09	0.03±0.04
NGC 5316–31	4825±58	1.65±0.17	2.82±0.19	-0.09±0.09 (41, 8)
NGC 5316–35	4716±49	2.17±0.16	2.31±0.10	0.01±0.09 (50, 13)
NGC 5316–45	4347±20	1.36±0.11	2.16±0.06	-0.13±0.06 (44, 11)
NGC 5316–72	4388±16	1.45±0.15	2.28±0.08	-0.15±0.06 (41, 9)
Mean $\pm \sigma_n$	4569±119	1.66±0.18	2.39±0.15	-0.09±0.04
NGC 2682–141	4854±34	2.73±0.10	1.80±0.07	0.06±0.07 (53, 11)
NGC 2682–151	4871±34	2.79±0.12	1.67±0.07	0.09±0.08 (55, 11)
NGC 2682–244	5175±30	3.18±0.09	1.62±0.06	0.09±0.07 (61, 13)
Mean $\pm \sigma_n$	4967±104	2.90±0.14	1.70±0.05	0.08±0.01

Table 4. Abundance ratios $[x/Fe]$ for the elements calculated in this work. These ratios were calculate from $[X/Fe] = [X/H] - [Fe/H]$ where $[X/H]$ is obtained from $[X/H] = \log(N_X/N_H)_\star - \log(N_X/N_H)_\odot$.

star	[Mg/Fe]	[Al/Fe]	[Si/Fe]	[Ca/Fe]	[Ti/Fe]	[Sr/Fe]	[Y/Fe]	[Zr/Fe]	[Ba/Fe]	[La/Fe]	[Ce/Fe]	[Nd/Fe]	[Eu/Fe]
IC 4756-12	0.04	0.07	0.11	0.13	0.07	0.09	0.15	-0.09	0.05	0.21	0.18	0.20	0.03
IC 4756-14	0.04	0.11	0.18	0.09	-0.03	-0.03	0.16	-0.11	0.11	0.38	0.24	0.25	0.13
IC 4756-28	0.08	0.28	0.20	0.10	0.00	-0.01	0.09	-0.13	0.15	0.33	0.14	0.01	0.11
IC 4756-38	-0.04	0.04	0.07	0.06	0.00	0.07	0.14	0.01	0.15	0.29	0.15	0.16	0.15
IC 4756-42	-0.07	0.02	0.09	0.06	-0.02	0.01	0.08	-0.02	0.10	0.18	0.11	0.03	0.16
IC 4756-44	-0.07	0.05	0.06	0.08	-0.01	0.10	0.16	-0.07	0.23	0.63	0.20	0.14	0.07
IC 4756-52	0.02	0.16	0.22	0.04	-0.08	-0.12	0.09	-0.26	0.13	0.33	0.09	0.18	0.13
IC 4756-101	-0.06	0.01	0.05	0.05	0.01	0.13	0.11	-0.04	0.16	0.27	0.04	0.29	0.11
IC 4756-109	0.00	0.12	0.12	0.12	0.04	0.10	0.13	-0.01	0.12	0.33	0.16	0.19	0.12
IC 4756-125	0.03	0.13	0.13	0.07	0.03	0.10	0.07	-0.02	0.04	0.23	0.13	0.19	0.10
IC 4756-164	-0.06	0.07	0.05	0.07	0.03	0.14	0.09	0.05	0.14	0.40	0.27	0.27	0.12
Mean $\pm\sigma_n$	-0.01 \pm 0.02	0.10 \pm 0.02	0.12 \pm 0.02	0.08 \pm 0.01	0.01 \pm 0.01	0.05 \pm 0.02	0.12 \pm 0.01	-0.06 \pm 0.03	0.13 \pm 0.02	0.33 \pm 0.04	0.16 \pm 0.02	0.17 \pm 0.03	0.11 \pm 0.01
NGC 5822-6	0.05	0.13	0.07	0.06	0.04	-0.03	0.02	0.12	0.38	0.23	0.19	0.23	0.06
NGC 5822-8	0.09	0.08	0.16	0.09	-0.02	0.08	0.13	-0.09	0.29	0.20	0.22	0.24	0.03
NGC 5822-102	0.12	0.10	0.03	0.08	0.05	0.00	0.08	0.17	0.38	0.36	0.17	0.09	0.17
NGC 5822-224	0.03	0.10	0.03	0.07	0.05	0.02	0.20	0.01	0.42	0.40	0.25	0.35	0.18
NGC 5822-240	0.20	0.31	0.10	0.03	0.07	-0.08	-0.06	0.00	0.32	0.41	0.25	0.28	—
NGC 5822-316	0.12	0.01	0.04	0.04	0.03	-0.01	0.03	-0.06	0.24	0.31	0.27	0.12	0.09
NGC 5822-348	0.07	0.01	0.12	0.12	0.15	0.05	0.10	-0.01	0.20	0.34	0.31	0.22	0.14
NGC 5822-375	0.25	0.13	0.09	0.05	0.02	0.05	0.08	-0.02	0.29	0.39	0.24	0.23	0.13
NGC 5822-443	0.17	0.11	0.12	0.04	0.05	0.09	0.15	0.00	0.29	0.40	0.26	0.19	0.15
Mean $\pm\sigma_n$	0.12 \pm 0.02	0.11 \pm 0.03	0.08 \pm 0.01	0.06 \pm 0.01	0.05 \pm 0.01	0.02 \pm 0.02	0.08 \pm 0.03	0.01 \pm 0.03	0.31 \pm 0.02	0.34 \pm 0.02	0.24 \pm 0.01	0.22 \pm 0.03	0.12 \pm 0.02
NGC 6940-28	0.06	0.05	0.05	0.04	-0.02	0.27	0.00	0.09	0.17	0.18	0.09	0.04	0.10
NGC 6940-30	0.11	0.11	0.08	0.08	0.01	0.03	0.04	0.03	0.25	0.25	0.10	0.30	0.13
NGC 6940-67	0.06	0.10	0.08	0.06	0.04	0.14	0.00	0.06	0.14	0.20	0.21	0.21	0.06
NGC 6940-87	0.04	-0.01	0.06	0.04	0.00	0.03	0.05	-0.15	0.10	0.09	0.14	0.22	0.02
NGC 6940-101	0.10	0.19	0.17	0.14	0.04	0.24	0.25	-0.01	0.17	0.33	0.24	0.18	0.01
NGC 6940-105	0.12	0.22	0.18	0.08	0.03	0.02	0.09	-0.02	0.15	0.26	0.18	0.26	0.13
NGC 6940-108	0.02	0.07	0.00	-0.05	0.03	0.33	0.26	0.24	0.14	0.34	0.25	0.22	—
NGC 6940-132	0.09	0.14	0.17	0.15	0.00	0.10	0.13	0.02	0.15	0.27	0.20	0.25	0.19
NGC 6940-138	0.10	0.12	0.09	0.06	0.04	0.13	0.10	0.03	0.08	0.32	0.07	0.18	—
NGC 6940-139	0.12	0.14	0.12	0.12	0.03	0.17	0.10	0.05	0.11	0.27	0.19	0.18	0.13
NGC 6940-152	0.11	0.16	0.15	0.10	0.04	0.09	0.08	0.01	0.17	0.35	0.20	0.15	0.17
Mean $\pm\sigma_n$	0.08 \pm 0.01	0.12 \pm 0.02	0.11 \pm 0.02	0.08 \pm 0.02	0.02 \pm 0.01	0.14 \pm 0.03	0.10 \pm 0.03	0.03 \pm 0.03	0.15 \pm 0.01	0.26 \pm 0.02	0.17 \pm 0.02	0.20 \pm 0.02	0.10 \pm 0.02
NGC 6633-78	0.06	0.20	0.09	-0.05	-0.10	-0.06	0.04	-0.14	0.09	0.27	0.10	0.08	0.12
NGC 6633-100	-0.03	0.10	-0.03	0.11	-0.05	0.12	0.04	-0.14	0.17	0.20	0.04	0.20	0.08
NGC 6633-106	-0.14	0.05	-0.03	0.02	-0.02	0.13	0.00	-0.24	0.35	0.18	0.02	0.06	0.13
NGC 6633-119	-0.05	0.03	-0.01	0.05	-0.01	0.16	0.09	-0.10	0.26	0.16	-0.03	-0.06	0.09
NGC 6633-126	-0.12	0.03	0.01	0.06	-0.01	0.20	0.05	-0.12	0.26	0.20	-0.01	0.03	0.15
Mean $\pm\sigma_n$	-0.06 \pm 0.04	0.08 \pm 0.03	0.01 \pm 0.02	0.04 \pm 0.03	-0.04 \pm 0.02	0.11 \pm 0.04	0.04 \pm 0.01	-0.15 \pm 0.02	0.23 \pm 0.04	0.20 \pm 0.02	0.02 \pm 0.02	0.06 \pm 0.04	0.11 \pm 0.01
NGC 5316-31	-0.03	0.20	0.04	-0.08	-0.14	0.06	0.04	0.02	0.20	0.00	-0.01	-0.12	0.05
NGC 5316-35	0.15	0.23	-0.01	-0.11	-0.07	0.01	0.02	-0.11	0.28	0.28	-0.07	0.30	0.17
NGC 5316-45	0.07	0.15	0.08	-0.14	-0.18	-0.06	0.03	-0.19	-0.03	0.11	0.09	0.11	0.09
NGC 5316-72	0.11	0.24	0.13	-0.09	-0.13	-0.11	0.12	-0.18	0.02	0.08	-0.10	-0.04	0.07
Mean $\pm\sigma_n$	0.07 \pm 0.04	0.21 \pm 0.02	0.06 \pm 0.03	-0.11 \pm 0.01	-0.13 \pm 0.02	-0.02 \pm 0.04	0.05 \pm 0.02	-0.11 \pm 0.05	0.12 \pm 0.07	0.12 \pm 0.06	-0.02 \pm 0.04	0.07 \pm 0.09	0.10 \pm 0.03
NGC 2682-141	0.13	0.18	0.21	0.05	0.03	-0.06	0.04	-0.04	-0.05	0.23	0.07	0.13	0.14
NGC 2682-151	0.11	0.14	0.23	0.02	0.08	0.08	0.03	-0.09	0.10	0.16	0.06	0.15	0.16
NGC 2682-244	0.07	0.17	0.11	0.04	0.08	-0.01	0.03	0.03	0.09	0.20	0.02	0.05	0.15
Mean $\pm\sigma_n$	0.10 \pm 0.02	0.16 \pm 0.01	0.18 \pm 0.04	0.04 \pm 0.01	0.06 \pm 0.02	0.01 \pm 0.04	0.03 \pm 0.00	-0.03 \pm 0.03	0.05 \pm 0.05	0.19 \pm 0.02	0.05 \pm 0.01	0.11 \pm 0.03	0.15 \pm 0.01

Table 5. Abundance ratios for Mg, Al, Si, Ca, Ti, Sr, Ba, and Eu in the cluster IC 4651.

Star	[Mg/Fe]	[Al/Fe]	[Si/Fe]	[Ca/Fe]	[Ti/Fe]	[Sr/Fe]	[Ba/Fe]	[Eu/Fe]
IC 4651-6333	0.07	0.18	0.08	0.06	0.03	-0.06	0.00	0.15
IC 4651-7646	0.05	0.18	0.07	-0.05	-0.07	-0.03	0.07	0.15
IC 4651-8540	0.00	0.13	-0.01	-0.17	-0.17	-0.07	0.01	0.18
IC 4651-9025	0.05	0.22	0.00	-0.10	-0.11	-0.05	0.13	0.17
IC 4651-9122	0.04	0.19	0.25	0.11	0.12	-0.01	0.18	0.13
IC 4651-9791	0.11	0.24	0.26	0.10	0.08	-0.03	0.03	0.10
IC 4651-14527	0.09	0.13	0.17	0.10	0.09	0.12	0.11	0.11
Mean $\pm\sigma_n$	0.06 \pm 0.01	0.18 \pm 0.02	0.12 \pm 0.04	0.01 \pm 0.04	0.00 \pm 0.04	-0.02 \pm 0.02	0.08 \pm 0.03	0.14 \pm 0.01

Table 6. Error propagation in the abundances for IC 4756–38. Second to sixth column gives the error from T_{eff} , $\log g$, $[\text{Fe}/\text{H}]$ and line to line scatter respectively. Last column represents the total abundance error.

Species	ΔT_{eff}	$\Delta \log g$	$\Delta \xi$	$\Delta [\text{Fe}/\text{H}]$	ΔAb	$\left(\sum \sigma^2\right)^{1/2}$
Fe I	0.02	0.00	0.02	0.01	0.01	0.03
Fe II	0.02	0.04	0.02	0.01	0.02	0.06
Mg I	0.01	0.01	0.01	0.00	0.03	0.03
Al I	0.01	0.01	0.01	0.00	0.02	0.02
Sr I	0.03	0.01	0.04	0.00	—	0.05
Y II	0.00	0.04	0.03	0.01	0.02	0.05
Zr I	0.04	0.01	0.00	0.01	0.06	0.07
La II	0.00	0.04	0.01	0.01	0.03	0.05
Ce II	0.01	0.04	0.01	0.01	0.01	0.04
Nd II	0.00	0.04	0.02	0.01	0.05	0.06

Table 7. Chemical clocks and abundance ratios in the clusters IC 4756, NGC 6940, NGC 5822, NGC 6633, NGC 5316 and NGC 2682. The ratios were obtained from the definition $[a/b] = \log (N_a/N_b)_\star - \log (N_a/N_b)_\odot$.

star	[Y/Mg]	[Y/Al]	[Y/Si]	[Y/Ca]	[Y/Ti]
IC 4756-12	0.11	0.08	0.03	0.01	0.07
IC 4756-14	0.12	0.05	-0.01	0.08	0.20
IC 4756-28	0.01	-0.20	-0.11	-0.02	0.08
IC 4756-38	0.18	0.10	0.07	0.08	0.12
IC 4756-42	0.15	0.06	0.00	0.03	0.10
IC 4756-44	0.23	0.10	0.03	0.01	0.09
IC 4756-52	0.07	-0.07	-0.12	0.06	0.18
IC 4756-101	0.17	0.10	0.06	0.05	0.09
IC 4756-109	0.13	0.01	0.01	0.01	0.09
IC 4756-125	0.04	-0.06	-0.05	0.00	0.05
IC 4756-164	0.15	0.02	0.04	0.03	0.06
Mean $\pm\sigma_n$	0.12 \pm 0.02	0.02 \pm 0.03	-0.01 \pm 0.02	0.03 \pm 0.01	0.10 \pm 0.01
IC 4651-6333	0.13	0.00	0.09	0.23	0.15
IC 4651-7646	0.03	-0.10	0.01	0.13	0.23
IC 4651-8540	-0.06	-0.01	0.01	0.16	0.21
IC 4651-9025	-0.02	0.03	0.03	0.13	0.14
IC 4651-9122	-0.04	-0.10	-0.09	-0.01	0.06
IC 4651-9791	0.11	-0.01	0.04	0.20	0.20
IC 4651-14527	0.22	0.18	0.15	0.23	0.23
Mean $\pm\sigma_n$	0.05 \pm 0.04	0.00 \pm 0.04	0.03 \pm 0.03	0.15 \pm 0.03	0.17 \pm 0.02
NGC 6940-28	-0.06	-0.05	-0.05	-0.04	0.02
NGC 6940-30	-0.07	-0.07	-0.04	-0.04	0.03
NGC 6940-67	-0.06	-0.10	-0.08	-0.07	-0.04
NGC 6940-87	0.01	0.06	-0.01	0.00	0.05
NGC 6940-101	0.15	0.06	0.09	0.12	0.22
NGC 6940-105	-0.03	-0.13	-0.09	0.01	0.06
NGC 6940-108	0.24	0.19	0.26	0.31	0.23
NGC 6940-132	0.04	-0.01	-0.04	-0.02	0.13
NGC 6940-138	0.00	-0.02	0.01	0.05	0.06
NGC 6940-139	-0.02	-0.04	-0.02	-0.03	0.07
NGC 6940-152	-0.03	-0.08	-0.07	-0.03	0.04
Mean $\pm\sigma_n$	0.02 \pm 0.03	-0.02 \pm 0.03	0.00 \pm 0.03	0.03 \pm 0.03	0.09 \pm 0.02
NGC 5822-6	-0.03	-0.03	-0.04	-0.03	-0.02
NGC 5822-8	0.05	0.05	-0.02	0.04	0.15
NGC 5822-102	-0.04	-0.04	0.05	0.00	0.02
NGC 5822-224	0.17	0.17	0.17	0.13	0.15
NGC 5822-240	-0.26	-0.26	-0.16	-0.09	-0.13
NGC 5822-316	-0.09	-0.09	-0.03	-0.03	-0.02
NGC 5822-348	0.03	0.03	-0.02	-0.02	-0.04
NGC 5822-375	-0.17	-0.17	-0.02	0.03	0.05
NGC 5822-443	-0.02	-0.02	0.03	0.11	0.10
Mean $\pm\sigma_n$	-0.04 \pm 0.04	-0.04 \pm 0.04	0.00 \pm 0.03	0.02 \pm 0.02	0.03 \pm 0.03
NGC 6633-78	-0.02	-0.16	-0.05	0.10	0.14
NGC 6633-100	0.07	-0.06	0.08	-0.06	0.10
NGC 6633-106	0.14	-0.05	0.03	-0.02	0.02
NGC 6633-119	0.14	0.06	0.10	0.04	0.10
NGC 6633-126	0.16	0.02	0.04	-0.02	0.06
Mean $\pm\sigma_n$	0.10 \pm 0.03	-0.04 \pm 0.04	0.04 \pm 0.03	0.01 \pm 0.03	0.08 \pm 0.02
NGC 5316-31	0.07	-0.16	0.00	0.12	0.18
NGC 5316-35	-0.13	-0.22	0.02	0.11	0.08
NGC 5316-45	-0.03	-0.12	-0.05	0.17	0.22
NGC 5316-72	0.01	-0.12	-0.01	0.22	0.25
Mean $\pm\sigma_n$	-0.02 \pm 0.04	-0.15 \pm 0.02	-0.01 \pm 0.01	0.16 \pm 0.02	0.18 \pm 0.04
NGC 2682-141	-0.10	-0.14	-0.16	-0.02	0.01
NGC 2682-151	-0.08	-0.12	-0.21	0.01	-0.06
NGC 2682-244	-0.05	-0.14	-0.08	-0.01	-0.05
Mean $\pm\sigma_n$	-0.07 \pm 0.01	-0.13 \pm 0.01	-0.15 \pm 0.03	-0.01 \pm 0.04	-0.03 \pm 0.03

Table 8. Results from the linear least square regression for the abundance ratios vs. age relations for the giant and dwarf stars presented in Luck (2015, 2018). The slopes (S) and y-axis intercept (y) parameters are presented, as well as the Pearson correlation coefficients (r) and p -values. The index g and d correspond to giants and dwarfs respectively.

Ratio	S_g	y_g	r_g	p_g	S_d	y_d	r_d	p_d
[Y/Mg]	-0.017±0.003	0.016±0.010	-0.17±0.04	1.0×10^{-7}	-0.020±0.002	0.118±0.009	-0.48±0.03	6.3×10^{-34}
[Y/Al]	-0.023±0.003	-0.072±0.010	-0.22±0.04	1.2×10^{-10}	-0.023±0.002	0.140±0.010	-0.49±0.03	1.2×10^{-35}
[Y/Si]	-0.032±0.004	-0.089±0.011	-0.28±0.03	8.4×10^{-17}	-0.014±0.001	0.071±0.008	-0.38±0.03	3.3×10^{-21}
[Y/Ca]	0.002±0.003	0.007±0.009	+0.02±0.03	0.572	-0.013±0.001	0.061±0.008	-0.37±0.03	3.1×10^{-20}
[Y/Ti]	-0.004±0.003	0.049±0.009	-0.05±0.04	0.139	-0.013±0.001	0.048±0.008	-0.36±0.04	3.0×10^{-19}

Table 9. Chemical clocks differences between giants and dwarfs stars within the same open clusters. Melotte 25 was studied by Luck (2015, 2018) whereas the others were studied by Blanco-Cuadros et al. (2015). The N_s corresponds to the number of giants and dwarfs studied in each cluster.

Cluster	[Y/Mg] _{gd}	[Y/Al] _{gd}	[Y/Si] _{gd}	[Y/Ca] _{gd}	[Y/Ti] _{gd}	$N_s (g, d)$
Melotte 25	0.05	0.15	0.23	—	0.07	(5, 42)
IC 4651	0.02	—	0.10	0.04	0.03	(6, 2)
IC 4756	0.05	—	0.07	0.02	0.04	(1, 3)
M 67	0.13	—	0.16	0.04	0.06	(28, 14)
NGC 2447	0.14	—	0.13	0.11	0.12	(3, 3)
NGC 2632	0.00	—	0.05	0.04	0.02	(11, 2)
NGC 3680	0.03	—	0.08	0.00	0.02	(2, 3)

Table 10. Comparisons star by star $\Delta[a/b]=[a/b]_{Li}-[a/b]_{tw}$, which is the literature value – this work. IC 4756 compared with Bagdonas et al. (2018), NGC 6940 with Bock Topcu et al. (2016), NGC 5822 with Peña Suárez et al. (2018) and NGC 5316 with Drazdauskas et al. (2016).

Star	$\Delta[Y/Mg]$	$\Delta[Y/Al]$	$\Delta[Y/Si]$	$\Delta[Y/Ca]$	$\Delta[Y/Ti]$
IC 4756-12	-0.23	-0.22	-0.18	-0.11	-0.03
IC 4756-14	-0.24	-0.13	-0.21	-0.13	-0.01
IC 4756-28	-0.10	0.11	-0.21	-0.03	0.03
IC 4756-38	-0.21	-0.02	-0.09	-0.03	0.08
IC 4756-42	-0.28	-0.05	-0.19	-0.09	0.01
IC 4756-44	-0.25	-0.15	-0.10	-0.11	0.00
IC 4756-52	-0.14	-0.07	-0.17	-0.12	0.01
IC 4756-101	-0.14	-0.05	-0.05	-0.03	0.10
IC 4756-109	-0.14	-0.03	-0.17	-0.13	0.02
IC 4756-125	-0.06	0.08	-0.04	-0.03	0.07
IC 4756-164	-0.27	-0.06	-0.12	-0.10	0.01
Mean± σ	-0.19±0.02	-0.05±0.03	-0.14±0.02	-0.08±0.01	0.03±0.01
NGC 6940-28	0.11	0.07	-0.05	-0.05	0.02
NGC 6940-30	0.17	0.13	-0.06	0.03	0.01
NGC 6940-87	0.01	-0.10	-0.09	-0.11	-0.01
NGC 6940-101	-0.11	-0.01	-0.19	-0.14	-0.18
NGC 6940-105	-0.03	0.04	-0.01	-0.17	-0.02
NGC 6940-108	-0.26	-0.28	-0.36	-0.08	-0.19
NGC 6940-132	-0.12	-0.11	-0.06	-0.17	-0.09
NGC 6940-138	-0.01	-0.02	-0.11	-0.10	-0.02
NGC 6940-139	0.10	0.07	-0.08	-0.02	-0.03
NGC 6940-152	-0.02	0.20	-0.03	-0.06	0.00
Mean± σ	-0.02±0.04	0.00±0.04	-0.10±0.03	-0.09±0.02	-0.05±0.02
NGC 5822-6	0.01	-0.10	-0.05	0.07	0.03
NGC 5822-8	0.05	-0.15	-0.07	0.01	-0.14
NGC 5822-102	0.12	0.01	-0.14	0.13	-0.01
NGC 5822-224	-0.06	-0.17	-0.26	0.04	-0.14
NGC 5822-240	0.19	0.17	0.07	0.07	0.14
NGC 5822-316	-0.15	-0.17	-0.06	0.03	0.03
NGC 5822-348	-0.18	-0.25	-0.07	0.02	0.05
NGC 5822-375	0.04	0.01	-0.07	-0.06	-0.04
NGC 5822-443	0.05	-0.05	-0.12	-0.08	-0.09
Mean± σ	0.01±0.04	-0.08±0.04	-0.09±0.03	0.03±0.02	-0.02±0.03
NGC 5316-31	0.24	-0.05	0.16	0.09	0.02
NGC 5316-35	0.20	0.13	0.15	0.10	0.09
NGC 5316-45	0.28	0.23	0.21	0.04	-0.01
NGC 5316-72	0.07	0.12	0.17	-0.01	-0.20
Mean± σ	0.20±0.05	0.11±0.06	0.17±0.01	0.05±0.02	-0.02±0.06

Table 11. Comparisons between [Luck \(2015\)](#) and our results.

Star	$\Delta[\text{Y}/\text{Mg}]$	$\Delta[\text{Y}/\text{Al}]$	$\Delta[\text{Y}/\text{Si}]$	$\Delta[\text{Y}/\text{Ca}]$	$\Delta[\text{Y}/\text{Ti}]$
NGC 2682-151	-0.05	-0.07	0.02	-0.05	0.03
NGC 2682-244	0.01	0.03	0.05	-0.02	0.06
IC 4651-8540	0.09	0.09	0.00	-0.05	-0.05
IC 4651-9122	-0.06	-0.14	-0.06	-0.09	-0.06
IC 4651-9791	-0.11	-0.08	-0.08	-0.06	-0.09
IC 4651-14527	-0.05	-0.06	-0.09	0.01	0.09
Mean $\pm\sigma_n$	-0.03 \pm 0.03	-0.04 \pm 0.03	-0.03 \pm 0.02	-0.04 \pm 0.01	0.00 \pm 0.03

Table 12. Comparisons between [Casali et al. \(2020\)](#) and our results.

OC	$\Delta[\text{Y}/\text{Mg}]$	$\Delta[\text{Y}/\text{Al}]$	$\Delta[\text{Y}/\text{Si}]$	$\Delta[\text{Y}/\text{Ca}]$	$\Delta[\text{Y}/\text{Ti}]$
NGC 6633	-0.02	0.19	0.03	0.08	0.11
NGC 2682	0.07	0.13	0.15	0.01	0.03

Table A1. Sample of stars studied in this work.

Star	Gaia DR2 ID	RA	DEC	V	(B-V)
NGC 5316–31	5867065827625365504	13 53 33.68	–61 50 18.62	9.39	1.43
NGC 5316–35	5867065621466916992	13 53 31.67	–61 51 49.98	9.44	1.48
NGC 5316–45	5867065312229279616	13 54 01.31	–61 50 48.66	9.55	1.61
NGC 5316–72	5867064934272149120	13 53 53.63	–61 51 37.12	9.84	1.59
NGC 6633–78	4477460391998886144	18 27 14.28	+07 00 32.75	7.30	1.43
NGC 6633–100	4477223378527434880	18 27 54.74	+06 36 00.34	8.31	1.08
NGC 6633–106	4477273268868842752	18 28 00.18	+06 54 51.43	8.69	1.03
NGC 6633–119	4477253305860760960	18 28 17.64	+06 46 00.03	8.98	0.98
NGC 6633–126	4477249113972647168	18 28 22.97	+06 42 29.25	8.77	1.03
NGC 5822–6	5887669507333898880	15 04 21.25	–54 23 05.63	10.78	1.02
NGC 5822–8	5887667033432920192	15 04 39.43	–54 21 04.05	10.40	1.05
NGC 5822–102	5887670705571768064	15 03 49.43	–54 20 10.62	10.85	1.03
NGC 5822–224	5887646451945778176	15 03 22.91	–54 26 32.60	10.83	1.04
NGC 5822–240	5887641435423836544	15 04 30.39	–54 31 44.77	9.49	1.34
NGC 5822–316	5887629100276804352	15 04 30.53	–54 35 48.74	10.52	1.03
NGC 5822–348	5887691806775861248	15 03 00.46	–54 28 17.56	10.91	1.02
NGC 5822–375	5887695517658166912	15 03 15.84	–54 16 39.12	9.71	1.22
NGC 5822–443	5887699640826811520	15 02 54.11	–54 12 51.50	9.72	1.22
IC 4756–12	4284658038773033728	18 35 47.43	+05 20 17.11	9.54	1.03
IC 4756–14	4284662849136453376	18 35 58.46	+05 24 59.99	8.86	0.86
IC 4756–28	4283901746580386816	18 36 33.23	+05 12 42.78	9.01	1.32
IC 4756–38	4283997575895463680	18 37 05.21	+05 17 31.62	9.83	1.10
IC 4756–42	4284806438475643776	18 37 20.77	+05 53 43.11	9.46	0.97
IC 4756–44	4283983552796484864	18 37 30.30	+05 12 15.72	9.77	1.08
IC 4756–52	4283984931511649792	18 37 35.83	+05 15 37.82	8.06	1.37
IC 4756–101	4283940671842998272	18 38 43.79	+05 14 19.94	9.36	1.02
IC 4756–109	4283990119832758528	18 38 52.93	+05 20 16.51	9.05	1.05
IC 4756–125	4283939920251942144	18 39 17.88	+05 13 48.73	9.36	1.01
IC 4756–164	4283961979205354496	18 40 18.52	+05 18 51.73	9.27	1.08
NGC 6940–28	1857093354284218624	20 33 25.02	+28 00 46.97	11.56	1.12
NGC 6940–30	1857476671523723904	20 33 29.80	+28 17 04.93	10.98	1.21
NGC 6940–67	1857474541219852288	20 34 04.12	+28 16 48.62	10.96	0.88
NGC 6940–87	1857478252061220096	20 34 14.70	+28 22 15.89	11.32	1.08
NGC 6940–101	1857484299385864832	20 34 23.64	+28 24 25.64	11.27	1.10
NGC 6940–105	1857458009880137728	20 34 25.46	+28 05 05.62	10.66	1.24
NGC 6940–108	1857461553227085056	20 34 25.68	+28 13 41.61	11.19	1.04
NGC 6940–132	1857481894204245504	20 34 40.11	+28 26 38.93	10.97	1.10
NGC 6940–138	1857460105824232448	20 34 45.88	+28 09 04.73	11.35	1.07
NGC 6940–139	1857461793756724608	20 34 47.60	+28 14 47.29	11.38	1.08
NGC 6940–152	1857466844638231296	20 34 56.64	+28 14 27.14	10.83	1.09
IC 4651–6333	5949565621044529664	17 24 33.40	–49 54 56.09	10.75	0.96
IC 4651–7646	5949565170038446592	17 24 42.00	–49 59 06.00	10.36	1.04
IC 4651–8540	5949565895922433408	17 24 47.00	–49 54 07.00	10.89	1.13
IC 4651–9025	5949553590806611328	17 24 50.00	–49 57 27.00	10.90	1.13
IC 4651–9122	5949553973093167104	17 24 50.07	–49 56 56.08	10.70	0.80
IC 4651–9791	5949577646955571712	17 24 54.15	–49 53 07.52	10.43	1.33
IC 4651–14527	5949576581802598016	17 25 24.00	–49 55 47.00	10.94	1.14
NGC 2682–141	604917629355042176	08 51 22.80	+11 48 01.78	10.35	1.22
NGC 2682–151	604921512005266048	08 51 26.18	+11 53 51.98	10.39	1.19
NGC 2682–244	604904950611554432	08 51 50.20	+11 46 06.92	10.70	1.02

APPENDIX A: TABLES

Table A2: List of absorption lines for IC 4756 stars

Wavelength (Å)	Species	χ (eV)	$\log gf$	E12 (mÅ)	E14 (mÅ)	E28 (mÅ)	E38 (mÅ)	E42 (mÅ)	E44 (mÅ)	E52 (mÅ)	E101 (mÅ)	E109 (mÅ)	E125 (mÅ)	E164 (mÅ)	Juno
5711.09 ¹	12	4.34	-1.73	124.7	136.6	133.7	117	113.9	112.1	143.3	120.1	124.2	120.4	121.8	101.4
6318.71 ²	12	5.11	-1.94	58.4	67.4	66.9	53.6	55.5	57.7	71.8	57.1	55.3	—	61.2	41.3
6319.24 ²	12	5.11	-2.17	36.7	45.6	47.2	32.2	33.3	31.1	46.3	29.2	36.5	—	36.7	28.8
7387.69 ³	12	5.75	-1.25	70.2	77	76.7	74.1	67.4	67.9	85.9	72.3	81.7	73.1	69.3	72.7

7691.55 ²	12	5.75	-1	71.7	—	—	—	—	—	—	—	—	—	—	56.2
8712.69 ⁴	12	5.93	-1.31	52.7	—	—	—	—	—	—	—	—	—	—	52.8
8717.83 ⁵	12	5.93	-1.05	83.2	89.7	79.5	—	75.5	71.2	90.6	77.3	80.9	73.5	73.5	79.8
8736.02 ⁵	12	5.94	-0.63	114.6	120.6	120.7	117.2	105.9	116.2	124.5	113.8	115.7	110.3	111.1	143.6
6696.02 ³	13	3.14	-1.481	54.1	71.4	76.3	50.9	49.6	54.5	90.6	51.6	57.9	55.3	58.7	34.3
6698.67 ⁶	13	3.14	-1.63	37.3	54.3	56.2	36.2	32.8	36.3	65.2	33.2	39.2	38.1	40.2	20.5
7835.32 ⁶	13	4.04	-0.58	49.6	54.9	73.5	49.9	47.1	50	77.2	49.7	57.6	46.1	52.2	36.7
7836.13 ⁶	13	4.02	-0.4	68	74.2	81.7	62.2	—	65.9	85.5	61.4	69.2	64.8	67.1	54.9
8772.88 ⁶	13	4.02	-0.25	78.7	102.1	109.4	83.1	80.1	—	110.9	—	89.6	—	90.4	72.7
8773.91 ⁶	13	4.02	-0.07	—	114.1	129.6	—	95.8	100.2	129.7	97.2	111.1	104.4	—	93
5488.98 ^x	14	5.61	-1.69	34.7	39.5	33.8	35.4	35.8	33.8	35.2	36.6	36.0	34.6	34.4	25.3
5517.54 ^x	14	5.08	-2.50	22.8	28.3	24.3	23.8	23.1	20.9	28.9	23.8	24.7	25.5	26.4	12.3
5665.55 ^x	14	4.92	-1.94	65.3	—	74.1	59.7	59.4	60.6	80.3	63.9	71.1	60.9	66.6	40.6
5684.48 ^x	14	4.95	-1.55	—	—	—	—	—	74.1	—	—	—	78.7	—	61.1
5690.43 ^x	14	4.93	-1.77	64.3	68.9	67.1	63.1	—	62.2	70.5	66.5	67.8	63.3	68.8	47.9
6125.02 ^x	14	5.61	-1.46	47.7	51.2	51.3	43.9	43.8	41.6	58.1	44.9	47.9	44.0	46.5	31.5
6142.48 ^x	14	5.62	-1.29	43.9	45.6	45.8	43.6	47.1	43.6	44.3	42.4	45.4	43.3	40.9	34.1
6145.02 ^x	14	5.62	-1.31	52.9	—	46.1	47.5	—	46.7	48.6	46.9	49.5	50.6	46.3	37.5
6243.82 ^x	14	5.62	-1.24	58.3	56.3	58.2	57.8	55.9	54.1	—	50.9	60.0	56.7	54.6	42.1
6244.47 ^x	14	5.62	-1.09	57.3	57.2	58.7	61.3	57.8	57.5	60.1	52.5	64.0	57.6	56.5	42.0
6414.98 ^x	14	5.87	-1.03	58.6	—	52.2	51.3	58.5	52.9	58.4	53.3	61.1	59.2	56.6	45.1
6721.85 ^x	14	5.86	-1.12	59.0	62.2	59.4	60.2	56.0	57.3	63.6	59.1	67.8	60.5	62.3	42.5
6741.63 ^x	14	5.98	-1.43	19.5	21.6	24.5	20.9	—	—	26.4	23.4	—	25.0	23.7	14.1
6848.58 ^x	14	5.86	-1.52	28.1	29.4	—	—	27.3	25.1	—	28.0	30.9	25.5	25.9	16.5
7003.57 ^x	14	5.96	-0.94	64.4	—	56.4	62.3	—	—	60.2	60.9	62.3	63.5	59.9	57.8
5260.39 ^x	20	2.52	-1.72	—	—	67.1	54.8	—	51.3	—	53.0	—	49.8	55.7	29.7
5512.98 ^x	20	2.93	-0.46	106.6	122.1	122.7	103.7	100.6	104.1	132.3	100.8	112.0	102.0	106.2	83.7
5581.97 ^x	20	2.52	-0.560	124.3	139.4	140.8	116.5	117.2	116.0	—	116.5	126.9	116.8	125.3	92.5
5590.11 ^x	20	2.52	-0.56	108.4	—	—	114.4	109.7	—	—	112.0	—	111.7	122.3	89.4
5867.56 ^x	20	2.93	-1.56	49.2	58.6	59.8	37.6	42.1	37.0	67.3	41.1	50.0	40.4	44.8	22.8
6161.30 ^x	20	2.52	-1.27	102.0	114.8	119.1	93.3	91.7	95.7	140.2	91.7	101.2	92.1	102.2	64.5
6166.44 ^x	20	2.52	-1.14	100.5	118.4	113.5	94.2	95.0	93.9	133.6	95.5	103.3	97.0	100.5	70.5
6169.04 ^x	20	2.52	-0.79	117.8	139.6	136.2	115.2	112.2	118.9	149.3	114.7	125.7	117.3	120.3	89.3
6169.56 ^x	20	2.53	-0.48	135.1	—	153.1	131.4	130.5	136.0	—	130.3	140.1	132.2	136.1	110.0
6455.60 ^x	20	2.52	-1.33	87.4	110.6	109.7	87.9	84.2	84.1	123.2	86.6	96.3	84.5	90.6	54.6
6471.66 ^x	20	2.53	-0.69	122.9	141.7	142.1	117.3	115.1	118.5	—	118.0	128.6	119.0	123.2	89.1
6493.78 ^x	20	2.52	-0.11	153.2	—	—	—	148.3	—	—	146.9	—	142.3	—	122.2
6499.65 ^x	20	2.52	-0.81	120.2	139.9	140.8	115.6	111.0	113.1	—	120.3	122.6	113.4	122.9	87.2
6572.78 ^x	20	0.00	-4.24	93.2	—	—	—	—	95.9	—	—	110.0	96.1	—	29.9
7326.15 ^x	20	2.93	-0.21	131.4	—	148.3	—	—	135.8	—	—	144.0	125.6	—	108.2
5159.05	26	4.28	-0.65	4	90.7	86.5	79.8	86.6	77.4	—	79.6	83.5	83	83.5	68.6
5242.49	26	3.63	-0.97	115.3	119.4	123.4	107.8	107.9	110.4	140.5	107.1	114.7	109.8	110.7	85.9
5253.03	26	2.28	-3.79	60.2	65.4	67.6	45.9	52.4	45.9	88.8	47.1	52	41.2	51.1	17.1
5288.52	26	3.69	-1.51	85.6	102.1	112.1	82.9	87.8	79.2	121.4	82.4	86.4	84.1	93.5	58.6
5321.1	26	4.43	-1.19	61.4	70.7	73.5	59.2	59.3	57.8	85.2	59.8	66	59.1	61.9	42.1
5322.04	26	2.28	-2.84	100.3	119.8	121	91.5	94.5	97.2	135.5	95.2	109.4	98	101.8	62.1
5364.87	26	4.45	0.23	129.1	141	138.4	128.6	135	141	151.8	132	130.2	129.6	140.6	132.9
5367.46	26	4.42	0.439	137.8	149.5	143.1	139.9	144.6	145.1	158.7	138.1	138.6	138.8	146.2	145.1
5373.7	26	4.47	-0.71	80.1	89.8	84.6	83.3	79.7	79.1	100.3	80.3	83.1	81	82.2	62.6
5389.47	26	4.42	-0.25	101.5	113.6	106.5	98.7	97.3	96.9	120	—	101.5	103	101.5	81.9
5410.91	26	4.47	0.4	132.8	138.6	137.7	131.5	125.1	128.1	—	124.6	133.3	131.7	127.1	130.9
5417.03	26	4.42	-1.53	55.3	63.9	60.8	54.6	52.9	54	74	51.5	57.8	52.2	58	35.2
5441.33	26	4.31	-1.58	49.9	71.2	65	52.4	52.3	54.8	74.4	52.2	56.4	55.4	48.9	31.5
5445.04	26	4.39	0.041	123.6	140	134.6	125.8	130.7	122.3	153.1	128.1	135.6	126.2	130.2	122.2
5522.44	26	4.21	-1.4	63.3	68.9	71.8	63.5	61	60.5	81.8	61.9	64.7	66.1	60.6	45.1
5554.89	26	4.55	-0.38	122.6	137.3	136.4	120.5	118.3	122.7	139.9	120.7	129.4	118.9	125.4	100.1
5560.21	26	4.43	-1.04	72.4	76.8	75.6	72.9	64.9	66.9	84.7	67.6	71.4	69.6	67.8	51.1
5584.76	26	3.57	-2.17	63	77.2	78.4	58.4	57.8	61.7	90.8	62.7	70.1	63.3	63.8	39.2
5624.02	26	4.39	-1.33	65.1	76.6	82.5	72.5	69.1	62.3	93.5	69	73.8	70.2	71.6	52.3
5633.94	26	4.99	-0.12	78.5	88.1	85.4	81.8	79.3	77.5	98.6	83.2	85.2	68.5	83.5	65.2
5635.82	26	4.26	-1.74	51.8	58.4	56.5	51.6	50.3	50.6	68.8	52.8	54.3	53.4	54.6	34
5638.26	26	4.22	-0.72	101.6	114.9	115.1	94.1	95.7	99.5	119.3	98.4	101.6	103.2	103.1	77.4
5691.49	26	4.3	-1.37	68.1	72.4	82	59.9	63.4	60.3	94.8	68.2	75.4	—	70.1	40.7
5705.46	26	4.3	-1.36	61	70.6	72.3	56.9	61.9	56.9	77.9	58.8	63.8	59.6	62.4	38.8
5717.83	26	4.28	-0.979	87.2	100.5	98	85	87.6	81.2	106	85.8	88.5	85.4	88.7	63.1
5731.76	26	4.26	-1.15	77.5	88.6	89.6	78.2	79.2	78.7	100.5	82.7	83.9	84	86.6	57.4
5806.72	26	4.61	-0.9	71.8	85.5	86.3	73.2	73.6	75	92.5	77.5	74.8	78	76.9	53.9

5814.8	26	4.28	-1.82	39.3	48.5	51.7	40	38.3	39	58.6	39.3	46.2	38.8	40.1	23.4
5852.21	26	4.55	-1.18	59.7	84.1	84.7	65.4	54.2	63.8	—	63	72.3	64.5	64.4	39.9
5883.81	26	3.96	-1.21	86.1	100.6	97.6	92.6	84.5	90.7	111.8	88.4	92.7	92.3	90.8	70.5
5916.24	26	2.45	-2.99	95.3	113.1	120.9	94	85.9	93.2	139.6	95.3	103.2	98	101.3	53.3
5934.65	26	3.93	-1.02	98.5	114.4	112	99.9	97.9	96.6	134.2	100.4	106.6	—	103.4	75
6024.05	26	4.55	-0.06	118.2	133.9	129.6	125.7	122.4	130.5	137.5	123.8	127.7	117.8	128.1	110.4
6027.05	26	4.08	-1.09	87.2	95	93.1	90.5	88.1	88.6	110	89.9	95	84	95.6	62.5
6056.00	26	4.73	-0.4	84.9	91.3	88.8	86.2	86.4	91.4	105.1	89.1	88.2	92.2	87.5	71.1
6079.00	26	4.65	-0.97	62.2	71.8	70.7	63.6	56	60.8	77.3	65.5	64.3	61	67.8	47.4
6093.64	26	4.61	-1.35	47.6	57.7	59.4	48.5	49.6	49.2	65.9	47.3	53.8	48.9	54.6	30.1
6096.66	26	3.98	-1.78	56.3	72.3	71.5	59.3	61.3	61.5	84	60.8	63.9	61.8	62.6	37.2
6120.24	26	0.91	-5.95	27.4	56.7	61.6	23.7	24.2	30.7	78.1	21.7	31.2	26.6	21	5.1
6151.61	26	2.18	-3.29	86.3	113	114	86.6	81.2	84.9	127.6	84.8	93.3	89.1	90.9	49.2
6157.72	26	4.08	-1.11	90.8	118	112.6	92.6	90.3	90	122.8	92.9	102.4	93	103.9	63.5
6165.36	26	4.14	-1.47	65.1	80.3	79.5	70.1	63.5	64.8	90.7	67.9	71.9	68.3	72.9	44
6170.5	26	4.8	-0.38	107.1	—	—	107.8	109.4	105.4	—	105.2	120.6	—	120	82.9
6173.33	26	2.22	-2.88	108.5	135.4	134.1	106.8	103	102.5	153.1	108.7	118.9	107.3	115.4	67.7
6187.99	26	3.94	-1.57	76.8	88.6	89.9	70.1	68.5	72.4	101.3	74.6	77.6	74.4	77.8	47.7
6200.31	26	2.61	-2.44	108.1	130.8	132.9	111.8	103.4	108.9	150.6	—	121.6	109.5	109.6	71.7
6322.68	26	2.59	-2.43	117	135.9	134.4	108.4	111.7	109.6	—	113.6	126.3	116.6	120.3	78.6
6380.74	26	4.19	-1.32	77.3	99.1	94	79.6	73.9	85.1	109.3	74.6	81.5	77.2	78.6	53.8
6392.53	26	2.28	-4.03	55	63.2	72.1	40.3	43.2	43.8	85.7	45.7	55.9	41.4	47.1	18.2
6419.95	26	4.73	0.09	101.6	117.4	114.6	101.3	100.2	105.9	125	104.1	108.3	—	108.8	87
6469.19	26	4.84	-0.62	85	102.1	100	84.2	80.9	82.8	104.9	81.9	90.4	—	92.1	58.4
6518.36	26	2.83	-2.3	90.6	111.6	108.8	84.5	83	87.3	—	86.5	97.3	89.7	92	58.1
6574.22	26	0.99	-5.02	81	108.1	113.2	76	72.5	76.1	135.9	76.3	87.8	76.3	85.2	29
6591.31	26	4.59	-2.07	21.8	29.1	28.7	22.4	17.7	21.4	38	22.7	22.4	—	24.5	10.5
6593.87	26	2.44	-2.42	125.7	160	158.5	127.5	126.1	133	—	122.9	142.6	—	136.8	87.5
6597.56	26	4.8	-0.92	60.3	67	70.4	66	60.3	65.7	76.6	64.3	67.5	64.3	64.4	42.4
6608.02	26	2.28	-4.03	48.4	75.9	78.6	44	45.1	50.2	94.9	44.6	57.1	51.9	54.6	17.1
6609.11	26	2.56	-2.69	113.1	139.9	140.4	105.7	107.2	104.5	—	105.1	116.7	111.3	116.1	68.2
6646.93	26	2.61	-3.99	37.2	62.5	60.3	32.1	33.6	32	72.5	30.3	40.3	28.1	35.1	8.2
6653.85	26	4.14	-2.52	21.1	29.1	28.6	18.8	17.5	19.9	32	20	21.1	16.7	23.7	10.9
6699.14	26	4.59	-2.19	19.8	25.6	26.6	13.1	18.6	17.8	29.8	16.9	18.9	14.2	18	7.5
6703.56	26	2.76	-3.16	73.9	98.3	90.2	69.2	69	72.4	113.7	71.7	78.9	71.3	75.4	37.8
6704.48	26	4.22	-2.66	12.1	22.1	17.7	12.8	12.3	15.4	25.7	10.4	12.3	10.4	15	6.1
6710.31	26	1.8	-4.88	57.6	96.5	91.9	54.4	56	55.6	112.8	57.2	67.9	52.7	66.6	15.7
6713.74	26	4.79	-1.6	34.4	46.4	44.6	35.2	36.5	38.3	52.9	32.9	39.6	33.6	38.7	21.4
6739.52	26	1.56	-4.95	42.1	68.2	72.2	42.1	38.4	42.1	88.9	39.8	49.9	35.4	47.9	11.8
6750.15	26	2.42	-2.62	115.1	146.2	144.9	108.6	106.6	116	—	111.2	124.4	117.4	119.5	76.2
6752.70	26	4.64	-1.2	66	84.1	—	—	—	58.4	—	58.6	70.4	—	63.5	38.2
6783.70	26	2.59	-3.98	38.3	74.8	79	43.9	46.4	47.4	92.7	45.8	51.3	35.6	46.5	14.3
6793.25	26	4.07	-2.47	26.3	40.8	37.1	25.9	27	28.6	46	25.1	32.3	24.7	33	13.2
6806.84	26	2.73	-3.21	70.8	97	94.8	72.8	66.9	68.5	110.9	70.9	80.1	70.1	77.2	34
6810.26	26	4.61	-0.99	67.2	78.7	73.7	67.5	68.2	70.4	84.5	70.7	74.1	62.3	71.8	50
6820.37	26	4.64	-1.17	61	74.9	75.4	58.6	57.6	62.4	84.4	66.7	68.2	58.5	68.4	40.9
6851.63	26	1.61	-5.32	25.9	48.2	56.5	24.5	24.2	25.1	78.7	22	35.8	23.3	25.6	6.7
6858.15	26	4.61	-0.93	68.2	83	78.6	70.1	72.3	70.3	87.6	72.6	80.6	71.3	75.9	50.2
7132.98	26	4.08	-1.61	63.7	80.8	73.8	59.2	66.1	57.2	99.4	67.2	69.9	67.8	74.9	42.5
6745.95	26	4.07	-2.77	—	20.3	19.6	14.6	16.4	14.2	—	—	16.9	15	14.8	8.3
6436.40	26	4.19	-2.46	—	—	—	—	—	—	48.1	—	—	—	—	11.1
6551.67	26	0.99	-5.79	—	—	—	—	—	—	99.7	—	—	—	—	6.1
4993.34	26.1	2.81	-3.67	58	55.2	54.1	54.8	54.7	57.7	60.4	57.6	58.4	65.5	62.6	38
5132.65	26.1	2.81	-4	39.6	40.3	34.2	41	38.6	35.4	48.6	40.3	42.5	44	41.4	23.8
5197.55	26.1	3.23	-2.25	110.7	105.8	106.9	106.6	106.1	104.7	—	107.2	109	109.3	113.9	81.9
5234.61	26.1	3.22	-2.24	105.1	105.7	101.8	103.1	102.1	105.8	101	105.1	105.6	105.1	106.5	81.9
5284.09	26.1	2.89	-3.01	85.8	79.8	82.8	83.8	84.8	82.3	—	85.9	91.3	92.8	87.8	66.7
5325.55	26.1	3.22	-3.17	60.5	57.7	52.3	59.1	60.1	56.6	53	62.4	63.3	64.2	60.4	38.7
5414.04	26.1	3.22	-3.62	48.4	36.4	40.8	44.5	41.3	39.2	39.5	41.7	45.9	42.3	40.8	25.9
5425.24	26.1	3.2	-3.21	61.3	58.2	54.4	58.5	59.7	61.5	59.7	58.5	63.5	65.2	60.9	39.6
5991.36	26.1	3.15	-3.56	50.4	50.7	53.2	53.6	53	50.3	46.6	56.1	58.9	53.1	58	29.9
6084.09	26.1	3.2	-3.8	42.6	39.4	39.1	40.6	39.8	37.7	35.7	43.2	41.1	44.5	42	22.2
6149.24	26.1	3.89	-2.72	50	44	45.7	48.1	53.2	44.4	48.7	55.9	55.1	51.3	51.8	37.7
6247.54	26.1	3.89	-2.34	69.3	61	57.1	67.2	75.8	61.4	57.6	71.6	75.5	76.8	75.9	55.9
6416.92	26.1	3.89	-2.68	53.7	53.8	52.6	55.5	55.6	52.1	51.1	57.4	58.6	58.9	59	39.6
6432.68	26.1	2.89	-3.58	62.9	64.3	57.2	59.2	62	59	63.2	61.1	65.7	67.4	65.8	43.1
4607.34	38	0	0.283	79.9	99.1	102	76.9	72.9	78.8	118.8	79.1	88	80.2	85.8	41.0

4883.68 ⁷	39.1	1.08	0.07	100.8	125.3	130.5	93.6	95.8	106.8	—	96.9	105.4	105.4	96.7	60.1
5087.43 ⁷	39.1	1.08	-0.17	84.5	85.9	90.3	85	78.9	77.6	—	78.7	88.7	85.4	82.9	48.8
5200.42 ⁷	39.1	0.99	-0.57	82.1	94.8	73.1	79.4	75	—	106.7	81.4	89.2	79.6	83	38.9
5289.82 ⁸	39.1	1.03	-1.85	21.5	29.8	29.6	23	19.8	20.4	39.2	21.2	28.1	22	26	5.2
5402.78 ⁶	39.1	1.84	-0.44	48	48.5	50.5	38.2	37	35.4	52.8	41.1	44.8	38.2	42.1	13
5205.72 ⁷	39.1	1.03	-0.34	—	—	—	—	—	—	—	75.9	—	—	—	41.4
6127.46 ⁹	40	0.15	-1.06	19.1	39.6	46	14.8	—	16.2	62.9	15.2	23.5	14.8	21.4	3.8
6134.57 ⁹	40	0	-1.28	11.1	32.4	—	10.2	9.3	11.7	58.9	—	15.7	10.9	15.4	2.2
6143.18 ⁹	40	0.07	-1.1	13.8	39.8	—	18.2	—	—	70	13.8	22.7	14	18.7	3
5385.13 ¹⁰	40	0.52	-0.64	—	27.5	25.5	—	8.9	8.2	39.1	—	—	—	—	1.9
5303.53 ⁸	57.1	0.32	-1.35	26.7	39.2	40.8	24.7	21.2	39.2	53.1	23.3	32	22.7	32.8	3.6
6390.48 ⁷	57.1	0.32	-1.41	23.3	46.7	49.4	23.7	20.1	—	59.2	25.6	35	25.8	23.5	3.9
5880.63 ¹¹	57.1	0.24	-1.83	—	24.9	—	—	—	—	35.2	—	16.1	12.1	21.2	1.4
5187.46 ⁸	58.1	1.21	0.3	29.5	44.6	43	30.1	25	28.6	52.6	25	36.4	29.8	36	7.5
5274.24 ⁸	58.1	1.28	0.389	40.4	49.8	45.2	35.1	30.7	29.2	55.9	30.6	43.7	37.4	38.9	9.8
5472.3 ⁸	58.1	1.25	-0.19	17.7	26.2	23.1	10.8	14.5	20.3	23.4	10.9	14.9	13.8	22.7	2.4
4628.16 ⁷	58.1	0.52	0.01	—	—	—	—	—	—	87.1	—	—	—	—	17.7
4811.34 ⁸	60.1	0.06	-1.015	53.7	75.9	75.6	51.2	43.8	54.7	85.8	50	55.7	50.4	53.9	9.3
4959.12 ⁸	60.1	0.06	-0.916	63.8	90.6	91.9	73.8	63.3	67.2	115.4	78.2	84.5	75.8	78.5	32.4
5130.59 ⁷	60.1	1.3	0.1	42.2	—	—	37.5	—	—	—	—	—	—	44.5	12.6
5234.19 ⁷	60.1	0.55	-0.46	53	—	—	48.6	—	—	—	38.9	—	44.4	56.4	5.6
5319.81 ⁷	60.1	0.55	-0.35	61.2	—	—	—	—	—	87.9	56.4	63.8	55.3	62	13
5740.88 ⁸	60.1	1.16	-0.56	15.8	27.8	10.5	11	9.9	10.5	32.3	17.2	18.8	15.2	15.7	2.4

¹ Reddy et al. (1999); ² Castro et al. (1997); ³ McWilliam et al. (1994); ⁴ Edvardsson et al. (1993); ⁵ Wiese et al. (1969); ⁶ Reddy et al. (2003); ⁷ Smith et al. (1996); ⁸ Van Winckel et al. (2000); ⁹ Sneden et al. (1996); ¹⁰ Antipova et al. (2005); ¹¹ Reyniers et al. (2004).

Table A3: List of absorption lines for NGC 2682 stars

Wavelength (Å)	Species	χ (eV)	log g f	E 141 (mÅ)	E 151 (mÅ)	E 244 (mÅ)	Juno
5711.09	12	4.34	-1.94	143.3	145	130.9	101.4
6318.71	12	5.11	-1.25	78.6	75.6	67.3	41.3
7387.69	12	5.75	-1.05	98.1	—	87.8	72.7
8717.83	12	5.93	-1.63	103.2	94.1	93.2	79.8
8736.02	12	5.94	-0.63	141.5	140.7	—	143.6
8712.69	12	5.93	-1.31	—	76.8	71.1	52.8
6319.24	12	5.11	-2.17	—	—	41.9	28.8
6696.02	13	3.14	-1.48	79.4	—	—	34.3
6698.67	13	3.14	-1.58	60.8	62.1	48.9	20.5
7835.32	13	4.04	-0.4	70.9	70.2	69.7	36.7
7836.13	13	4.02	-0.283	91.8	84	75.8	54.9
8772.88	13	4.02	-0.25	—	—	98.8	72.7
5488.98	14	5.61	-1.69	—	44.9	42.9	25.3
5517.54	14	5.08	-2.50	32.8	—	27.8	12.3
5665.55	14	4.92	-1.94	73.1	79.5	67.7	40.6
5684.48	14	4.95	-1.55	—	—	—	61.1
5690.43	14	4.93	-1.77	80.8	77.4	71.0	47.9
6125.02	14	5.61	-1.46	54.6	—	47.6	31.5
6142.48	14	5.62	-1.29	—	—	—	34.1
6145.02	14	5.62	-1.31	—	57.9	—	37.5
6243.82	14	5.62	-1.24	—	—	—	42.1
6244.47	14	5.62	-1.09	65.4	72.4	62.8	42.0
6414.98	14	5.87	-1.03	—	—	—	45.1
6721.85	14	5.86	-1.12	—	67.9	55.5	42.5
6741.63	14	5.98	-1.43	—	—	—	14.1
6848.58	14	5.86	-1.52	—	37.5	—	16.5
7003.57	14	5.96	-0.94	—	75.4	—	57.8
5260.39	20	2.52	-1.72	—	69.8	—	29.7
5512.98	20	2.93	-0.46	121.5	118.8	107.6	83.7
5581.97	20	2.52	-0.56	143.3	132.7	121.8	92.5
5590.11	20	2.52	-0.57	133.6	—	114.5	89.4
5867.56	20	2.93	-1.57	67.4	61.1	47.7	22.8
6161.30	20	2.52	-1.27	125.1	117.4	95.1	64.5
6166.44	20	2.52	-1.14	122.5	114.3	95.8	70.5
6169.04	20	2.52	-0.80	143.6	134.2	117.8	89.3

6169.56	20	2.53	-0.48	—	150.2	134.5	110.0
6455.60	20	2.52	-1.34	111.9	110.4	92.5	54.6
6471.66	20	2.53	-0.69	140.4	138.6	121.5	89.1
6493.78	20	2.52	-0.11	—	—	—	122.2
6499.65	20	2.52	-0.82	140.5	138.5	122.5	87.2
6572.78	20	0.00	-4.24	—	—	94.2	29.9
7326.15	20	2.93	-0.21	—	—	—	108.2
5022.87	22	0.83	-0.43	—	145.4	119.3	70.6
5039.96	22	0.02	-1.13	—	—	128.0	71.1
5064.65	22	0.05	-0.99	—	—	140.1	85.2
5147.48	22	0.00	-2.01	—	119.4	—	34.8
5210.39	22	0.05	-0.88	—	—	145.1	88.2
5219.70	22	0.02	-2.29	121.6	121.7	86.3	28.2
5295.77	22	1.07	-1.63	73.3	73.9	46.5	12.6
5866.45	22	1.07	-0.84	132.8	130.3	100.4	48.7
6091.17	22	2.27	-0.42	70.6	68.0	—	14.9
6126.22	22	1.07	-1.42	100.6	97.1	69.1	23.2
6258.10	22	1.44	-0.35	130.7	128.9	96.9	51.0
6261.10	22	1.43	-0.48	—	—	102.3	48.9
5242.49	26	3.63	-0.79	130.2	128.9	112.7	85.9
5253.03	26	2.28	-3.51	79.8	75.1	55.3	17.1
5288.52	26	3.69	-1.19	107.1	—	93.2	58.6
5321.1	26	4.43	-1.84	73.9	76.9	58.7	42.1
5322.04	26	2.28	-2.23	119.5	120.5	99.3	62.1
5364.87	26	4.45	0.71	149.5	144.7	144.1	132.9
5373.7	26	4.47	-0.25	96.2	88.4	79.8	62.6
5389.47	26	4.42	-0.53	113.9	116	102.1	81.9
5417.03	26	4.42	-1.58	66	67.5	57.7	35.2
5441.33	26	4.31	-1.041	71.4	66.5	55.3	31.5
5445.04	26	4.39	0.4	150.8	146.8	134.1	122.2
5522.44	26	4.21	-1.38	78.7	78.8	67.8	45.1
5554.89	26	4.55	-0.04	138.9	138.1	127.9	100.1
5560.21	26	4.43	-1.17	81.8	78.3	72.6	51.1
5584.76	26	3.57	-2.33	83.2	—	—	39.2
5624.02	26	4.39	-1.12	86.4	—	81.1	52.3
5633.94	26	4.99	-0.74	95.2	88.1	88.1	65.2
5635.82	26	4.26	-1.72	65.7	69.5	59.4	34
5638.26	26	4.22	-0.36	121	111.5	104.6	77.4
5705.46	26	4.3	-1.979	76.7	72.5	58.5	38.8
5717.83	26	4.28	-0.15	106.8	106.9	—	63.1
5731.76	26	4.26	-1.9	97.3	92.8	80.6	57.4
5806.72	26	4.61	-0.82	90.9	87	78.3	53.9
5814.8	26	4.28	-1.21	58.4	55.2	45.4	23.4
5883.81	26	3.96	-1.99	115.3	110.5	98.8	70.5
5916.24	26	2.45	-2.02	121.3	114.7	—	53.3
5934.65	26	3.93	-1.09	112.5	—	100.4	75
6027.05	26	4.08	-1.4	103.4	102	86.9	62.5
6056	26	4.73	-0.97	96.8	98.5	90	71.1
6079	26	4.65	-0.35	80.8	77.8	66.1	47.4
6093.64	26	4.61	-1.78	63.6	64.8	50.8	30.1
6096.66	26	3.98	-1.95	74.4	73.1	59.4	37.2
6120.24	26	0.91	-5.29	62.9	59.6	31.6	5.1
6151.61	26	2.18	-3.11	112	109.6	89.8	49.2
6157.72	26	4.08	-1.47	113.4	112.5	85.3	63.5
6165.36	26	4.14	-1.88	81.5	83.5	70.7	44
6173.33	26	2.22	-2.57	138.4	133.4	110	67.7
6187.99	26	3.94	-1.44	90.6	90.5	75.7	47.7
6200.31	26	2.61	-2.32	132.1	130	115.6	71.7
6380.74	26	4.19	-1.09	98.2	95.8	89.1	53.8
6419.95	26	4.73	-0.46	125.2	—	—	87
6436.4	26	4.19	-2.02	39.5	—	30	11.1
6574.22	26	0.99	-5.92	112.1	109	84.1	29
6597.56	26	4.8	-0.03	75.1	68.6	64.5	42.4
6608.02	26	2.28	-4.52	78.3	76.5	54.1	17.1
6653.85	26	4.14	-2.16	31.8	—	—	10.9
6703.56	26	2.76	-3.6	104.6	94.4	70.2	37.8
6713.74	26	4.79	-1.95	47.7	45.6	40.1	21.4

6739.52	26	1.56	-4.21	67.7	64.4	46.6	11.8
6806.84	26	2.73	-3.99	100.6	96.4	74.1	34
6810.26	26	4.61	-0.17	87.1	78.6	67.8	50
6820.37	26	4.64	-1.93	84.7	79.3	63.2	40.9
6858.15	26	4.61	-0.67	87.1	82	77.3	50.2
5691.49	26	4.3	-1.37	—	76.2	65.3	40.7
5852.21	26	4.55	-1.18	—	83.6	69.9	39.9
6024.05	26	4.55	-0.06	—	138.6	130.4	110.4
6322.68	26	2.59	-2.43	—	132.8	117.4	78.6
6518.36	26	2.83	-2.3	—	111.6	—	61.3
6609.11	26	2.56	-2.69	—	137.6	115.6	68.2
6699.14	26	4.59	-2.19	—	27.6	—	7.5
6704.48	26	4.22	-2.66	—	22.2	—	6.1
6750.15	26	2.42	-2.62	—	144.4	118.9	76.2
6392.53	26	2.28	-4.03	—	—	56.1	18.2
6469.19	26	4.84	-0.62	—	—	89.5	58.4
6593.87	26	2.44	-2.42	—	—	125.9	87.5
6710.31	26	1.8	-4.88	—	—	64.2	15.7
6745.95	26	4.07	-2.77	—	—	18.1	8.3
6752.7	26	4.64	-1.2	—	—	70.6	38.2
6793.25	26	4.07	-2.47	—	—	31.1	13.2
4993.34	26.1	2.81	-3.24	62.9	65.1	58.4	38
5234.61	26.1	3.22	-2.17	101.8	106.9	106.8	81.9
5325.55	26.1	3.22	-3.62	56.4	59.6	57.7	38.7
5414.04	26.1	3.22	-3.21	41.3	45.9	42.3	25.9
5425.24	26.1	3.2	-3.56	59.1	60.4	57.4	39.6
5991.36	26.1	3.15	-3.8	50.6	—	50.3	29.9
6084.09	26.1	3.2	-3.72	40.7	39.4	44.3	22.2
6149.24	26.1	3.89	-2.34	49.8	47.8	46.6	37.7
6247.54	26.1	3.89	-2.68	72.5	65.7	69.7	55.9
6416.92	26.1	3.89	-2.58	53.2	49.4	55.9	39.6
6432.68	26.1	2.89	-3.73	67.3	64.5	58.9	43.1
5197.55	26.1	3.23	-2.25	—	103.3	106.3	81.9
5132.65	26.1	2.81	-4	—	—	46.2	23.8
4607.34	38	0	0.17	100.1	101.1	78.5	41
5087.43	39.1	1.08	-0.57	92.7	89.1	84.4	48.8
5200.42	39.1	0.99	-0.85	91.9	—	73.5	38.9
5289.82	39.1	1.03	-1.64	28.6	26.4	19.7	5.2
5402.78	39.1	1.84	-0.44	—	43.4	33	13
5385.13	40	0.52	-0.28	27.5	23.2	14.6	1.9
6134.57	40	0	-1.1	34.1	31.4	—	2.2
6143.18	40	0.07	-1.35	40.3	36.5	20.3	3
6127.46	40	0.15	-1.06	—	—	18.5	3.8
5303.53	57.1	0.32	-1.41	30.5	32	21.6	3.6
6390.48	57.1	0.32	-1.74	40.7	28.5	24.1	3.9
4628.16	58.1	0.52	-0.3	72.3	68.6	53.5	17.7
5187.46	58.1	1.21	0.389	34.3	29.4	—	7.5
5274.24	58.1	1.28	0.015	44	42.4	28.9	9.8
5472.3	58.1	1.25	-0.19	—	15.7	—	2.4
4811.34	60.1	0.06	-1.916	66.1	60.7	42.7	9.3
4959.12	60.1	0.06	-0.1	95.2	91.7	73.3	32.4
5130.59	60.1	1.3	0.35	58.7	—	—	12.6
5319.81	60.1	0.55	-0.56	61.3	—	44.5	13
5740.88	60.1	1.16	0	19.7	17.4	—	2.4
5234.19	60.1	0.55	-0.46	—	43.8	—	5.6

Table A4: List of absorption lines for NGC 5316 stars

Wavelength (Å)	Species	χ (eV)	$\log gf$	E31 (mÅ)	E35 (mÅ)	E45 (mÅ)	E72 (mÅ)	Juno
5711.09	12	4.34	-1.73	150.0	151.4	—	—	101.4
6318.71	12	5.11	-1.94	66.9	85.9	87.1	89.7	41.3
8736.02	12	5.94	-0.63	135.6	138.2	—	129.1	143.6
7387.69	12	5.75	-1.25	—	89.1	87.9	94.1	72.7
8717.83	12	5.93	-1.05	—	—	86.5	96.3	79.8

4730.04 ⁶¹⁰	12	4.34	-2.39	—	—	—	110.5	55.9
6698.67	13	3.14	-1.63	59.2	68	78.6	81.7	20.5
7836.13	13	4.02	-0.4	92.5	95.7	95.3	104.1	54.9
8772.88	13	4.02	-0.25	108.8	—	—	—	72.7
6696.02	13	3.14	-1.481	—	93.1	—	—	34.3
5488.98	14	5.61	-1.69	38.9	35.1	33.4	40.1	25.3
5517.54	14	5.08	-2.50	24.5	30.1	26.4	29.8	12.3
5665.55	14	4.92	-1.94	94.1	—	—	—	40.6
5684.48	14	4.95	-1.55	—	87.8	83.7	—	61.1
5690.43	14	4.93	-1.77	81.1	79.7	70.2	82.9	47.9
6125.02	14	5.61	-1.46	51.0	58.1	53.2	—	31.5
6142.48	14	5.62	-1.29	50.9	44.5	40.1	—	34.1
6145.02	14	5.62	-1.31	66.0	61.6	49.1	54.4	37.5
6243.82	14	5.62	-1.24	79.7	53.1	—	58.1	42.1
6244.47	14	5.62	-1.09	72.1	55.2	—	63.1	42.0
6414.98	14	5.87	-1.03	58.3	54.2	—	—	45.1
6721.85	14	5.86	-1.12	—	—	60.9	—	42.5
6741.63	14	5.98	-1.43	—	—	18.3	—	14.1
6848.58	14	5.86	-1.52	32.2	—	30.2	—	16.5
7003.57	14	5.96	-0.94	—	60.4	55.5	59.6	57.8
5260.39	20	2.52	-1.72	65.0	76.7	—	—	29.7
5512.98	20	2.93	-0.46	124.1	132.4	—	142.9	83.7
5581.97	20	2.52	-0.56	—	151.6	—	—	92.5
5590.11	20	2.52	-0.57	—	—	—	—	89.4
5867.56	20	2.93	-1.57	—	66.9	73.3	68.6	22.8
6161.30	20	2.52	-1.27	131.9	135.5	137.3	136.8	64.5
6166.44	20	2.52	-1.14	124.4	127.1	137.5	143.4	70.5
6169.04	20	2.52	-0.80	149.4	145.0	—	—	89.3
6169.56	20	2.53	-0.48	—	—	—	—	110.0
6455.60	20	2.52	-1.34	120.1	129.1	126.7	130.3	54.6
6471.66	20	2.53	-0.69	—	—	—	—	89.1
6493.78	20	2.52	-0.11	—	—	—	—	122.2
6499.65	20	2.52	-0.82	—	151.9	—	—	87.2
6572.78	20	0.00	-4.24	142.5	—	—	—	29.9
7326.15	20	2.93	-0.21	—	—	—	—	108.2
5022.87	22	0.83	-0.43	—	—	—	—	70.6
5039.96	22	0.02	-1.13	—	—	—	—	71.1
5064.65	22	0.05	-0.99	—	—	—	—	85.2
5113.45	22	1.44	-0.78	82.5	102.1	117.5	127.1	24.4
5147.48	22	0.00	-2.01	—	—	—	—	34.8
5210.39	22	0.05	-0.88	—	—	—	—	88.2
5219.70	22	0.02	-2.29	—	149.3	—	—	28.2
5295.77	22	1.07	-1.63	66.2	86.1	111.3	—	12.6
5866.45	22	1.07	-0.84	151.0	—	—	—	48.7
6091.17	22	2.27	-0.42	52.7	86.1	92.2	92.2	14.9
6126.22	22	1.07	-1.42	97.2	—	149.7	147.7	23.2
6258.10	22	1.44	-0.35	147.7	145.1	—	—	51.0
6261.10	22	1.43	-0.48	149.2	—	—	—	48.9
7138.91	22	1.44	-1.59	—	73.3	91.2	92.2	6.8
5253.03	26	2.28	-3.79	87.5	86.1	109.3	106.2	17.1
5321.1	26	4.43	-1.19	94.3	—	90.4	93.2	42.1
5373.7	26	4.47	-0.71	122.2	105.2	112	119.1	62.6
5389.47	26	4.42	-0.25	142.6	—	134.2	136.2	81.9
5417.03	26	4.42	-1.53	82.3	78.1	88.8	86.8	35.2
5441.33	26	4.31	-1.58	83.6	83.3	89.2	86.5	31.5
5522.44	26	4.21	-1.4	104.7	90.1	104.3	99.6	45.1
5560.21	26	4.43	-1.04	93.4	89.2	100.3	99.6	51.1
5584.76	26	3.57	-2.17	94.9	—	107.8	109.8	39.2
5624.02	26	4.39	-1.33	103.1	104.9	103.5	109.1	52.3
5633.94	26	4.99	-0.12	117.3	103.7	98.9	106.3	65.2
5635.82	26	4.26	-1.74	74.6	—	85.4	88.9	34
5638.26	26	4.22	-0.72	134.9	126.6	135.1	142	77.4
5691.49	26	4.3	-1.37	114.1	—	101.2	103.8	40.7
5705.46	26	4.3	-1.36	94.7	83	92.6	93.6	38.8

¹⁰ Reddy et al. (2003)

5731.76	26	4.26	-1.15	113.6	106.8	121.5	114.3	57.4
5806.72	26	4.61	-0.9	113.9	104.1	110	104.9	53.9
5814.8	26	4.28	-1.82	63.9	63.1	70.1	65.7	23.4
5852.21	26	4.55	-1.18	106.2	—	—	—	39.9
5883.81	26	3.96	-1.21	140.9	129.1	133.1	133.7	70.5
6027.05	26	4.08	-1.09	131.6	118.1	126.4	—	62.5
6056.00	26	4.73	-0.4	130.8	108.3	114.5	114.9	71.1
6079.00	26	4.65	-0.97	98.5	84.9	97.6	99	47.4
6093.64	26	4.61	-1.35	83.5	70.2	82.5	81.1	30.1
6096.66	26	3.98	-1.78	86.3	88.9	94.5	96.1	37.2
6120.24	26	0.91	-5.95	68.7	83.5	105.3	104	5.1
6165.36	26	4.14	-1.47	107.7	96.7	101.7	113.7	44
6187.99	26	3.94	-1.57	112	107.5	115.3	121.4	47.7
6380.74	26	4.19	-1.32	107.5	—	—	124.9	53.8
6574.22	26	0.99	-5.02	149.5	—	—	—	29
6597.56	26	4.8	-0.92	84.6	84.1	85.5	86.5	42.4
6608.02	26	2.28	-4.03	97.3	101.1	121.9	113.6	17.1
6703.56	26	2.76	-3.16	133.6	125.8	135.4	142.5	37.8
6710.31	26	1.8	-4.88	122.8	—	—	130	15.7
6713.74	26	4.79	-1.6	53.4	51.6	57.3	60.1	21.4
6739.52	26	1.56	-4.95	74	91.5	117.4	—	11.8
6806.84	26	2.73	-3.21	121.1	121.6	135.9	136.1	34
6810.26	26	4.61	-0.99	105.5	93.6	106.2	103.5	50
6820.37	26	4.64	-1.17	87.7	91	95.6	95.7	40.9
6851.63	26	1.61	-5.32	73.5	—	105	98.4	6.7
6858.15	26	4.61	-0.93	108.3	92.3	108.2	99.9	50.2
5242.49	26	3.63	-0.97	—	149.6	—	—	85.9
6151.61	26	2.18	-3.29	—	139.9	—	—	49.2
6518.36	26	2.83	-2.3	—	133.2	—	—	58.1
6699.14	26	4.59	-2.19	—	28.2	32	30.3	7.5
6704.48	26	4.22	-2.66	—	22.7	30.4	30	6.1
5717.83	26	4.28	-0.979	—	—	123.2	130.1	63.1
6419.95	26	4.73	-0.09	—	—	140.8	—	87
6646.93	26	2.61	-3.99	—	—	83.5	—	8.2
6745.95	26	4.07	-2.77	—	—	39	—	8.3
7132.98	26	4.08	-1.61	—	—	112.6	115.3	42.5
5132.65	26.1	2.81	-4	83.8	56.1	—	—	23.8
5414.04	26.1	3.22	-3.62	78	55.2	56.6	50.2	25.9
5425.24	26.1	3.2	-3.21	101.4	72.8	69.7	72.3	39.6
5991.36	26.1	3.15	-3.56	86	67	52.5	58.7	29.9
6084.09	26.1	3.2	-3.8	80.4	55.7	—	—	22.2
6149.24	26.1	3.89	-2.72	100.1	59.6	55.4	60.1	37.7
6247.54	26.1	3.89	-2.34	126.6	81.2	75.2	77	55.9
6416.92	26.1	3.89	-2.68	92.8	68.1	59.9	—	39.6
5234.61	26.1	3.22	-2.24	—	122.8	122.1	122.7	81.9
5325.55	26.1	3.22	-3.17	—	72.2	63.9	67.3	38.7
6432.68	26.1	2.89	-3.58	—	75.7	72.3	84.2	43.1
4993.34	26.1	2.81	-3.67	—	—	75.8	—	38
5284.09	26.1	2.89	-3.01	—	—	107.1	—	66.7
5197.55	26.1	3.23	-2.25	—	—	—	125.3	81.9
4607.34	38	0	0.283	134.5	122.4	143.4	142.7	41
5200.42	39.1	0.99	-0.57	137.8	111.9	133.6	—	38.9
5289.82	39.1	1.03	-1.85	54.6	45.5	52.9	52.3	5.2
5402.78	39.1	1.84	-0.44	86.8	58.4	59.8	80.4	13
5087.43	39.1	1.08	-0.17	—	118.7	—	—	48.8
5385.13	40	0.52	-0.64	28.8	34.9	66.6	61.1	1.9
6127.46	40	0.15	-1.06	45.2	59.5	—	—	3.8
6134.57	40	0	-1.28	31.1	52.8	93.2	79.2	2.2
6143.18	40	0.07	-1.1	46.4	60.9	97.6	98.2	3
5303.53	57.1	0.32	-1.35	45.7	55.6	63.3	56.8	3.6
6390.48	57.1	0.32	-1.41	58.2	68.3	70.9	70.3	3.9
5880.63	57.1	0.24	-1.83	—	—	39.5	—	1.4
5187.46	58.1	1.21	0.3	61.8	48.8	68.3	58	7.5
5274.24	58.1	1.28	0.389	65.2	55.5	71.5	67.5	9.8
5472.3	58.1	1.25	-0.19	40.8	21.4	49.3	25.1	2.4
4811.34	60.1	0.06	-1.015	83.6	96.8	110.9	95.5	9.3
4959.12	60.1	0.06	-0.916	140.1	135.1	—	135.9	32.4

5740.88	60.1	1.16	-0.56	32.5	39.1	44.5	38.3	2.4
5234.19	60.1	0.55	-0.46	—	82.8	—	—	5.6
5319.81	60.1	0.55	-0.35	—	—	104.1	—	13

Table A5: List of absorption lines for NGC 5822 stars

Wavelength (Å)	Species	χ (eV)	$\log gf$	E6 (mÅ)	E8 (mÅ)	E102 (mÅ)	E224 (mÅ)	E240 (mÅ)	E316 (mÅ)	E348 (mÅ)	E375 (mÅ)	E443 (mÅ)	Juno
5711.09	12	4.34	-1.73	117.5	124.9	116.8	114.1	141.6	124.9	118.9	143.8	142.1	101.4
6318.71	12	5.11	-1.94	52.7	59.8	56.3	60.9	80	60.8	57.2	73.9	70.5	41.3
7387.69	12	5.75	-1.25	73.1	79.9	81.3	84.3	93.2	85.1	81.4	—	96.8	72.7
8717.83	12	5.93	-1.05	87.7	—	—	88.3	103.2	103.4	84.5	110.9	—	79.8
8736.02	12	5.94	-0.63	125.2	128.1	139.8	123	140.8	148.5	135.3	—	147.8	143.6
6319.24	12	5.11	-2.17	—	45.1	41.8	40.6	—	46.9	44.2	—	—	28.8
8712.69	12	5.93	-1.31	—	58.1	—	69.7	—	65.9	62.6	84.3	—	52.8
7691.55	12	5.75	-1	—	—	—	—	—	89.8	91	105.2	100.1	56.2
6696.02	13	3.14	-1.481	52.7	—	—	52	—	57.7	57.7	79.4	76.4	34.3
6698.67	13	3.14	-1.63	40.3	40.2	29.3	41.6	70.6	37.4	36.3	57.3	56.3	20.5
7835.32	13	4.04	-0.58	59.3	50.5	52.2	60.3	—	—	—	—	—	36.7
7836.13	13	4.02	-0.4	69.3	64.7	66.2	72.7	96.8	66.6	65.7	79.8	82.5	54.9
8772.88	13	4.02	-0.25	—	—	79.8	95.5	—	—	—	—	—	72.7
8773.91	13	4.02	-0.07	—	—	—	100.5	—	—	—	—	—	93
7362.30	13	4.02	-0.748	—	—	—	—	—	42.3	—	—	—	31.3
5488.98	14	5.61	-1.69	—	—	30.5	—	—	36.2	—	—	—	25.3
5517.54	14	5.08	-2.50	24.0	26.4	18.7	23.1	—	—	23.6	28.8	30.6	12.3
5665.55	14	4.92	-1.94	59.5	64.7	55.6	62.9	—	66.4	65.5	—	—	40.6
5684.48	14	4.95	-1.55	—	—	68.5	—	—	—	—	—	—	61.1
5690.43	14	4.93	-1.77	63.5	68.3	59.0	63.8	68.8	67.3	—	—	—	47.9
6125.02	14	5.61	-1.46	45.4	44.4	39.3	43.5	—	46.6	45.4	49.4	45.8	31.5
6142.48	14	5.62	-1.29	44.5	47.8	40.5	—	42.3	47.8	—	—	49.2	34.1
6145.02	14	5.62	-1.31	48.1	51.8	41.7	—	—	—	—	—	52.7	37.5
6243.82	14	5.62	-1.24	51.2	62.3	50.8	56.3	50.1	55.4	59.3	53.4	57.3	42.1
6244.47	14	5.62	-1.09	53.1	65.3	49.2	57.7	56.3	58.1	57.9	54.8	60.5	42.0
6414.98	14	5.87	-1.03	50.0	—	—	51.7	48.6	54.9	—	52.1	52.2	45.1
6721.85	14	5.86	-1.12	58.4	57.9	54.5	56.3	—	61.2	60.1	60.1	—	42.5
6741.63	14	5.98	-1.43	22.5	24.2	20.3	22.7	—	—	23.4	21.8	—	14.1
6848.58	14	5.86	-1.52	24.9	26.2	18.3	24.9	—	30.2	29.7	28.0	32.4	16.5
7003.57	14	5.96	-0.94	—	—	59.9	65.4	59.6	—	—	60.3	—	57.8
5260.39	20	2.52	-1.72	53.7	—	—	—	78.7	57.1	—	—	—	29.7
5512.98	20	2.93	-0.46	101.8	108.0	—	101.8	127.4	110.5	109.0	122.5	120.7	83.7
5581.97	20	2.52	-0.56	115.8	122.9	114.3	116.4	146.3	122.6	117.7	136.7	140.3	92.5
5590.11	20	2.52	-0.57	—	—	—	—	133.6	117.6	—	133.5	—	89.4
5867.56	20	2.93	-1.57	39.7	46.2	40.8	45.3	65.2	45.3	46.6	—	59.8	22.8
6161.30	20	2.52	-1.27	—	96.3	89.0	88.4	122.5	97.8	97.2	110.3	122.1	64.5
6166.44	20	2.52	-1.14	87.5	104.1	94.2	94.4	129.7	102.3	97.2	120.4	119.8	70.5
6169.04	20	2.52	-0.80	107.7	123.3	—	113.7	—	116.0	121.3	140.3	137.6	89.3
6169.56	20	2.53	-0.48	—	127.2	—	—	—	129.5	135.6	—	—	110.0
6455.60	20	2.52	-1.34	82.3	87.8	81.7	86.6	118.1	88.9	90.3	115.5	111.7	54.6
6471.66	20	2.53	-0.69	115.5	120.0	112.4	120.2	146.8	120.6	124.7	147.8	146.4	89.1
6493.78	20	2.52	-0.11	147.8	145.4	145.5	—	—	—	150.0	—	—	122.2
6499.65	20	2.52	-0.82	111.7	122.6	113.2	116.4	149.4	121.7	118.1	144.4	143.5	87.2
6572.78	20	0.00	-4.24	—	—	—	—	—	—	—	—	—	29.9
7326.15	20	2.93	-0.21	—	—	—	—	—	—	—	—	—	108.2
5022.87	22	0.83	-0.43	110.3	114.4	—	110.4	—	118.7	116.4	149.7	—	70.6
5039.96	22	0.02	-1.13	117.8	120.5	115.3	—	—	126.5	126.7	—	—	71.1
5064.65	22	0.05	-0.99	—	—	—	—	—	—	—	—	—	85.2
5113.45	22	1.44	-0.78	57.3	65.6	—	59.5	109.7	66.7	67.7	—	93.3	24.4
5147.48	22	0.00	-2.01	85.6	89.2	83.5	84.7	143.3	—	88.2	121.6	130.6	34.8
5210.39	22	0.05	-0.88	—	140.2	133.4	—	—	141.4	142.3	—	—	88.2
5219.70	22	0.02	-2.29	68.6	85.7	36.8	80.4	143.7	78.7	85.4	119.8	121.9	28.2
5295.77	22	1.07	-1.63	41.4	40.2	—	43.2	95.3	42.2	45.3	77.4	80.3	12.6
5866.45	22	1.07	-0.84	95.7	93.2	—	97.4	—	98.9	98.9	128.2	138.8	48.7
6091.17	22	2.27	-0.42	32.4	38.6	37.8	39.5	86.5	46.4	45.2	68.7	69.8	14.9
6126.22	22	1.07	-1.42	60.3	71.2	61.1	62.2	122.2	66.4	67.8	104.2	103.3	23.2
6258.10	22	1.44	-0.35	89.2	100.3	90.4	91.5	147.0	95.9	98.8	123.3	125.7	51.0

6261.10	22	1.43	-0.48	95.2	—	90.5	94.9	—	94.7	100.3	127.8	—	48.9
7138.91	22	1.44	-1.59	—	—	—	—	—	—	—	—	—	6.8
5242.49	26	3.63	-0.97	111.1	112.5	117.7	109.6	130.7	114.4	114.3	127.2	131.3	85.9
5253.03	26	2.28	-3.79	49.3	—	48.2	51.4	84.5	57.3	47.8	76.7	65.8	17.1
5288.52	26	3.69	-1.51	84.5	88.2	82.1	85.3	—	93.6	82.3	112.2	113.7	58.6
5321.1	26	4.43	-1.19	56.3	62.5	57.5	61.4	79.4	64.5	67.1	75.1	76.1	42.1
5322.04	26	2.28	-2.84	94.4	104.5	93.5	97.3	131.1	101.2	97.6	123.8	118.2	62.1
5364.87	26	4.45	0.23	132.3	134.1	134.8	135.8	—	138.3	129.3	144.1	—	132.9
5367.46	26	4.42	0.439	137.2	—	142.1	139.2	—	144.6	143.1	—	—	145.1
5373.7	26	4.47	-0.71	73.8	81.3	77.8	80.8	93.7	83.7	80.9	94.2	96.2	62.6
5389.47	26	4.42	-0.25	96.4	93.3	92.2	98.4	117.3	103.3	99.3	113.7	110.4	81.9
5410.91	26	4.47	0.4	126.7	133.6	131.1	—	143.2	136	129.1	144.4	—	130.9
5417.03	26	4.42	-1.53	52.2	56.6	50.7	53.6	71.8	57.7	54.9	68.9	65.4	35.2
5441.33	26	4.31	-1.58	52.2	55.2	48.2	53.8	73.2	58.9	53.7	73.8	70.9	31.5
5445.04	26	4.39	0.041	131.5	130.2	127.2	120.1	143.2	136.4	128	148.1	145.1	122.2
5522.44	26	4.21	-1.4	61.1	69.9	61.6	63.5	80.5	67.9	62.5	85	79.7	45.1
5554.89	26	4.55	-0.38	116.6	—	117.2	121.4	142.7	125.2	121.4	140.1	138.2	100.1
5560.21	26	4.43	-1.04	66.6	73.1	66.6	68.3	81.5	71.6	72.4	82.3	81.7	51.1
5584.76	26	3.57	-2.17	59.4	69.2	69.4	60.4	—	67.5	61.6	81.8	—	39.2
5624.02	26	4.39	-1.33	70	73.4	67.3	70.3	92.4	77.3	72.6	89.6	89.3	52.3
5633.94	26	4.99	-0.12	78.1	82.5	82.7	82.2	94.6	85.2	77.3	95	97	65.2
5635.82	26	4.26	-1.74	51	53.3	45.4	50.7	67.7	57	58.7	65.3	71.6	34
5638.26	26	4.22	-0.72	94.8	101.1	92.3	95.1	117.3	101.4	102.1	114.1	115.4	77.4
5691.49	26	4.3	-1.37	66.9	—	67.3	69.6	—	63.6	63.2	87.4	72.1	40.7
5705.46	26	4.3	-1.36	57.5	61.7	54.4	56.4	76.8	65.3	59.3	76.3	72.9	38.8
5731.76	26	4.26	-1.15	72.2	79.2	68.2	76.5	99.9	84.7	85.5	98.2	97.4	57.4
5806.72	26	4.61	-0.9	72.8	—	68.8	69.6	92.1	77.1	76.5	89.3	87.6	53.9
5814.8	26	4.28	-1.82	37.2	41.4	37.9	39.3	57	42.6	40.9	55.3	51.4	23.4
5852.21	26	4.55	-1.18	61.2	65.7	61.1	65.6	—	68.6	64.3	86.9	88.5	39.9
5883.81	26	3.96	-1.21	89.6	90.6	80.2	87.6	119.3	94.4	91.3	106.2	105.5	70.5
5934.65	26	3.93	-1.02	93.4	101.2	96.4	96.5	132.3	104.2	101.3	—	117.5	75
6024.05	26	4.55	-0.06	119	126.3	112.4	119.7	134.8	131.7	117.3	138.3	135.3	110.4
6027.05	26	4.08	-1.09	83.3	89.4	81.3	84.5	106.5	86.3	85.7	98.5	104.6	62.5
6056	26	4.73	-0.4	80	88.6	78.5	83.2	96.3	—	90.4	101.8	113.8	71.1
6079	26	4.65	-0.97	59.3	68.1	62.7	61.3	77.5	68.1	67.4	77.1	77.4	47.4
6093.64	26	4.61	-1.35	46.7	52.6	45.3	47.6	64.2	50.5	49.2	60.6	61.3	30.1
6096.66	26	3.98	-1.78	56.9	61.8	50.2	55.1	79.8	62.4	58.4	77.4	78.6	37.2
6151.61	26	2.18	-3.29	84.8	91.6	80.3	84.3	125.5	90.9	86.3	114.3	114.7	49.2
6157.72	26	4.08	-1.11	90.1	81.4	78.5	92.6	—	98.2	93.2	103.3	119.9	63.5
6165.36	26	4.14	-1.47	63.3	67.7	61.1	64.1	88.5	71.1	67.8	86.3	89.9	44
6170.5	26	4.8	-0.38	100.8	—	—	104.3	—	109.2	106.1	—	106.3	82.9
6173.33	26	2.22	-2.88	104.6	114.3	101.1	103.2	—	112.3	105.4	140.4	132.4	67.7
6187.99	26	3.94	-1.57	67.4	75.5	65.6	70.3	96.5	79.7	74.6	94.8	91.6	47.7
6200.31	26	2.61	-2.44	101.3	114.5	106.3	106.2	141.5	114.3	109.4	133.2	136.7	71.7
6322.68	26	2.59	-2.43	109.6	117.2	107.9	112.1	148.2	121	110.6	141.1	139.2	78.6
6380.74	26	4.19	-1.32	78.8	83.3	72.5	78.2	105.3	80.2	72.7	100.6	96.4	53.8
6392.53	26	2.28	-4.03	42.4	52.2	41.7	43.3	84.4	51.5	48.3	75.3	72.3	18.2
6419.95	26	4.73	-0.09	100.5	104.1	96.7	100.6	121.6	105.3	102.7	120.6	119.5	87
6469.19	26	4.84	-0.62	80.4	—	85.7	83.5	—	86.8	81.9	—	102.5	58.4
6518.36	26	2.83	-2.3	86.4	91.1	91.3	93.3	129.3	93.1	90.3	114.2	114.4	58.1
6574.22	26	0.99	-5.02	75.8	86.4	69.7	72.4	133.2	83	81.1	121.4	121.3	29
6593.87	26	2.44	-2.42	120.4	—	—	121.2	—	133.4	124.2	—	—	87.5
6597.56	26	4.8	-0.92	58.5	60.1	56.8	57.3	72.3	62.1	61.3	76.4	73.2	42.4
6608.02	26	2.28	-4.03	49.4	54.3	47.4	49.7	95.3	55.3	51.3	81.4	79.2	17.1
6609.11	26	2.56	-2.69	104.4	115.3	103.1	105.1	—	114.7	105.9	145.2	142	68.2
6703.56	26	2.76	-3.16	70.3	78.6	67.6	71.6	105.1	75.8	72.2	100.4	98.9	37.8
6710.31	26	1.8	-4.88	53.3	62.7	54.6	59.4	—	62.2	—	98.2	—	15.7
6713.74	26	4.79	-1.6	32.3	36.6	28.4	33.9	48.7	36.3	35.8	48.2	45.1	21.4
6739.52	26	1.56	-4.95	36.4	43.3	32.7	45.1	84	43.5	40.3	68.3	—	11.8
6750.15	26	2.42	-2.62	107.5	118.2	108.4	111.3	—	116.3	110.3	141.2	146	76.2
6783.7	26	2.59	-3.98	42.3	47.7	47.2	46	—	—	—	72.3	76.3	14.3
6806.84	26	2.73	-3.21	69.6	77.7	66.3	69.6	108.7	74.9	68.8	91.4	101.6	34
6810.26	26	4.61	-0.99	67.8	71.1	62.7	65.4	85.9	72.2	71.8	82.3	81.4	50
6820.37	26	4.64	-1.17	59	65.6	58.2	62.7	84.4	66.3	63	77.3	75.6	40.9
6851.63	26	1.61	-5.32	28.5	34.3	—	—	64.3	26.9	—	48.6	—	6.7
6858.15	26	4.61	-0.93	67.8	73	66.8	70.3	84.3	73.2	72.3	81.1	79.4	50.2
5159.05	26	4.28	-0.65	—	84.3	—	—	—	91.6	85.4	—	—	68.6

5916.24	26	2.45	-2.99	—	98.8	86.3	90.4	138.2	98.1	92.4	124.2	125.9	53.3
6120.24	26	0.91	-5.95	—	32.2	—	25.6	76.2	30.1	28.4	60.7	64.4	5.1
6551.67	26	0.99	-5.79	—	35.5	—	30.6	72.8	30.5	29.9	63.3	61.8	6.1
6752.7	26	4.64	-1.2	—	62.1	52.8	64.7	—	60.4	51.7	70.6	83.7	38.2
6793.25	26	4.07	-2.47	—	29.3	23	—	44.3	30.8	28.9	40.5	44.1	13.2
5717.83	26	4.28	-0.979	—	—	83.3	92.4	104.2	95.3	—	105.5	102.3	63.1
6436.4	26	4.19	-2.46	—	—	21.3	28.6	46.7	25.8	23.9	40.4	36.6	11.1
6646.93	26	2.61	-3.99	—	—	31.7	34.9	—	34.8	34.1	—	60.1	8.2
6591.31	26	4.59	-2.07	—	—	—	27.7	27.7	28.9	24.9	25.1	—	10.5
6653.85	26	4.14	-2.52	—	—	—	—	39.8	23.8	20.9	30.2	33.7	10.9
6699.14	26	4.59	-2.19	—	—	—	—	—	17.8	16.3	26.6	24.3	7.5
6704.48	26	4.22	-2.66	—	—	—	—	—	13.7	12.9	20.7	20.8	6.1
6745.95	26	4.07	-2.77	—	—	—	—	—	—	16.1	—	24.2	8.3
4993.34	26.1	2.81	-3.67	55.7	58.8	55.2	60.2	62.8	72.1	58.7	67.4	—	38
5132.65	26.1	2.81	-4	41.1	49.4	43.7	—	48.6	48.5	43.5	48.6	44.3	23.8
5197.55	26.1	3.23	-2.25	104.2	—	—	—	—	—	—	112.6	—	81.9
5234.61	26.1	3.22	-2.24	106	—	110.3	109	100.2	105.3	105.7	108.3	106.5	81.9
5284.09	26.1	2.89	-3.01	82.5	87.1	—	—	—	92	87.2	95.5	96.4	66.7
5325.55	26.1	3.22	-3.17	56.3	59.9	56	58.7	53.1	—	54.4	60.3	61.1	38.7
5414.04	26.1	3.22	-3.62	44.3	48	40.5	43.3	43.3	48.9	44.2	44.4	45.3	25.9
5425.24	26.1	3.2	-3.21	57.4	61.5	54.5	58.6	55.7	63.6	61.5	60.5	—	39.6
5991.36	26.1	3.15	-3.56	50.1	50.1	50.2	51.4	50.5	57.4	50.7	55.4	—	29.9
6084.09	26.1	3.2	-3.8	39.7	39.5	34.7	37.9	39.9	43.8	36.4	43.7	—	22.2
6149.24	26.1	3.89	-2.72	50.2	49	51.5	53.3	44.1	57.3	49.3	53.3	51	37.7
6247.54	26.1	3.89	-2.34	75	71.5	75.2	78.1	62.1	—	68.7	—	66.4	55.9
6416.92	26.1	3.89	-2.68	55.7	57.4	56.9	55.4	52.2	58.7	52.5	56.9	56.3	39.6
6432.68	26.1	2.89	-3.58	—	67.3	59.7	—	—	66.9	60.5	60.2	62.4	43.1
4607.34	38	0	0.283	70.3	82.1	71.9	73.2	127.5	78.5	76.7	104.2	107.8	41
5087.43	39.1	1.08	-0.17	80.8	86.9	82.2	87.4	93.2	85.5	81.6	98.7	100.9	48.8
5200.42	39.1	0.99	-0.57	72.2	84.3	76.6	—	105.3	76.6	75.8	96.4	98.4	38.9
5205.72	39.1	1.03	-0.34	71.2	—	—	—	—	—	76.9	—	101.1	41.4
5289.82	39.1	1.03	-1.85	20.4	23.3	18.9	27.5	42.2	22.1	19.4	29.7	31.3	5.2
5402.78	39.1	1.84	-0.44	34.6	43.3	36.8	43	—	37.3	37.8	50.3	50.7	13
4883.68	39.1	1.08	0.07	—	102.8	—	—	—	99.2	95.2	—	—	60.1
5385.13	40	0.52	-0.64	13.3	10.8	12.4	10.6	46.5	10.1	—	29.4	34.6	1.9
6127.46	40	0.15	-1.06	18.4	19.8	18.2	19.3	65.1	15.5	17.4	42.3	45.4	3.8
6134.57	40	0	-1.28	15	13.2	17.4	12.7	59.8	11.1	13.7	39.4	38.3	2.2
6143.18	40	0.07	-1.1	—	—	18.2	17.8	70.5	18.5	15.9	46.2	46.9	3
5303.53	57.1	0.32	-1.35	23.8	30.3	23.5	29.5	51.5	27.6	24.4	45.6	45.2	3.6
5880.63	57.1	0.24	-1.83	11.6	11.6	17	17.8	39	16.6	15.8	27.6	26.8	1.4
6390.48	57.1	0.32	-1.41	22.3	25.1	26	32	57.4	28.4	25.7	47.6	45.6	3.9
4628.16	58.1	0.52	-0.74	59.8	66.2	60	61.6	90.3	68.1	65.8	83.6	80.3	17.7
5187.46	58.1	1.21	0.3	30.2	36.4	28	34.2	53.2	37.2	39.4	49.8	48.5	7.5
5274.24	58.1	1.28	0.389	35.4	42.4	—	42.4	58.8	43.7	37.6	54.1	55.2	9.8
5472.3	58.1	1.25	-0.19	15.7	18.4	—	17.7	33.6	21.6	16.8	—	23.9	2.4
4811.34	60.1	0.06	-1.015	47	54.6	46.7	58.6	86.4	52.3	52.3	68.7	66.3	9.3
4959.12	60.1	0.06	-0.916	71.2	—	68.2	76.8	114.1	72.7	71.3	96.9	106	32.4
5234.19	60.1	0.55	-0.46	39.9	—	—	44.7	—	—	—	—	—	5.6
5319.81	60.1	0.55	-0.35	54.4	61.8	49.5	53.3	87.5	55.7	52.7	79.4	—	13
5740.88	60.1	1.16	-0.56	17.6	15.3	10	20.1	32	17.3	15.3	25.5	20.1	2.4
5311.46 ¹¹	60.1	0.98	-0.56	—	22.2	—	23.9	—	—	—	32.1	—	2.3
5130.59	60.1	1.3	0.1	—	—	—	—	—	43.6	—	—	—	12.6

Table A6: List of absorption lines for NGC 6633 stars

Wavelength (Å)	Species	χ (eV)	$\log g f$	E78 (mÅ)	E100 (mÅ)	E106 (mÅ)	E119 (mÅ)	E126 (mÅ)	Juno
5711.09	12	4.34	-1.73	149.3	127.4	114.1	116	115.9	101.4
6318.71	12	5.11	-1.94	72.8	59.1	52.6	50.6	51.6	41.3
7387.69	12	5.75	-1.25	86.2	79.2	64.9	63.3	67.2	72.7
8736.02	12	5.94	-0.63	124.3	—	—	110.4	107.4	143.6
4730.04	12	4.34	-2.39	—	80.6	75.3	72.9	75.7	55.9

¹¹ Smith et al. (1996)

6319.24	12	5.11	-2.17	—	37.3	36.9	33.6	34.1	28.8
8717.83	12	5.93	-1.05	—	81.4	66.9	67.1	73.2	79.8
7691.55	12	5.75	-1	—	—	—	56.5	54.6	56.2
6696.02	13	3.14	-1.481	94.6	63.2	47.9	47.1	55.2	34.3
6698.67	13	3.14	-1.63	74.7	43.2	37.7	31.2	36.8	20.5
7836.13	13	4.02	-0.4	94.2	72.5	68.6	59.7	65.9	54.9
8772.88	13	4.02	-0.25	101.9	100.1	83.4	—	107.1	72.7
7835.32	13	4.04	4.04	—	58.3	54.9	46.2	56.7	36.7
8773.91	13	4.02	-0.07	—	—	126.1	—	126.3	93
5488.98	14	5.61	-1.69	37.4	37.6	36.2	—	38.2	25.3
5517.54	14	5.08	-2.50	24.1	18.8	23.8	19.5	21.9	12.3
5665.55	14	4.92	-1.94	—	66.3	63.3	58.6	62.1	40.6
5684.48	14	4.95	-1.55	80.3	75.7	72.5	67.7	75.1	61.1
5690.43	14	4.93	-1.77	65.7	68.7	67.5	54.9	—	47.9
6125.02	14	5.61	-1.46	—	45.0	45.7	38.2	43.8	31.5
6142.48	14	5.62	-1.29	40.9	40.1	44.3	37.4	41.6	34.1
6145.02	14	5.62	-1.31	49.9	48.3	42.9	40.2	45.8	37.5
6243.82	14	5.62	-1.24	48.5	51.1	60.9	58.1	57.6	42.1
6244.47	14	5.62	-1.09	65.9	51.8	53.6	53.5	60.1	42.0
6414.98	14	5.87	-1.03	44.8	58.5	53.0	52.3	52.3	45.1
6721.85	14	5.86	-1.12	—	—	—	—	57.8	42.5
6741.63	14	5.98	-1.43	—	—	—	—	23.9	14.1
6848.58	14	5.86	-1.52	—	—	—	—	26.4	16.5
7003.57	14	5.96	-0.94	—	—	—	—	—	57.8
5260.39	20	2.52	-1.72	83.5	60.5	51.8	—	51.7	29.7
5512.98	20	2.93	-0.46	131.7	112.2	107.2	96.8	104.2	83.7
5581.97	20	2.52	-0.56	—	129.1	116.4	112.1	118.3	92.5
5590.11	20	2.52	-0.57	144.1	122.1	—	107.3	112.5	89.4
5867.56	20	2.93	-1.57	78.0	—	45.6	36.4	41.6	22.8
6161.30	20	2.52	-1.27	132.2	105.5	89.1	85.9	95.0	64.5
6166.44	20	2.52	-1.14	80.9	104.2	95.4	93.4	92.9	70.5
6169.04	20	2.52	-0.80	—	125.4	112.2	109.2	114.9	89.3
6169.56	20	2.53	-0.48	—	139.7	130.3	129.6	137.7	110.0
6455.60	20	2.52	-1.34	128.9	98.4	89.0	84.0	86.0	54.6
6471.66	20	2.53	-0.69	—	130.7	122.3	115.7	124.5	89.1
6493.78	20	2.52	-0.11	—	—	—	—	—	122.2
6499.65	20	2.52	-0.82	—	—	113.2	108.9	—	87.2
6572.78	20	0.00	-4.24	—	—	88.3	—	—	29.9
7326.15	20	2.93	-0.21	—	—	—	131.3	135.8	108.2
5022.87	22	0.83	-0.43	—	—	111.4	—	110.4	70.6
5039.96	22	0.02	-1.13	—	—	—	—	114.5	71.1
5064.65	22	0.05	-0.99	—	—	—	—	128.7	85.2
5113.45	22	1.44	-0.78	115.2	68.1	—	54.2	56.3	24.4
5147.48	22	0.00	-2.01	—	—	—	—	84.7	34.8
5210.39	22	0.05	-0.88	—	—	137.1	—	133.4	88.2
5219.70	22	0.02	-2.29	—	—	—	—	72.0	28.2
5295.77	22	1.07	-1.63	104.2	48.2	41.6	37.7	36.2	12.6
5866.45	22	1.07	-0.84	—	—	—	87.6	93.6	48.7
6091.17	22	2.27	-0.42	95.1	44.9	—	—	35.6	14.9
6126.22	22	1.07	-1.42	135.3	71.1	64.7	55.8	60.1	23.2
6258.10	22	1.44	-0.35	—	97.1	90.9	84.2	87.8	51.0
6261.10	22	1.43	-0.48	—	101.8	93.7	82.3	—	48.9
7138.91	22	1.44	-1.59	—	—	—	—	24.6	6.8
5321.1	26	4.43	-1.19	90.4	67.6	60.9	58	58.5	42.1
5373.7	26	4.47	-0.71	104	83.7	78	79.2	82	62.6
5389.47	26	4.42	-0.25	125.7	106.1	99.3	92	99.9	81.9
5417.03	26	4.42	-1.53	80.3	58.4	54.5	52.7	58.4	35.2
5441.33	26	4.31	-1.58	81.1	55.6	55.8	48.8	51.5	31.5
5445.04	26	4.39	0.041	154.8	139.7	135.2	130.6	133.7	122.2
5560.21	26	4.43	-1.04	94.8	73.5	69.9	61.7	67.4	51.1
5584.76	26	3.57	-2.17	98.4	70.6	65.9	58	62.9	39.2
5624.02	26	4.39	-1.33	103.1	78.6	—	75.7	72.2	52.3
5633.94	26	4.99	-0.12	101.3	84.8	83	83.5	86.7	65.2
5635.82	26	4.26	-1.74	78.9	—	54.3	49	51.9	34
5638.26	26	4.22	-0.72	128.5	103.7	97.4	95.8	97.3	77.4
5705.46	26	4.3	-1.36	82.5	64.9	59.9	58.9	60.7	38.8
5717.83	26	4.28	-0.979	111.4	91.7	93.5	83.6	94.5	63.1

5731.76	26	4.26	-1.15	104.9	88.7	83.5	77	86.3	57.4
5916.24	26	2.45	-2.99	147.3	105.8	99.5	88.6	92.8	53.3
6024.05	26	4.55	-0.06	149.7	132.3	128.3	123.2	125.4	110.4
6027.05	26	4.08	-1.09	113.2	96.9	91.8	86.4	91.8	62.5
6056	26	4.73	-0.4	107	90.8	94.1	82.9	83.6	71.1
6079	26	4.65	-0.97	85	69.9	64.5	62	61.7	47.4
6093.64	26	4.61	-1.35	71.4	55.7	49.5	46.5	53.6	30.1
6096.66	26	3.98	-1.78	87.1	67	64.3	55.9	60.8	37.2
6120.24	26	0.91	-5.95	91.4	38.5	31.4	25.3	27.4	5.1
6151.61	26	2.18	-3.29	144.3	97.7	87.9	82.6	87.7	49.2
6165.36	26	4.14	-1.47	95.8	76.5	70.1	65.2	68	44
6187.99	26	3.94	-1.57	101.8	80.5	73.6	70.4	68.7	47.7
6380.74	26	4.19	-1.32	108.7	87.7	88.4	73.7	74.3	53.8
6419.95	26	4.73	-0.09	128.7	108.9	103.1	97.3	98.3	87
6597.56	26	4.8	-0.92	85.3	68.2	65.3	57.2	59.9	42.4
6608.02	26	2.28	-4.03	103.8	56.5	52.2	44.1	47.2	17.1
6609.11	26	2.56	-2.69	164.4	117.9	108.1	98.8	105.6	68.2
6699.14	26	4.59	-2.19	28	18	21.7	12.1	17.2	7.5
6703.56	26	2.76	-3.16	122.6	85.7	78.1	66.4	75.9	37.8
6704.48	26	4.22	-2.66	28.5	18.9	15.4	11.3	13.8	6.1
6710.31	26	1.8	-4.88	116.3	67.6	63.5	52.4	55.8	15.7
6713.74	26	4.79	-1.6	51.5	41.2	38.6	36.7	38.3	21.4
6739.52	26	1.56	-4.95	101.6	54.8	51.4	35.6	36.7	11.8
6745.95	26	4.07	-2.77	33.5	—	—	—	—	8.3
6806.84	26	2.73	-3.21	115.9	82.1	73.7	61.9	71	34
6810.26	26	4.61	-0.99	90.2	77.6	70	62.1	69.8	50
6820.37	26	4.64	-1.17	89.1	68.4	62.9	60.8	64.1	40.9
6851.63	26	1.61	-5.32	88.5	39.4	35	25.7	31.3	6.7
6858.15	26	4.61	-0.93	88.9	73.9	73.4	63.4	70.8	50.2
7132.98	26	4.08	-1.61	96	75.2	71.8	64.4	73.3	42.5
5242.49	26	3.63	-0.97	—	116.7	110.8	108.2	109.3	85.9
5253.03	26	2.28	-3.79	—	51.2	45.1	42.5	40.7	17.1
5288.52	26	3.69	-1.51	—	91.6	94.1	82.2	93.1	58.6
5322.04	26	2.28	-2.84	—	109.3	100.8	96.8	97.7	62.1
5364.87	26	4.45	0.23	—	137.9	144.9	134.8	137.4	132.9
5367.46	26	4.42	0.439	—	146.2	146.4	142.2	144.5	145.1
5410.91	26	4.47	0.4	—	133.8	133.4	126.9	131	130.9
5691.49	26	4.3	-1.37	—	75.6	69	62.6	64.4	40.7
5852.21	26	4.55	-1.18	—	71.9	70.2	57.2	65.4	39.9
5883.81	26	3.96	-1.21	—	97.4	91.9	81.9	88.4	70.5
6157.72	26	4.08	-1.11	—	99.1	96.8	92.4	96.4	63.5
6173.33	26	2.22	-2.88	—	120.4	112.3	100.5	107.1	67.7
6200.31	26	2.61	-2.44	—	117.3	110.8	104.9	104.2	71.7
6322.68	26	2.59	-2.43	—	124.5	114.1	108.3	111.4	78.6
6392.53	26	2.28	-4.03	—	56.3	50.2	40.5	44.7	18.2
6574.22	26	0.99	-5.02	—	89.3	77	66.8	77.8	29
6750.15	26	2.42	-2.62	—	126.5	112.6	109.4	115.6	76.2
6752.7	26	4.64	-1.2	—	69.3	64.8	65.4	68.4	38.2
5522.44	26	4.21	-1.4	—	—	71.1	56.7	65.4	45.1
5554.89	26	4.55	-0.38	—	—	120.6	116.4	121.2	100.1
6646.93	26	2.61	-3.99	—	—	36.5	28	33.7	8.2
4993.34	26.1	2.81	-3.67	63.5	—	62.9	54.1	60.3	38
5234.61	26.1	3.22	-2.24	106.2	112.4	109.1	102.7	104.9	81.9
5325.55	26.1	3.22	-3.17	57.1	66.8	59.3	60.7	66.3	38.7
5414.04	26.1	3.22	-3.62	43.5	52.3	49.8	41.7	43.2	25.9
5425.24	26.1	3.2	-3.21	58.3	66	67.2	57.2	59.2	39.6
5991.36	26.1	3.15	-3.56	49.3	58.9	55.6	55.3	57.5	29.9
6084.09	26.1	3.2	-3.8	37.2	46.1	45.4	40.1	—	22.2
6149.24	26.1	3.89	-2.72	47.5	55.2	54.1	53.4	52.1	37.7
6247.54	26.1	3.89	-2.34	63.3	74.8	81.7	72.8	73.5	55.9
6432.68	26.1	2.89	-3.58	64.5	72.5	66.4	58.9	67.5	43.1
5132.65	26.1	2.81	-4	—	51.7	52.8	45.2	46.1	23.8
5197.55	26.1	3.23	-2.25	—	108.7	—	109.2	109.3	81.9
5284.09	26.1	2.89	-3.01	—	93	—	88.9	89.7	66.7
6416.92	26.1	3.89	-2.68	—	59.7	59.2	53.4	58	39.6
4607.34	38	0	0.283	130.9	88.4	81.5	78.1	82.1	41
4883.68	39.1	1.08	0.07	129.1	100.6	97.4	94.8	92.9	60.1

5200.42	39.1	0.99	-0.57	111.9	84.6	78.5	74.4	78.1	38.9
5289.82	39.1	1.03	-1.85	44.1	23.6	20.8	20.2	21	5.2
5402.78	39.1	1.84	-0.44	53.7	44.7	38.6	36.6	33.6	13
5087.43	39.1	1.08	-0.17	—	92.3	77	82.4	83.1	48.8
5385.13	40	0.52	-0.64	55.3	—	—	6.1	7	1.9
6134.57	40	0	-1.28	79.9	13.3	10.2	7.5	10.9	2.2
6143.18	40	0.07	-1.1	87.5	19.5	14.3	12.1	13.6	3
6127.46	40	0.15	-1.06	—	22.8	10.8	11.5	12.8	3.8
5303.53	57.1	0.32	-1.35	53.6	30	25.3	20.6	21.5	3.6
5880.63	57.1	0.24	-1.83	41.4	13.9	—	—	9.8	1.4
6390.48	57.1	0.32	-1.41	68.7	34.3	27.3	18.4	27.2	3.9
5187.46	58.1	1.21	0.3	58.9	32.2	31.3	21.7	23.5	7.5
5274.24	58.1	1.28	0.389	64.5	43.1	32	30.8	31.1	9.8
5472.3	58.1	1.25	-0.19	30.4	14.2	14	7.1	11	2.4
4628.16	58.1	0.52	-0.74	—	63.2	—	—	—	17.7
4811.34	60.1	0.06	-1.015	90	57.9	45.3	35.4	40.8	9.3
4959.12	60.1	0.06	-0.916	126.5	88.3	70.6	63.3	70.6	32.4
5234.19	60.1	0.55	-0.46	65.1	43.1	36.8	21.1	—	5.6
5319.81	60.1	0.55	-0.35	88.3	64.9	—	—	—	13
5740.88	60.1	1.16	-0.56	30.6	21.1	—	—	11.1	2.4
5130.59	60.1	1.3	0.1	—	—	—	30.6	—	12.6
5311.46 ⁷¹²	60.1	0.98	-0.56	—	—	—	—	11.8	2.3

Table A7: List of absorption lines for NGC 6940 stars

Wavelength (Å)	Species	χ (eV)	log gf	E28 (mÅ)	E30 (mÅ)	E67 (mÅ)	E87 (mÅ)	E101 (mÅ)	E105 (mÅ)	E108 (mÅ)	E132 (mÅ)	E138 (mÅ)	E139 (mÅ)	E152 (mÅ)	Juno
5711.09	12	4.34	-1.73	129	135	134.2	121.6	131.6	138	117.5	131.9	125.9	128.6	130.6	101.4
6318.71	12	5.11	-1.94	53.5	64.5	64.9	60.9	58.7	64.8	56.9	67.5	55.5	65.8	63.5	41.3
8712.69	12	5.93	-1.31	70.5	—	—	—	69.9	75.7	56.2	86.4	72.3	—	88	52.8
8717.83	12	5.93	-1.05	101.4	90.5	—	—	114.1	98.4	—	110.2	—	100.9	93.7	79.8
8736.02	12	5.94	-0.63	140.4	150	144.7	—	—	139.5	—	148.9	—	147.1	146.7	143.6
7387.69	12	5.75	-1.25	—	90	90.7	87.2	93.2	89.3	88.8	96.2	82.6	96.1	97.4	72.7
7691.55	12	5.75	-1	—	95.2	80.3	100.1	99.6	105.9	—	—	83.2	—	100.1	56.2
6319.24	12	5.11	-2.17	—	—	—	—	—	—	43.7	—	—	—	—	28.8
6696.02	13	3.14	-1.481	58.3	—	—	63.6	—	—	—	—	—	—	—	34.3
6698.67	13	3.14	-1.63	43.1	54.6	50	42.4	55.5	60.9	38	55.5	48.6	51.3	54.1	20.5
7835.32	13	4.04	-0.58	56.1	—	—	57.6	—	—	—	—	—	—	—	36.7
7836.13	13	4.02	-0.4	70.1	79.2	76.6	—	82.2	88.4	65.9	82.8	67.4	76.1	81.1	54.9
8772.88	13	4.02	-0.25	90.5	—	—	—	—	—	—	—	—	—	—	72.7
8773.91	13	4.02	-0.07	113.1	—	—	—	—	—	—	—	—	—	—	93.0
5488.98	14	5.61	-1.69	39.8	—	43.5	45.4	—	43.7	26.7	47.9	—	44.8	45.7	25.3
5517.54	14	5.08	-2.50	—	30.3	—	34.2	—	33.6	21.8	32.8	—	—	—	12.3
5665.55	14	4.92	-1.94	65.3	73.1	—	69.1	73.4	72.7	60.2	74.1	62.2	65.4	74.1	40.6
5684.48	14	4.95	-1.55	83.3	80.2	—	80.1	—	—	—	—	—	—	—	61.1
5690.43	14	4.93	-1.77	66.8	70.9	79.3	69.7	78.3	—	59.5	81.7	—	—	78.2	47.9
6125.02	14	5.61	-1.46	49.1	48.9	49.3	49.3	55.7	50.2	43.8	57.8	45.9	—	53.5	31.5
6142.48	14	5.62	-1.29	—	52.2	49.0	—	—	52.3	40.3	—	48.9	—	—	34.1
6145.02	14	5.62	-1.31	48.9	—	60.1	53.3	58.8	58.6	—	65.2	51.7	55.4	57.6	37.5
6243.82	14	5.62	-1.24	60.2	67.2	—	57.4	63.9	71.7	54.6	—	56.6	—	67.1	42.1
6244.47	14	5.62	-1.09	62.6	63.1	—	56.8	68.9	67.5	55.8	71.7	56.3	60.9	65.8	42.0
6414.98	14	5.87	-1.03	—	—	—	—	—	—	—	—	—	—	63.9	45.1
6721.85	14	5.86	-1.12	60.7	63.6	66.4	65.7	63.6	68.1	55.1	74.2	60.9	66.6	68.1	42.5
6741.63	14	5.98	-1.43	—	—	—	—	—	—	—	—	—	—	25.2	14.1
6848.58	14	5.86	-1.52	—	—	—	—	—	—	—	35.8	29.5	31.2	—	16.5
7003.57	14	5.96	-0.94	65.5	—	—	—	—	—	—	—	—	—	—	57.8
5260.39	20	2.52	-1.72	60.4	65.9	61.5	64.2	—	—	44.0	—	—	—	—	29.7
5512.98	20	2.93	-0.46	105.5	119.5	112.5	—	114.9	122.9	106.1	119.0	106.5	112.1	119.6	83.7
5581.97	20	2.52	-0.56	120.9	130.2	128.6	126.5	134.2	140.7	118.5	134.8	121.2	126.9	135.9	92.5
5590.11	20	2.52	-0.57	—	132.2	128.0	123.5	—	—	—	—	—	—	—	89.4
5867.56	20	2.93	-1.57	46.8	54.6	56.1	52.8	55.9	61.5	—	60.2	44.7	51.2	59.4	22.8
6161.30	20	2.52	-1.27	95.8	116.9	101.0	101.3	111.5	113.6	85.0	117.2	97.5	103.7	109.2	64.5

¹² Smith et al. (1996)

6166.44	20	2.52	-1.14	101.0	109.6	111.0	103.9	109.3	118.9	89.1	—	98.4	106.8	114.9	70.5
6169.04	20	2.52	-0.80	117.3	128.5	126.4	123.9	126.5	137.1	111.6	137.3	117.1	127.6	131.2	89.3
6169.56	20	2.53	-0.48	135.3	149.2	139.3	—	—	—	129.7	—	134.8	144.8	—	110.0
6455.60	20	2.52	-1.34	90.5	—	100.1	94.9	102.5	108.6	78.9	107.3	88.2	94.6	102.6	54.6
6471.66	20	2.53	-0.69	122.8	137.2	135.1	128.3	130.4	—	125.1	136.9	121.1	128.4	138.1	89.1
6493.78	20	2.52	-0.11	—	—	—	—	—	—	—	—	—	—	—	122.2
6499.65	20	2.52	-0.82	122.7	—	129.8	124.2	130.6	139.6	—	136.6	120.7	128.7	134.8	87.2
6572.78	20	0.00	-4.24	—	—	—	—	—	—	—	112.8	97.2	106.2	119.4	29.9
7326.15	20	2.93	-0.21	—	—	—	—	—	—	123.1	—	—	—	150.6	108.2
5022.87	22	0.83	-0.43	118.2	124.8	126.0	—	119.0	136.7	—	—	114.1	115.4	—	70.6
5039.96	22	0.02	-1.13	120.6	140.2	126.3	126.9	128.4	—	118.9	128.9	122.3	127.8	—	71.1
5064.65	22	0.05	-0.99	128.9	—	144.1	—	—	—	—	149.7	134.3	148.5	—	85.2
5113.45	22	1.44	-0.78	—	—	—	—	—	83.9	—	—	—	—	75.4	24.4
5147.48	22	0.00	-2.01	84.2	105.3	95.6	93.5	—	114.1	80.8	102.7	—	92.2	102.5	34.8
5210.39	22	0.05	-0.88	—	—	—	—	145.3	—	—	150.6	143.0	144.3	—	88.2
5219.70	22	0.02	-2.29	84.7	104.2	96.9	87.8	87.8	110.8	77.1	92.1	90.4	86.6	99.8	28.2
5295.77	22	1.07	-1.63	43.2	52.7	50.5	50.1	49.7	67.6	34.7	54.3	49.6	50.1	55.1	12.6
5866.45	22	1.07	-0.84	91.4	115.6	103.8	100.3	110.3	131.1	93.7	110.7	108.6	101.8	122.3	48.7
6091.17	22	2.27	-0.42	50.0	60.1	52.3	48.8	50.5	64.2	31.2	52.7	44.4	46.5	57.8	14.9
6126.22	22	1.07	-1.42	67.5	78.2	76.0	73.4	75.9	96.3	—	79.1	73.6	66.1	79.4	23.2
6258.10	22	1.44	-0.35	—	104.1	—	—	—	—	—	103.2	—	95.4	—	51.0
6261.10	22	1.43	-0.48	100.1	118.7	112.7	—	108.8	139.5	90.7	117.3	99.0	105.9	121.5	48.9
5242.49	26	3.63	-0.97	119.8	121.9	117	120.3	118.8	123.4	111.2	121.2	117.7	116.7	120.2	85.9
5253.03	26	2.28	-3.79	50.4	66.3	57.9	59.4	57.8	65	39.8	63.5	51.4	59.9	64.3	17.1
5288.52	26	3.69	-1.51	89.8	96.4	98.5	86.7	94.3	109.5	100.2	101.9	93.2	92.4	104.2	58.6
5321.1	26	4.43	-1.19	63.5	70.9	73.4	72.4	67	74.1	75.4	71.4	65.5	68.2	69.5	42.1
5322.04	26	2.28	-2.84	101.5	115.9	108.5	105.3	105.8	120.7	98.2	110.7	103.3	101.4	114.6	62.1
5364.87	26	4.45	0.23	139.7	142.7	147.6	133.5	146.5	143.1	139.2	145.2	134.2	143.1	144.9	132.9
5367.46	26	4.42	0.439	141.9	146.2	—	147.9	148.8	150.1	146.5	149.3	148.2	145.6	—	145.1
5373.7	26	4.47	-0.71	81.3	87.5	89.4	91.2	87.7	—	88.1	88	82.5	84.7	94.8	62.6
5389.47	26	4.42	-0.25	101.5	106.8	105.8	100.5	104.9	112	—	107.5	100.1	104.2	109.3	81.9
5410.91	26	4.47	0.4	137.8	139.3	135.2	131.7	—	—	—	138.5	134	137.3	—	130.9
5417.03	26	4.42	-1.53	59.7	59.6	59.9	68.4	55.8	64.6	52.2	63.7	57.6	56.1	61.9	35.2
5441.33	26	4.31	-1.58	61.2	63.8	62.9	64.3	63.6	68.5	59	64.6	55.9	55.6	62.7	31.5
5445.04	26	4.39	0.041	130.8	141.1	—	135.2	134.8	142.4	136	135.1	132.3	134.1	140.6	122.2
5522.44	26	4.21	-1.4	69.1	72.1	78.1	72.3	65.9	76.4	61.3	72.4	66.5	69.6	76.6	45.1
5554.89	26	4.55	-0.38	123.9	138.1	133.3	127.7	134.1	137.8	120	137.1	123.1	128.5	137.8	100.1
5560.21	26	4.43	-1.04	69.7	77.6	73.2	71.2	—	78.3	72.5	77.1	70.8	72.3	76.1	51.1
5584.76	26	3.57	-2.17	67.2	84.3	70.1	72.6	79.1	—	—	80.7	76.6	76.7	79.6	39.2
5624.02	26	4.39	-1.33	72.6	91.5	81.7	79.2	74.3	78.2	75.1	83.9	72.8	—	87.2	52.3
5633.94	26	4.99	-0.12	82.1	92.6	88.9	90.5	89	90.5	79.3	92.4	84	—	91.1	65.2
5635.82	26	4.26	-1.74	58.8	61.4	57.6	—	64.6	63.8	46.4	57.8	54.9	55	59.4	34
5638.26	26	4.22	-0.72	103.4	104.7	102.1	100.2	106.5	111.2	95.7	107.6	98.4	107.2	109.9	77.4
5691.49	26	4.3	-1.37	71.6	80.6	73.3	71.5	78.1	86.2	74.2	83.1	72.1	77.7	83.4	40.7
5705.46	26	4.3	-1.36	68.7	73.5	72	72.1	63.5	76.3	59.2	69.8	60.1	61.4	72.9	38.8
5717.83	26	4.28	-0.979	95.4	109.9	101.9	91.8	—	—	101.3	105.5	95.3	98.4	107	63.1
5731.76	26	4.26	-1.15	82.7	83.9	86.6	88.9	86.6	89.9	85.7	89	80.1	84.1	86.8	57.4
5806.72	26	4.61	-0.9	80.9	83.6	76.9	77.8	81	86.8	73.9	85.1	73.4	79	86.3	53.9
5814.8	26	4.28	-1.82	50	44.4	45.3	47.4	43	50.9	33.7	50.5	44.7	42.3	48.1	23.4
5852.21	26	4.55	-1.18	62.5	79.5	73.8	75	70.1	83.9	59	72.5	66.2	72.8	78.6	39.9
5883.81	26	3.96	-1.21	93.9	104.4	98.7	93.8	93.4	107.1	102.9	104.6	91.1	102.7	104.5	70.5
5916.24	26	2.45	-2.99	93.4	116.7	109.1	99.2	103.5	124.7	93.1	110.2	102.6	100.9	109.1	53.3
5934.65	26	3.93	-1.02	103	113.2	105.3	106.6	107.1	110.4	94.7	109.2	98.1	101.7	107.3	75
6024.05	26	4.55	-0.06	122.5	129.6	132.7	126.6	139	131.3	133.5	138	132	129.4	136.6	110.4
6027.05	26	4.08	-1.09	92.1	100.3	92.4	98.5	89.5	96.3	89.7	93.9	89.5	93.7	99.3	62.5
6056	26	4.73	-0.4	89.3	99.1	92.3	97.8	95.6	99.5	83.9	94.4	88.2	93.6	94.3	71.1
6079	26	4.65	-0.97	65.1	72.5	75.2	70.2	64.8	76.4	62.1	73	67	66.2	75	47.4
6093.64	26	4.61	-1.35	52.5	58.7	54.7	51	54.8	58.3	44	56.2	48.3	56.1	52.2	30.1
6096.66	26	3.98	-1.78	65	68.5	66	68.1	64.7	69.3	53.9	71.4	60.6	63.7	67.9	37.2
6120.24	26	0.91	-5.95	33.7	39.4	41.4	31.4	30.9	48.9	15.6	38.1	30.6	32.4	41.7	5.1
6151.61	26	2.18	-3.29	94.3	100.6	93.2	96.5	93.9	106.6	84.2	99.3	92.4	93.8	101.1	49.2
6157.72	26	4.08	-1.11	99.6	110.3	100.8	93.8	102.1	112.1	91.1	105.2	92.7	97.7	106.6	63.5
6165.36	26	4.14	-1.47	72.1	78.7	77.9	78.7	75.4	83.5	68	78.7	69.6	75	80.5	44
6173.33	26	2.22	-2.88	109.1	124.4	124.3	117.2	115.3	132.3	109.4	123.1	111.9	114.8	123.9	67.7
6187.99	26	3.94	-1.57	83.4	84.9	78.1	76.4	77.2	89.3	75	83.4	74.3	75.6	83.6	47.7
6200.31	26	2.61	-2.44	115.4	126.6	122.3	121.7	115.5	128.1	117.4	121.1	112.2	112.3	121.8	71.7
6322.68	26	2.59	-2.43	116.2	125.4	119.8	115.1	116.2	131.6	114.5	126	116.7	120.1	128.6	78.6

6380.74	26	4.19	-1.32	88.2	92.6	91.2	—	94.2	103.6	90.8	97.7	83.4	84.6	—	53.8
6392.53	26	2.28	-4.03	55.9	—	61.6	64.2	50.6	65.1	—	54.9	—	59.6	65.4	18.2
6419.95	26	4.73	-0.09	102.7	—	121.5	—	119.4	121.8	125.9	128.7	111.5	111.8	128.1	87
6436.4	26	4.19	-2.46	33.8	41.6	38.3	33.3	31.7	39.1	26.4	36.7	27.9	30.2	34.6	11.1
6469.19	26	4.84	-0.62	89.4	102	93.2	87.3	92.4	103.1	80.7	98.3	85.7	91.4	—	58.4
6518.36	26	2.83	-2.3	91.6	102.1	99.7	94.4	—	117.5	86.8	104.8	96.1	97.4	107.4	58.1
6574.22	26	0.99	-5.02	82.8	96.7	89.5	90.3	86.5	109.6	69.7	92.5	84.8	86.3	94.1	29
6591.31	26	4.59	-2.07	30.3	31.3	30.4	—	25.7	30.3	—	33.6	24.3	27.8	36.1	10.5
6593.87	26	2.44	-2.42	139.1	148.3	136.9	142.8	134.9	148.9	130.2	146	131.3	135.6	144	87.5
6597.56	26	4.8	-0.92	60.5	65.1	67.5	72.5	65.6	72.1	—	63.3	61	65.5	66	42.4
6608.02	26	2.28	-4.03	52.7	64	53.7	61.3	61.9	72.4	47.2	62.5	56.1	53.1	64.4	17.1
6609.11	26	2.56	-2.69	112.8	125.4	114.1	117.3	121.6	137.8	110.5	124.2	112.6	113	125.1	68.2
6703.56	26	2.76	-3.16	77.5	88.2	84.5	91.2	81.2	98.9	74.6	90.3	74.9	78.9	86.4	37.8
6704.48	26	4.22	-2.66	16.2	20.3	23.1	21.2	20.5	19.9	14.2	20	18.8	14.9	17.4	6.1
6710.31	26	1.8	-4.88	62.3	80.3	72.6	68.5	69.5	90.6	56.8	76.3	61	67.9	76.1	15.7
6713.74	26	4.79	-1.6	42.8	42	39.6	43.9	40.7	45.8	30	42.2	35.6	35.8	42.3	21.4
6739.52	26	1.56	-4.95	44.4	49.1	43.6	49.9	—	66.3	37	51	—	44.6	53.1	11.8
6750.15	26	2.42	-2.62	120	129.4	127.5	122.4	119.9	139.1	111.5	125.1	117.8	119.6	130.2	76.2
6752.7	26	4.64	-1.2	60.2	77.2	—	69.4	71.4	80.3	—	80.4	64.9	71.9	74	38.2
6793.25	26	4.07	-2.47	27.4	—	—	28.9	—	—	22.2	—	—	—	32.7	13.2
6806.84	26	2.73	-3.21	76	85.2	76.4	74.4	77.9	93.3	71.4	83.7	72.2	76.1	87.1	34
6810.26	26	4.61	-0.99	72.6	75.2	72.9	73.4	69.1	79.9	70.6	80.5	68.3	72.5	76.2	50
6820.37	26	4.64	-1.17	65.6	73.2	73	75.1	68.1	75.9	60.8	71.6	61.8	64.6	71.9	40.9
6858.15	26	4.61	-0.93	73.6	80	82.9	80.6	77.2	86.1	72.5	80.2	72.5	78.7	81	50.2
6551.67	26	0.99	-5.79	—	51.6	46.3	45.5	36.4	63.4	—	53	41.1	—	51.9	6.1
6646.93	26	2.61	-3.99	—	50.4	44.4	42.4	41.8	60.1	—	47.6	36.3	37.7	—	8.2
6653.85	26	4.14	-2.52	—	27.5	22.6	28.4	26.3	30.4	22	27.2	24.2	23.6	27.1	10.9
6699.14	26	4.59	-2.19	—	30.4	24	23.9	20.3	30.1	12.4	22.9	19.9	—	24.8	7.5
6745.95	26	4.07	-2.77	—	19	—	—	—	—	—	—	—	—	21.1	8.3
6851.63	26	1.61	-5.32	—	47	41.6	42	35	54.2	21.5	39.8	35.2	42.1	37.6	6.7
7132.98	26	4.08	-1.61	—	72	76.6	—	—	—	—	—	—	—	—	42.5
6170.5	26	4.8	-0.38	—	—	117.5	—	—	—	115	—	—	113.2	—	82.9
6783.7	26	2.59	-3.98	—	—	—	—	—	70.3	—	63.3	50.8	52.3	64.7	14.3
4993.34	26.1	2.81	-3.67	59.6	—	68.4	56.9	52.9	62.6	—	63.1	60.6	—	63.2	38
5132.65	26.1	2.81	-4	42.1	55.5	49.5	41.7	44.7	—	37.7	44.4	45.1	43.6	43.9	23.8
5197.55	26.1	3.23	-2.25	107.4	110.6	106.9	—	—	110.1	115	111.1	102	108.5	—	81.9
5234.61	26.1	3.22	-2.24	111.8	—	104	105.3	102.7	101.4	—	110.7	102.5	103.8	103.8	81.9
5284.09	26.1	2.89	-3.01	86.6	95.7	—	—	87.5	—	—	—	—	—	—	66.7
5325.55	26.1	3.22	-3.17	62	56.9	60.7	62.5	58	58.5	—	60.9	60.8	—	60.2	38.7
5414.04	26.1	3.22	-3.62	42.2	46.9	50.4	44.1	43.2	—	43.1	—	43.9	—	45.5	25.9
5425.24	26.1	3.2	-3.21	67.9	66.4	60.9	64.8	59.1	59.4	69.1	60.3	58.5	63.2	61.6	39.6
5991.36	26.1	3.15	-3.56	52.3	56.3	—	52.5	52.1	53.6	—	60	51.2	53.6	54.4	29.9
6084.09	26.1	3.2	-3.8	40.3	47.8	44.4	—	—	45.2	—	46.7	40.5	42.6	42.6	22.2
6149.24	26.1	3.89	-2.72	51.5	54.3	56.5	53	46.7	48.4	55.6	—	52.8	53.2	57.6	37.7
6247.54	26.1	3.89	-2.34	70.6	74.8	73.8	72.8	68.6	65.8	76.8	74.4	70.4	79.2	75.2	55.9
6416.92	26.1	3.89	-2.68	55.2	61.2	56.6	58.7	55.3	60.6	61.4	57.4	55.1	56.8	59.7	39.6
6432.68	26.1	2.89	-3.58	61.8	64.2	66.6	63.9	57.9	61.6	64.3	63.4	66.2	65.8	63.2	43.1
4607.34	38	0	0.283	88.7	91.4	89.7	82.6	93	98.1	93.1	91.2	84.7	88	94.1	41
4883.68	39.1	1.08	0.07	91.1	—	—	—	—	—	—	—	—	—	—	60.1
5087.43	39.1	1.08	-0.17	81.7	88.5	81.6	81.6	88.7	92.1	95.9	91.7	85.9	87.8	87.8	48.8
5200.42	39.1	0.99	-0.57	73.2	85.1	77.9	75.6	88.2	92.3	—	87.5	80.8	81.7	84.6	38.9
5205.72	39.1	1.03	-0.34	75.7	—	—	—	—	—	—	—	—	—	—	41.4
5289.82	39.1	1.03	-1.85	20.4	26.1	—	23.3	30	30.1	28.3	28.6	25.1	26.7	25.7	5.2
5402.78	39.1	1.84	-0.44	—	46.6	40.4	42.8	43.5	49.1	43.1	46.1	39.8	40.1	44.5	13
5385.13	40	0.52	-0.64	14.3	21	17.1	—	13.3	26.9	—	19.7	—	15	17.4	1.8
6127.46	40	0.15	-1.06	26.5	26	22.9	20.1	24.1	—	22.8	27.9	25.2	24.4	29.1	3.8
6134.57	40	0	-1.28	17.4	26.7	28.2	18.4	19.5	31.6	12.9	26.1	19.9	23.8	24.4	2.2
6143.18	40	0.07	-1.1	28.4	33.3	27.2	21.6	22.9	—	—	30.2	23.8	17.7	29.1	3
5303.53	57.1	0.32	-1.35	25.1	31.9	22.4	18.2	28.5	34.2	23.7	31.5	27.3	25.9	35.7	3.6
6390.48	57.1	0.32	-1.41	22.9	28.2	32.2	26.2	29	42.2	24.2	33.1	33.9	32	34	3.9
5880.63	57.1	0.24	-1.83	—	20.2	—	11	—	—	—	—	17	—	—	1.4
4628.16	58.1	0.52	-0.74	57.6	66.4	69.7	62	63.5	—	63.1	67.9	55.9	67.4	71.5	17.7
5187.46	58.1	1.21	0.3	29	31.2	36.7	36.4	31.9	42.1	—	37.3	29.5	31.4	30.1	7.5
5274.24	58.1	1.28	0.389	34	43.8	40.4	35.7	44.1	47.4	35.1	43.2	39.4	40.3	47.8	9.8
5472.3	58.1	1.25	-0.19	13.5	19.1	18.4	—	—	23.9	14	21.2	—	17.3	18.8	2.4
4811.34	60.1	0.06	-1.015	43.9	65.2	48.2	57.6	53.8	72.7	37	66.5	55.2	57.9	59.9	9.3
4959.12	60.1	0.06	-0.916	70.5	90.1	84.6	75.7	75.1	96.1	—	85.3	75.5	76.5	80.3	32.4

5130.59	60.1	1.3	0.1	38.9	—	—	—	—	—	—	—	—	—	44.9	12.6
5319.81	60.1	0.55	-0.35	50.6	67	61	61	—	—	—	61.4	60.1	54.3	64.1	13
5740.88	60.1	1.16	-0.56	12.7	—	19.8	—	15	23.6	—	19.8	—	—	17.2	2.4
5234.19	60.1	0.55	-0.46	—	57.8	40.6	—	31.2	—	32.9	57.1	—	—	—	5.6
5311.46 ¹³	60.1	0.98	-0.56	—	—	—	—	—	—	—	—	—	18.8	—	2.3

This paper has been typeset from a \LaTeX file prepared by the author.

¹³ [Smith et al. \(1996\)](#)